University of New Mexico
UNM Digital Repository

Nuclear Engineering ETDs | Engineering ETDs

6-24-2010

Development of sensitivity analysis with the use of TSUNAMI-3D sensitivity coefficients for benchmark uncertainty analysis

Allison Barber

Follow this and additional works at: https://digitalrepository.unm.edu/ne_etds

Recommended Citation
Barber, Allison. "Development of sensitivity analysis with the use of TSUNAMI-3D sensitivity coefficients for benchmark uncertainty analysis." (2010). https://digitalrepository.unm.edu/ne_etds/22

This Thesis is brought to you for free and open access by the Engineering ETDs at UNM Digital Repository. It has been accepted for inclusion in Nuclear Engineering ETDs by an authorized administrator of UNM Digital Repository. For more information, please contact disc@unm.edu.

www.manaraa.com

Development of Sensitivity Analysis with the Use of TSUNAMI-3D Sensitivity Coefficients for Benchmark Uncertainty Analysis

BY

Allison Delo Barber

B.S. Nuclear Engineering

University of New Mexico, 2008

THESIS

Submitted in Partial Fulfillment of the
Requirements for the Degree of

Master of Science

Nuclear Engineering

The University of New Mexico
Albuquerque, New Mexico
May, 2010

www.manaraa.com

©2010, Allison Delo Barber

www.manaraa.com

DEDICATION

This work has taken me into a field that I would have not been exposed to if other paths had been taken. Without Justin, I am not sure where I would be today. With his help I have been able to endure more than I would alone. To my parents who have never doubted that I could achieve great things.

www.manaraa.com

ACKNOWLEDGMENTS

I would like to acknowledge Ken for giving me an amazing opportunity to work in an environment where I only see growth and learning. The advisors for this work have been a tremendous assistance. Dr. Busch you have been there since I first walked into your office as a scared sophomore not knowing what direction to go in. Dr. Prinja you have always fascinated me with how fast you derive the diffusion equation but also how much I have learned from each class I take. Gary you have taught me so much in the area of this work, and I have had more opportunities than other students in my position. I hope that I have produced work that you are as proud of, as I am.

www.manaraa.com

Development of Sensitivity Analysis with the Use of TSUNAMI-3D Sensitivity Coefficients for Benchmark Uncertainty Analysis

by

Allison Delo Barber

ABSTRACT OF THESIS

Submitted in Partial Fulfillment of the
Requirements for the Degree of

Master of Science

Nuclear Engineering

The University of New Mexico
Albuquerque, New Mexico

May, 2010

www.manaraa.com

Development of Sensitivity Analysis with the Use of TSUNAMI-3D Sensitivity Coefficients for Benchmark Uncertainty Analysis

By

Allison Delo Barber

B.S., Nuclear Engineering, University of New Mexico, 2008

M.S., Nuclear Engineering, University of New Mexico, 2010

ABSTRACT

The uncertainty of a critical benchmark experiment is a very important result. This value tells how well each parameter in the system is known and therefore how well the multiplication factor is known. The current method of uncertainty analysis for benchmark evaluations is tedious and time consuming. If the time required for the uncertainty analysis can be decreased and also offer a robust analysis, this would greatly enhance the results produced from the benchmark experiments.

Four experiments were chosen for evaluation in the work. The direct uncertainty analysis was performed as described in the International Handbook of Evaluated Criticality Safety Benchmark Experiments Uncertainty Guidelines. The process was duplicated from the benchmark evaluations to ensure the process was well understood as well as validate the computer code and cross section library used in this work. First order

www.manaraa.com

derivative equations were developed to correlate the direct uncertainty analysis values with the sensitivity coefficients produced from the TSUNAMI-3D computer code. TSUNAMI-3D produces sensitivities to the nuclear data, while the direct uncertainty analysis required sensitivities to the material, and physical properties.

The goal of this work was to implement the sensitivities in the nuclear data with the first order derivative equations to offer a robust uncertainty analysis that required less time and produces a better analysis than current processes.

www.manaraa.com

Table of Contents

www.manaraa.com

www.manaraa.com

www.manaraa.com

www.manaraa.com

List of Figures

www.manaraa.com

www.manaraa.com

List of Tables

www.manaraa.com

www.manaraa.com

CHAPTER 1

1.1 Introduction

When a criticality safety benchmark evaluation is performed, a detailed uncertainty analysis of the experiment is conducted. This analysis determines the overall uncertainty in the multiplication factor for the experiment. The uncertainty analysis is performed by first gathering each uncertainty in the physical and material properties for the experiment. Next a computer model is generated for the nominal case. The nominal experimental model is perturbed for each uncertainty individually, which creates hundreds of input files. The time required to run all of the input files can be weeks and even months. Caution must be taken when creating the perturbed input files, as to ensure that all aspects of the parameter variation are correctly handled. One example of this is when analyzing the effect of the clad outer diameter. If the inner clad diameter is not modified in addition to the clad outer diameter, the result in the sensitivity will be a function of the outer clad diameter as well as the thickness of the cladding. Without the change in the clad inner diameter, the clad thickness as well as the volume fraction of the moderator will change, resulting in a sensitivity for more than one parameter. It is difficult to separate the two modifications, but the change in the gap thickness (i.e., change in clad inner diameter) has less of a neutronic effect on the system than the change in the volume fraction of the moderator. Each of these precautions is discussed in the direct uncertainty analysis section.

When a computational model is generated, there is an associated uncertainty with that computational model. That uncertainty only represents the uncertainty in the nuclear

www.manaraa.com

data and does not represent how well the physical and material parameters of the system are known.

Thus, there are three types of uncertainties: those associated with physical proprieties (dimensions, locations, etc.), with material properties (impurities, densities, etc.), and with nuclear properties (cross sections, nu, etc.). Automatic evaluations of nuclear data uncertainty can be done with Tool for Sensitivity and Uncertainty Analysis Methodology Implementation (TSUNAMI)[1]; however, the code only evaluates sensitivities for nuclear data uncertainties. TSUAMI is also used for evaluating similarities among experiments.

Uncertainty analysis for benchmark evaluations is a painstaking process. The evaluator needs to evaluate the uncertainties for all physical and material properties. The process requires a perturbation for each parameter individually, which requires hundreds of computer runs. To accurately determine the solution changes due to the small perturbations of the system model each run requires significant computer time to reach adequate convergence. A simpler and less time consuming process is needed; however the robustness of the process must be maintained.

The code TSUNAMI-3D in the SCALE 5.1 code package is currently used to determine a correlation among experiments for the goal of determining applicable benchmark evaluations.[2,3,4] The goal of this work is to show that TSUNAMI-3D could be used as a sensitivity and uncertainty analysis tool for an individual experiment, rather than using the more tedious direct uncertainty process of perturbing each parameter individually. A secondary goal is the application of this analysis approach before or

www.manaraa.com

while performing an experiment. If the pertinent sensitivities could be determined up front, then the parameters to which the experiment is most sensitive could be identified. Additional measurements could be made to reduce the sensitivities and offer an even more robust uncertainty analysis. Effort could be focused on these parameters to reduce their uncertainties and hence reduce the overall uncertainty in the experimental results.

The International Handbook of Evaluated Criticality Safety Benchmark Experiments (IHECSBE)[5] contains over five hundred individual experiments. The purpose of a benchmark experiment is to provide a comprehensive set of benchmark data that can be used for comparison of proposed experiments, reactor design, and validation of computer codes and nuclear data used in computer codes. The accuracy of the overall uncertainty associated with each benchmark is very important. The final calculated uncertainty comes from many different parts of the system: how close the system is to critical, the masses and compositions of content in the system, and its physical dimensions. When all of these values and associated uncertainties are determined, an overall uncertainty for the system can be calculated. This will give an estimate of how well the configuration and the neutronic state of the system are known.

The work performed here will evaluate the process currently used in uncertainty analysis for three critical experiments from the IHECSBE, and for the Seven Percent Critical Experiment (7uPCX) being performed at Sandia National Laboratories, andle also implementing a different method of uncertainty analysis using the TSUNAMI-3D code. The three experiments from the IHECSBE are LEU-COMP-THERM-023[6], LEU-COMP-THERM-070[7], and LEU-COMP-THERM-079[8]. These experiments were chosen

www.manaraa.com

to represent different physical and material properties for a range of experiments. The uncertainty analysis provided in the benchmark evaluations was replicated to ensure correct modeling, and the developed sensitivity and uncertainty analysis was applied to each critical experiment. The results of these evaluations are presented in a later chapter.

The KENO V.a and TSUNAMI-3D code systems from the SCALE 5.1 code package were used to evaluate all experimental models.[9] The SCALE5.1 code package was developed at Oak Ridge National Laboratory and is a well accepted tool. KENO V.a is a module in the CSAS5 sequence that calculates the multiplication factor for the system using Monte Carlo techniques. TSUNAMI-3D is a three-dimensional Monte Carlo code that determines the sensitivity of particular constituents in the experimental model. The sensitivity/uncertainty analysis from TSUNAMI-3D gives the sensitivity of the multiplication factor to the nuclear data. A more detailed overview of these programs is provided in Appendix A.

Once the uncertainty analysis process is determined, the opportunity to design experiments with TSUNAMI-3D is possible. Experiments are designed with the goal of determining how different parameters affect systems. Examples are v arious enrichments, burnable poisons, pitch variations. With an anticipated outcome for a critical experiment, it is possible to perform the uncertainty analysis.

First the sensitivity theory is discussed and how it was implemented in the work evaluated here. Following the sensitivity theory, the process of sensitivity analysis is discussed. The next chapter discusses perturbation theory for the purpose of understanding how TSUNAMI-3D calculates the sensitivity coefficients. After the

www.manaraa.com

perturbation theory has been described, the process of how TSUANMI-3D calculates the sensitivity coefficients is discussed. Chapter 5 discusses the experiments evaluated in this work and the direct uncertainty analysis is provided for each experiment. Chapter 6 develops the equations used for a new approach to sensitivity analysis for benchmark and experiment evaluation. Correlations are made between the new approach to sensitivity analysis and the traditional direct uncertainty analysis method. Finally chapter 7 contains the conclusions made from all of the evaluations and discusses possibilities for future work.

www.manaraa.com

CHAPTER 2

2.1 Sensitivity Theory

Sensitivity Analysis (SA) studies how a variation in the result of a computational model can be qualitatively understood based on how different sources of variation and the information put into a model.[10] The definition of sensitivity analysis is the evaluation of the relationship between the information flowing in and out of a model.

The goal of sensitivity analysis is to determine how the solution to a computational model depends on the parameters of the system. A local sensitivity analysis can use partial derivatives to quantify the effects of variation in individual system parameters on the system output.[10] In the work described below, the parameters are material compositions, system properties, and physical dimensions. The results of the sensitivity analysis can provide valuable information about the model as well as the software used for the model.

A large number of sensitivity analysis methods have been developed: including the use of Green's Functions, a One-Factor-at-a-Time (OAT) approach, Importance Measures, Derivatives, Local Methods, Regression Method (Standardized Regression Coefficients), Morris, Variance Based Methods and Monte Carlo Filtering.[11] The different methods offer a range of advantages and disadvantages, so choosing a method for uncertainty analysis should consider the objective of the analysis. While other factors may influence which method is used, the analysis objective of the sensitivity analysis should be given the most weight.

www.manaraa.com

2.2 Sensitivity Theory Process

The following offers a general example of sensitivity analysis. Below is a simple example of how sensitivity of a parameter in a general function is determined.

Given the following function,

$$y = f(\alpha_1, \alpha_2, ..., \alpha_n). \tag{1}$$

where the variables ($\alpha_1, \alpha_2, ..., \alpha_n$) are the various parameters of the function. The sensitivity of the function y with respect to a parameter in that function, is given by the following equation

$$S_{\alpha_j} = \frac{\frac{\partial y}{y}}{\frac{\partial \alpha_j}{\alpha_j}} = \left(\frac{\alpha_j}{y}\right)\frac{\partial y}{\partial \alpha_j} \tag{2}$$

S_{α_j} is often referred to as the sensitivity coefficient.

The function, y, is the multiplication factor and the variables are parameters such as:

- macroscopic absorption cross section, Σ_a
- fission cross section, Σ_f
- chi, χ
- nu, υ
- scattering cross section, Σ_s

www.manaraa.com

- temperature, T
- water height, h_{water}
- fuel radius, r_{fuel}
- pitch, P
- and other parameters in the system

$$k_{eff} = k_{eff}(\Sigma_a, \Sigma_f, \Sigma_s, \chi, \upsilon, T, h_{water}, r_{fuel}, P...) \quad (3)$$

The sensitivity represents the relative change in a function as a result of a change in a parameter. The method of sensitivity analysis implemented in this work is the OAT approach.[12] This method requires that each parameter in the system is perturbed, while maintaining all other parameters at the nominal value.[12] Reference 12 describes the OAT method as only valid when the purpose of the sensitivity analysis is to assess the relative importance of the system parameters, and is only justified when the model is proven to be linear. This is the case for the critical benchmark evaluations.

The method of perturbing one parameter at a time and running a Monte Carlo code is very time consuming requiring a large amount of computing time. Utilizing perturbation theory and sensitivity analysis could allow for a more automated process as well as saving time spent running the hundreds of input files that are required to obtain good statistical results from direct uncertainty analysis.

www.manaraa.com

CHAPTER 3

3.1 Perturbation Theory

Adjoint-based first-order linear perturbation theory is used to compute the sensitivities of the nuclear data to the multiplication factor. The computed sensitivities can be referenced to the effect of a particular nuclide or nuclide-reaction combination on the multiplication factor, k_{eff}. Monte Carlo techniques are implemented to determine the neutron flux moments and/or the angular fluxes, which then generate the scattering terms of the sensitivity coefficients.[13]

The following is a general review of perturbation theory from a range of textbooks and references.[14,15,16,17]

The time-independent neutron transport equation describes the behavior of the angular flux in a reactor.

$$\hat{\Omega}\cdot\nabla\phi\left(\vec{r},E,\hat{\Omega}\right)+\Sigma_t\left(\vec{r},E\right)\phi\left(\vec{r},E,\hat{\Omega}\right)=\int_{4\pi}d\hat{\Omega}'\int_0^{\infty}dE'\,\Sigma_s\left(\vec{r},E'\rightarrow E,\hat{\Omega}'\cdot\hat{\Omega}\right)\phi\left(\vec{r},E',\hat{\Omega}'\right)$$

$$+\frac{1}{k}\frac{\chi(\vec{r},E)}{4\pi}\int_{4\pi}d\hat{\Omega}\int_0^{\infty}dE'\,\nu(\vec{r},E')\Sigma_f(\vec{r},E')\phi\left(\vec{r},E',\hat{\Omega}'\right) \qquad (4)$$

The left side of the equation represents the loss terms, while the right side of the equation represents the production of neutrons. In Equation 4, ϕ is the angular-dependent neutron flux, Σ_t is the total macroscopic cross-section, χ is the average number of fission neutrons emitted, ν is the average number of fissions neutron emitted from fission, Σ_f is

www.manaraa.com

the macroscopic cross section for fission, Σ_s is the macroscopic scattering cross section, Ω is the direction, r is the point, E is the energy, and k is the multiplication factor.

For the development of perturbation theory, it is necessary to define an inner product. The inner product (f,g), where $f(\vec{r},E,\vec{\Omega},t)$ and $g(\vec{r},E,\vec{\Omega},t)$ are any two real functions of phase space, is defined as

$$\langle f,g\rangle \equiv \int_0^t \int_0^\infty \int_R \int_{4\pi} f(\vec{r},E,\vec{\Omega},t)g(\vec{r},E,\vec{\Omega},t)d\vec{\Omega}drdEdt \,. \tag{5}$$

where the integration is over the phase space. The definition of inner product is then used to define as operator $M^\dagger$ that is adjoint to the operator M as follows;

$$\langle f,Mg\rangle = \langle g,M^\dagger f\rangle \tag{6}$$

where the homogenous boundary conditions, $f(\tilde{r}_s)=0=g(\tilde{r}_s)$, have been assumed.

The next step in perturbation theory is to represent the transport equation in operator notation

$$M\phi = \frac{1}{k}F\phi \tag{7}$$

where $M\phi$ is the migration and loss of neutrons and $1/k\,F\phi$ is the modified source of fission neutrons.[15] Equation 8 below represents the adjoint problem

$$M^\dagger\phi^\dagger = \frac{1}{k^\dagger}F^\dagger\phi^\dagger \,. \tag{8}$$

www.manaraa.com

The † symbol represents the adjoint of the term. It should be noted that for the fundamental mode, the adjoint multiplication factor is equal to the unperturbed multiplication factor, $k^{\dagger} = k$.

To show that $k^{\dagger} = k$, the following derivation is provided.

$$M\Psi = \frac{1}{k} F\Psi \tag{9}$$

$$M^{\dagger}\Psi^{\dagger} = \frac{1}{k^{\dagger}} F^{\dagger}\Psi^{\dagger} \tag{10}$$

Equation **9** is the transport equation in operator notation and Equation 10 is the adjoint transport equation.

$$\left\langle \Psi^{\dagger}, M\Psi \right\rangle = \left\langle \Psi, M^{\dagger}\Psi^{\dagger} \right\rangle \tag{11}$$

$$\left\langle \Psi^{\dagger}, F\Psi \right\rangle = \left\langle \Psi, F^{\dagger}\Psi^{\dagger} \right\rangle \tag{12}$$

Equation 11 and Equation 12 are the definition of the adjoints.

The next step is the take the inner product of Equation 9 and Equation 10 and set them equal to one another. The result is Equation 13.

$$\left\langle \Psi^{\dagger}, M\Psi \right\rangle - \left\langle \Psi, M^{\dagger}\Psi^{\dagger} \right\rangle = \frac{1}{k}\left\langle \Psi^{\dagger}, F\Psi \right\rangle - \frac{1}{k^{\dagger}}\left\langle \Psi, F^{\dagger}\Psi^{\dagger} \right\rangle \tag{13}$$

www.manaraa.com

Because the left hand side is the definition of the adjoint and is equal to zero, the following relationship can be made.

$$0 = \left(\frac{1}{k} - \frac{1}{k^{\dagger}} \right) \left\langle \Psi^{\dagger}, F\Psi \right\rangle \tag{14}$$

Through complex proofs, it can be shown that the following is true.

$$\begin{aligned} &\Psi > 0 \\ &\Psi^{\dagger} > 0 \\ &F\Psi^{\dagger} > 0 \\ &\left\langle \Psi^{\dagger}, F\Psi \right\rangle > 0 \end{aligned} \tag{15}$$

Given that all of the terms are positive, the only possibility for Equation 14 to be true is that the adjoint keff must be equal to the unperturbed keff (for the fundamental mode).

As an example, a perturbation is made in the migration and loss terms; this could be representative of a change in the microscopic absorption cross section. In Equation 16 M' is the new perturbed operator.

$$M' = M + \delta M \tag{16}$$

To calculate the change in k from the change in migration and/or loss terms, the scalar product of the following equation is taken with the adjoint flux. Equation 17 is the perturbed problem.

$$M'\phi' = \frac{1}{k'} F\phi' \tag{17}$$

www.manaraa.com

Where the perturbation δM in the operator is the following equation

$$M' = M + \delta M \,. \tag{18}$$

Inserting (18) into (17) and taking the scalar product of Equation 17 and the adjoint flux is

$$\left\langle \phi^{\dagger}, M\phi' \right\rangle + \left\langle \phi^{\dagger}, \delta M\phi' \right\rangle = \frac{1}{k'}\left\langle \phi^{\dagger}, F\phi' \right\rangle \tag{19}$$

Then implementing the equation for the adjoint operator

$$\left\langle \phi^{\dagger}, M\phi' \right\rangle = \left\langle M^{\dagger}\phi^{\dagger}, \phi' \right\rangle = \left\langle \frac{1}{k}F^{\dagger}\phi^{\dagger}, \phi' \right\rangle = \frac{1}{k}\left\langle \phi^{\dagger}, F\phi' \right\rangle. \tag{20}$$

The result of the above equation is

$$\left(\frac{1}{k'} - \frac{1}{k}\right) = \frac{\left\langle \phi^{\dagger}, \delta M\phi' \right\rangle}{\left\langle \phi^{\dagger}, F\phi' \right\rangle}. \tag{21}$$

With the above equations, it is now possible to determine the change in k from the change in the migration and loss term, where the following relationship is implemented for convenience,

$$\rho = \frac{k-1}{k} \tag{22}$$

$$\Delta\rho = \rho' - \rho = \left(\frac{1}{k} - \frac{1}{k'}\right) \tag{23}$$

www.manaraa.com

where ρ is reactivity. Replacing the perturbed flux in Equation 21 with the unperturbed flux plus the change in that flux ($\phi+\delta\phi$) is shown in the following equation.

$$\Delta\rho = -\frac{\left\langle \phi^{\dagger}, \delta M\left(\phi+\delta\phi\right)\right\rangle}{\left\langle \phi^{\dagger}, F\left(\phi+\delta\phi\right)\right\rangle} \tag{24}$$

$$\Delta\rho = -\frac{\left\langle \phi^{\dagger}, \delta M\phi\right\rangle + \left\langle \phi^{\dagger}, \delta M\delta\phi\right\rangle}{\left\langle \phi^{\dagger}, F\phi\right\rangle + \left\langle \phi^{\dagger}, F\delta\phi\right\rangle} \tag{25}$$

$$\Delta\rho = -\frac{\left[\left\langle \phi^{\dagger}, \delta M\phi\right\rangle + \left\langle \phi^{\dagger}, \delta M\delta\phi\right\rangle\right]}{\left\langle \phi^{\dagger}, F\phi\right\rangle}\left[1+\frac{\left\langle \phi^{\dagger}, F\delta\phi\right\rangle}{\left\langle \phi^{\dagger}, F\phi\right\rangle}\right]^{-1} \tag{26}$$

$$\Delta\rho = -\frac{\left[\left\langle \phi^{\dagger}, \delta M\phi\right\rangle + \left\langle \phi^{\dagger}, \delta M\delta\phi\right\rangle\right]\left[1-\frac{\left\langle \phi^{\dagger}, F\delta\phi\right\rangle}{\left\langle \phi^{\dagger}, F\phi\right\rangle}\right]}{\left\langle \phi^{\dagger}, F\phi\right\rangle} \tag{27}$$

$$\Delta\rho = -\frac{\left\langle \phi^{\dagger}, \delta M\phi\right\rangle}{\left\langle \phi^{\dagger}, F\phi\right\rangle} - \frac{\left\langle \phi^{\dagger}, \delta M\delta\phi\right\rangle}{\left\langle \phi^{\dagger}, F\phi\right\rangle} + \frac{\left\langle \phi^{\dagger}, \delta M\phi\right\rangle\left\langle \phi^{\dagger}, F\delta\phi\right\rangle}{\left\langle \phi^{\dagger}, F\phi\right\rangle^{2}} + \ldots \tag{28}$$

Thus the change in reactivity due to the change in the M operator term is Equation 28.

Equation 28 is possible because it is assumed that the change in the migration and loss term is very small and thus the change in the flux is small as well. The change in reactivity is represented in terms of the unperturbed flux, rather than the perturbed flux, which is difficult to calculate. Neglecting second and higher order terms in all perturbed quantities, then the result for the first order perturbation theory is the following equation

www.manaraa.com

$$\Delta\rho \cong -\frac{\left\langle \phi^{\dagger}, \delta M \phi \right\rangle}{\left\langle \phi^{\dagger}, F\phi \right\rangle} \ . \tag{29}$$

The change in reactivity requires the calculation of the adjoint scalar flux. The SCALE 5.1 TSUNAMI code is used to generate the necessary terms to perform the perturbation theory. A description of the code TSUANMI and the processes that are run during the sensitivity coefficient calculation is attached in appendix A.

www.manaraa.com

CHAPTER 4

4.1 TSUNAMI-3D

TSUNAMI-3D[13] uses a three-dimensional Monte Carlo neutron transport analysis to determine the sensitivity and uncertainty associated with the nuclide/compositions of an experiment. The uncertainties in the cross section data are propagated to uncertainties in the multiplication factor by means of the sensitivity coefficients.

4.2 TSUNAMI Sensitivity Coefficient Generation

The Sensitivity Analysis Module for the SCALE Code System (SAMS) in the TSUNAMI code sequence calculates the effect of a change in a constituent component or cross section on the effective multiplication factor (k_{eff}) for a computational model.[14] The module was developed by Bradley T. Rearden for his doctoral dissertation at Texas A&M University in 1999.[14] The following describes the process for the sensitivity coefficient generation.

Sensitivity coefficients are generated using linear perturbation theory, relating the change in k_{eff} to the change in a particular parameter. By means of the transport equation, the relative change in k_{eff} from a small change in a macroscopic cross section is represented as a sensitivity coefficient.

www.manaraa.com

To obtain the equation for the sensitivity coefficients, the following derivation is performed.

$$[A-\lambda B]\phi=0 \tag{30}$$

$$[A'-\lambda' B']\phi'=0 \tag{31}$$

$$\left[A^{\dagger}-\lambda B^{\dagger}\right]\phi^{\dagger}=0 \tag{32}$$

$$A'=A+dA \tag{33}$$

$$B'=B+dB \tag{34}$$

$$\lambda'=\lambda+d\lambda \tag{35}$$

First starting with the operator notation form of the unperturbed transport equation (30), the perturbed transport equation (31) and the adjoint transport equation (32) and equations (33), (34) and (35) represent the perturbed parameters of the transport equations. From the previous discussion on perturbation theory A=M, B=F and λ=1/k.

Multiplying Equation 32 by the adjoint flux and Equation 31 by the perturbed flux, results in

$$\phi'[A'-\lambda' B']\phi^{\dagger}=0 \tag{36}$$

$$\phi^{\dagger}\left[A^{\dagger}-\lambda B^{\dagger}\right]\phi'=0 \tag{37}$$

www.manaraa.com

Subtracting Equation 36 from Equation 37 gives Equation 38 and integrating over phase space (volume, energy, and angles) results in Equation 39.

$$\phi^{\dagger}\left[A'-\lambda' B'\right]\phi'-\phi'\left[A^{\dagger}-\lambda B^{\dagger}\right]\phi^{\dagger}=0 \tag{38}$$

$$\left\langle \phi^{\dagger},\left[A'-\lambda' B'\right]\phi'\right\rangle-\left\langle \phi',\left[A^{\dagger}-\lambda B^{\dagger}\right]\phi^{\dagger}\right\rangle=0 \tag{39}$$

The next step is to distribute all terms and cancel all possible terms (Equations 40-44).

$$\left\langle \phi^{\dagger},\left[(A+dA)-(\lambda+d\lambda)(B+dB)\right]\phi'\right\rangle-\left\langle \phi^{\dagger},\left[A-\lambda B\right]\phi'\right\rangle=0 \tag{40}$$

$$\left\langle \phi^{\dagger},\left[A+dA-\lambda B-\lambda dB-d\lambda B-d\lambda dB-A+\lambda B\right]\phi'\right\rangle=0 \tag{41}$$

$$\left\langle \phi^{\dagger},\left[dA-\lambda dB-d\lambda B-d\lambda dB\right]\phi'\right\rangle=0 \tag{42}$$

$$\left\langle \phi^{\dagger},\left[dA-\lambda dB-d\lambda B-d\lambda dB\right](\phi+d\phi)\right\rangle=0 \tag{43}$$

$$\left\langle \phi^{\dagger},dA\phi-\lambda dB\phi-d\lambda B\phi-d\lambda dB\phi+dAd\phi-\lambda dBd\phi-d\lambda Bd\phi-d\lambda dBd\phi\right\rangle=0 \tag{44}$$

To proceed, the second order terms in Equation 44 can be neglected and the result is Equation 45.

$$\left\langle \phi^{\dagger},\left[dA-\lambda dB-d\lambda B\right]\phi\right\rangle=0 \tag{45}$$

From Equation 45 the yield for reactivity perturbation can be obtained.

$$\frac{d\lambda}{\lambda}=\frac{\left\langle \phi^{\dagger},\left[dA-\lambda dB\right]\phi\right\rangle}{\left\langle \phi^{\dagger},d\lambda B\phi\right\rangle} \tag{46}$$

www.manaraa.com

Taking note that $\lambda = 1/k$ and $d\lambda/\lambda = -dk/k$, the sensitivity to a cross section $(\Sigma(\vec{r}))$ perturbation is given by the following equation. Where $\vec{r}$ represents a point per unit volume $d\vec{r}$ in phase space.[9]

$$S_{\Sigma(\vec{r})} = \frac{dk/k}{d\Sigma(\vec{r})/\Sigma(\vec{r})} = \frac{-\dfrac{\left\langle \phi^{\dagger}, [dA - \lambda dB]\phi \right\rangle}{\left\langle \phi^{\dagger}, [\lambda B]\phi \right\rangle}}{d\Sigma(\vec{r})/\Sigma(\vec{r})} \tag{47}$$

Equation 47 can be simplified into the following form which also includes the operator terms. A more detailed description of the derivation of the sensitivity coefficient is given in reference 12.

$$S_{\Sigma(\vec{r})} = -\frac{\Sigma(\vec{r})}{k} \frac{\int \phi^{\dagger}(\xi) \left[\dfrac{dA[\Sigma(\xi)]}{d\Sigma(\vec{r})} - \dfrac{1}{k} \dfrac{dB[\Sigma(\xi)]}{d\Sigma(\vec{r})} \right] \phi(\xi) d\xi}{\int \phi^{\dagger}(\xi) \left[\dfrac{B[\Sigma(\xi)]}{k^2} \right] \phi(\xi) d\xi} \tag{48}$$

Where ξ denotes the phase space variables ($\vec{r}$, E, $\vec{\Omega}$).

The SAMS module in the TSUNAMI sequence automatically selects each sensitivity parameter that is available for calculation given available cross-section data, for each nuclide present in the system. For every nuclide provided, a sensitivity relative to the total, scatter, capture, fission cross-sections, average number of neutrons released per fission ($\bar{\nu}$) and fission spectrum (χ) is calculated. The cross-section-covariance data file is then used to produce the uncertainty information. The uncertainties produced from the forward and adjoint solutions are propagated through to the final sensitivity, implementing standard error propagation techniques.[18] It should be noted that the

www.manaraa.com

forward and adjoint uncertainties are treated as uncorrelated, while the flux moments are treated as fully correlated.

www.manaraa.com

CHAPTER 5 DIRECT UNCERTAINTY ANALYSIS

5.1 Methodology

Direct uncertainty analysis is used in the benchmark evaluation process. The following chapter shows the direct uncertainty analysis process for four experiments. Three critical benchmark evaluations and one experiment were chosen for the comparison of the direct uncertainty analysis, and the Sensitivity Analysis with First Order Derivatives (SAFOD) developed in Chapter 6. The standard direct uncertainty analysis is performed for all known uncertainties and compared to the evaluations presented in the IHECSBE.[5] This comparison is provided to understand how the evaluators performed the direct uncertainty analysis as well as to validate a newer version of the computer code being used in this work. The benchmark evaluations used earlier versions or different computer codes for their evaluations, also different cross section libraries were used. The following table displays the general characteristics of each experiment used in this work. One case from the three evaluations and two configurations of an unpublished experiment were evaluated here.

www.manaraa.com

Table 1. Benchmark Evaluations Description

LCT023	
Fuel Type	$U(10\%)O_2$
Fuel OD	0.416 cm
Clad Material	Stainless Steel 0X18H9T
Array Configuration	Hexagonal
Pitch	1.4 cm
Approach Variable	Water Height
Number of Fuel Rods	1503
LCT070	
Fuel Type	$U(6.5\%)O_2$
Fuel OD	0.7565 cm
Clad Material	Zr, Nb, Hf
Array Configuration	Hexagonal
Pitch	1.10 cm
Approach Variable	Water Height
Number of Fuel Rods	1081
LCT079	
Fuel Type	$U(4.31\%)O_2$
Fuel OD	1.2649 cm
Clad Material	Zircaloy-4
Array Configuration	Hexagonal
Pitch	2.0 cm
Approach Variable	Number of Fuel Rods
Number of Fuel Rods	253
7uPCX 0.800 cm Pitch	
Fuel Type	$U(6.90\%)O_2$
Fuel OD	0.52578 cm
Clad Material	Aluminum 3003
Array Configuration	Square
Pitch	0.800 cm
Approach Variable	Fuel Rods
Number of Fuel Rods	1197
7uPCX 0.855 cm Pitch	
Fuel Type	$U(6.90\%)O_2$
Fuel OD	0.52578 cm
Clad Material	Aluminum 3003
Array Configuration	Square
Pitch	0.855 cm
Approach Variable	Fuel Rods
Number of Fuel Rods	909

www.manaraa.com

When an experiment is performed, each parameter in the system is only known to a particular certainty. The physical parameters are usually measured and assigned an uncertainty. The material properties can be measured but are sometimes taken from a standard report, providing a range for each nuclide present in the material. The goal of a very detailed uncertainty analysis is to determine how each parameter affects the system and how the parameter uncertainties propagate to the uncertainties in the benchmark k_{eff}.

To start the uncertainty analysis, an inventory of each parameter is made. Table 2 shows a typical listing of parameters; more parameters can be included. Examples of additional parameters are metals present in the system or an absorber material is placed in the moderator.

Table 2. System Parameters

Physical Parameter
Pitch
Fuel Outer Diameter
Clad Outer Diameter
Clad Thickness
Moderator Height
Material Parameter
Fuel Enrichment
Clad Material
Temperature

Once the list of all possible parameters is made, the uncertainty in each parameter is found or estimated. The uncertainty in the physical parameters is determined from manufactured tolerances or from performing a series of measurements. The composition of a material is reported with a range of weight fraction present in the material.

www.manaraa.com

After all of the uncertainties have been compiled and a system model has been developed for a code package, an individual input file is created to perform the calculation for each uncertainty in each parameter. For example, the pitch is reported as pitch ± uncertainty; three input files are created: pitch, pitch + Δpitch, and pitch – Δpitch. Once the calculations have been run with sufficient histories to produce acceptable statistics, the results of the multiplication factor are plotted with the change in parameter. If one standard deviation is evaluated and the result is clearly linear, a least squares line is fit to the data where the slope of that line is the sensitivity of the multiplication factor to the parameter being evaluated. However, in the case in which one standard deviation is not a linear relationship, a second deviation is required to determine if there could still be linear relationship. There are particular cases where a second order or quadratic relationship exists.

Now that each uncertainty has been evaluated for the system, and a corresponding sensitivity, $^{\Delta k}/_{\Delta p}$, has been calculated, the uncertainty in the multiplication factor can be determined. The uncertainty in the multiplication factor is simply the sensitivity previously mentioned multiplied by the original uncertainty in the parameter. The overall uncertainty in the multiplication factor for the whole system is calculated by taking the square root of the sum of the squares of the individual uncertainties also known as sum in quadrature.

The process described above is carried out for the four experiments chosen. Each of the parameters is discussed, and the results of the direct uncertainty analysis are provided.

www.manaraa.com

A standard guide for evaluating uncertainties in a critical benchmark evaluation was developed by the ICSBEP subgroup.[20] This guide was developed to provide a recommended methodology on the treatment of the uncertainties.

Once the perturbations for the direct uncertainty analysis were performed, the multiplication factor was plotted against the change in parameter. A least squares trendline evaluation was performed on the data obtained, and a slope of the data (keff vs. parameter) was determined. That slope is the change in multiplication factor per the change in the perturbed parameter,

$$\frac{\delta k}{\delta P}. \tag{49}$$

From reference 21, the equation of a straight line that is fit to a set of data points is

$$y(x) = y(x \mid a,b) = a + bx. \tag{50}$$

The data consists of a measured value, y_i, an independent variable that is known exactly, x_i, and an uncertainty σ_i, that is associated with the measured value. The following equations are used to determine the parameters a and b for the straight line,

$$S \equiv \sum_{i=0}^{N-1} \frac{1}{\sigma_i^2} \tag{51}$$

$$S_x \equiv \sum_{i=0}^{N-1} \frac{x_i}{\sigma_i^2} \tag{52}$$

www.manaraa.com

$$S_y \equiv \sum_{i=0}^{N-1} \frac{y_i}{\sigma_i^2} \tag{53}$$

$$S_{xx} \equiv \sum_{i=0}^{N-1} \frac{x_i^2}{\sigma_i^2} \tag{54}$$

$$S_{xy} \equiv \sum_{i=0}^{N-1} \frac{x_i y_i}{\sigma_i^2} \tag{55}$$

$$S_y = aS + bS_x \tag{56}$$

$$S_{xy} = aS_x + bS_{xx} \tag{57}$$

$$\Delta \equiv SS_{xx} - (S_x)^2 \tag{58}$$

$$a = \frac{S_{xx}S_y - S_x S_{xy}}{\Delta} \tag{59}$$

$$b = \frac{SS_{xy} - S_x S_y}{\Delta} \tag{60}$$

$$\sigma_a^2 = \frac{S_{xx}}{\Delta} \tag{61}$$

$$\sigma_b^2 = \frac{S}{\Delta} \tag{62}$$

where N is the number of data points. Equation 59 is the y-intercept, and Equation 60 is the slope of the line. Equation 61 is the uncertainly of the calculated value for the y-intercept, and Equation 62 is the uncertainty in the calculated value for the slope. These

www.manaraa.com

equations were implemented to determine the sensitivity to each parameter and the associated uncertainty in the sensitivity.

www.manaraa.com

5.2 LEU-COMP-THERM-023

5.2.1 Experiment Description

The title of this critical experiment is Partially Flooded Uniform Lattices of Rods with U(10%)O_2 Fuel. This set of experiments was performed in 1965-1967 in RRC "Kurchatov Institute."[6] The set of experiments includes uniform hexagonal pitch and square pitched lattices fully flooded with water, hexagonally pitched, and partially flooded lattices. This particular benchmark evaluation consists of six critical experiments where the height of the water in the system is varied to obtain a critical system, and the pitch was constant throughout all six experiments. For simplicity only one of the six cases, case1, is evaluated in this work.

The experiment was performed in a stainless-steel tank that is 15 mm thick, with an inside diameter of 1590 mm and a total height of 2550 mm. The configuration includes two lattice plates to maintain the desired pitch of 1.4 cm.

www.manaraa.com

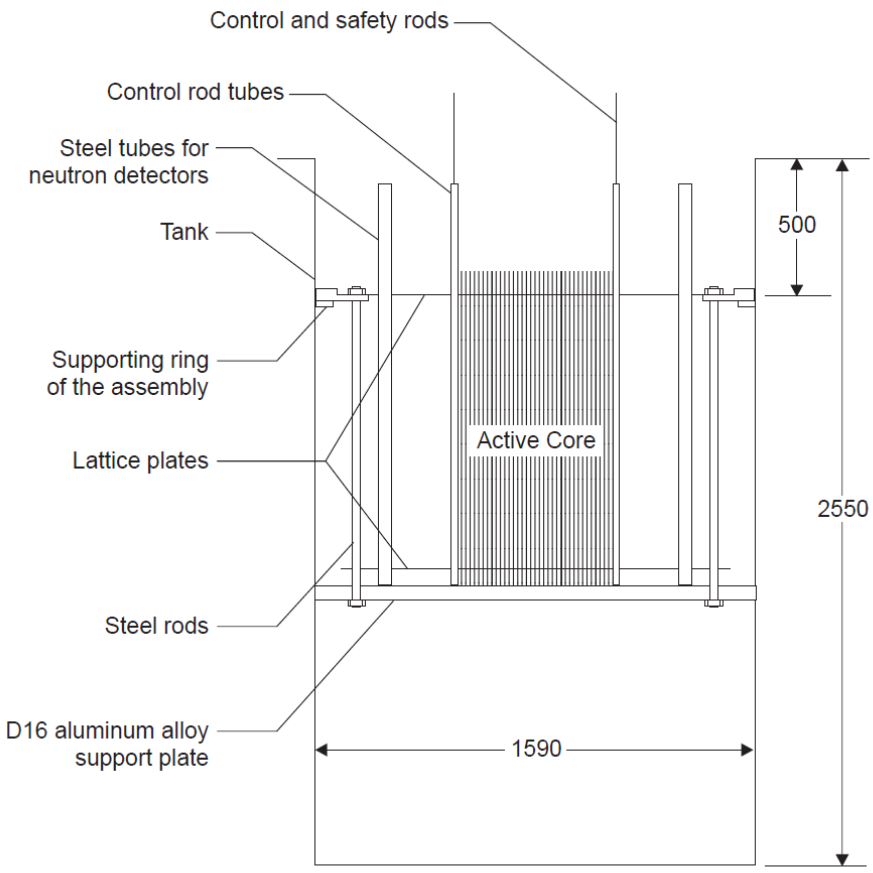

Figure 1. The Placement of Active Core in Tank. (dimensions given in mm)

Figure 1. Cross-Sectional View of LCT023 Core Tank (Fig. 1 from Ref. 6)

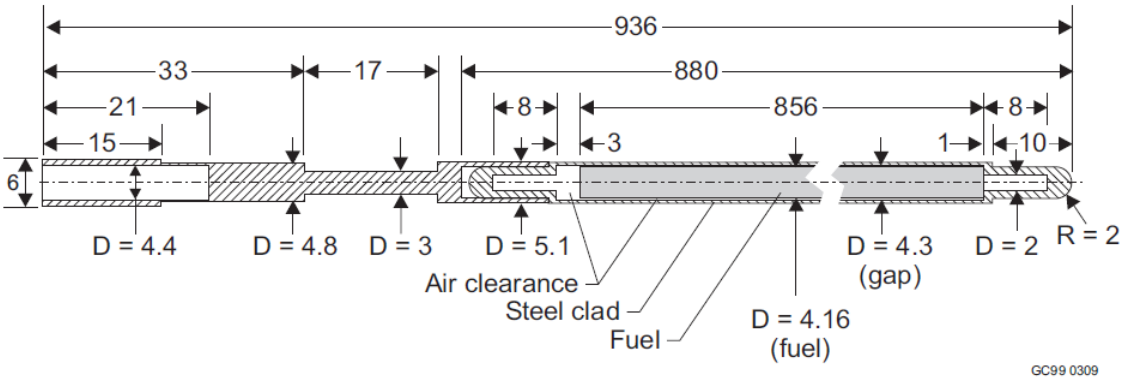

Figure 3. Fuel Rod.
(dimensions given in mm)

Figure 2. Fuel Rod for LCT023 (Fig. 3 from Ref. 6)

www.manaraa.com

Figure 1 displays the cross sectional view of the core layout. Figure 2 displays the details of the fuel rods.

Case 1 was chosen for evaluation. The number of fuel rods present in the system is 1503 and has a critical water height of 22.58 cm. Figure 3 displays the core layout of the experiment for case 1.

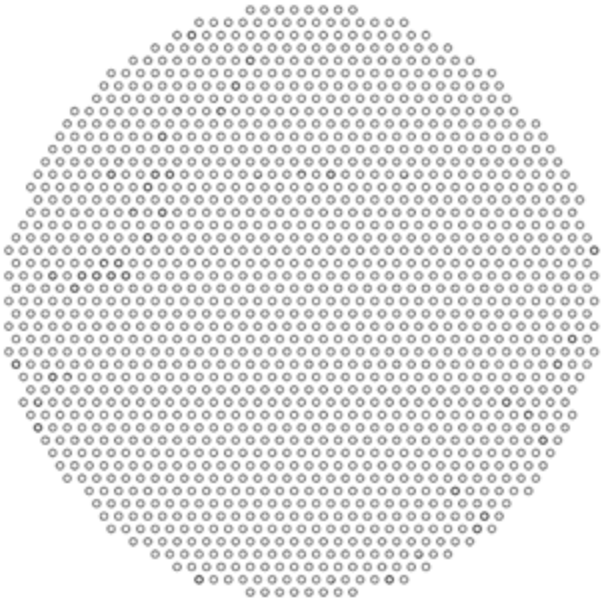

Figure 3. Fuel Rod Design in LCT023 (Ref. 6)

www.manaraa.com

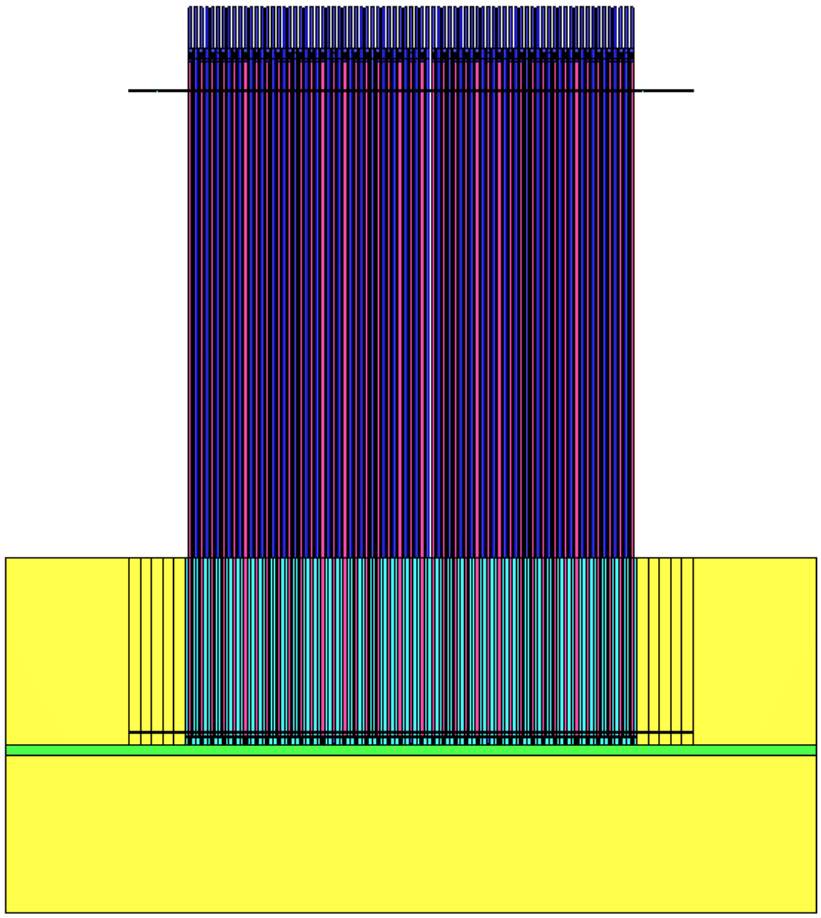

Figure 4. Vertical Section LCT023 (KENO 3D Model)

Figure 4 displays a vertical view of the core. It is important to note that there is a large amount of fuel above the water. The yellow and blue material is water, the pink is fuel and the blue is the cladding material.

www.manaraa.com

5.2.2 Direct Uncertainty Analysis of LCT023

The evaluation contained a well documented uncertainty analysis. The direct uncertainty analysis was repeated to ensure that the model was correct as well as that the method for obtaining the overall uncertainty in the system was understood.

Table 3 lists the uncertainties in each parameter and the corresponding change in the multiplication factor as a result of the change in parameter. The uncertainties are determined from a set of measurements on a physical parameter or material, or determined from scientific judgment.[20]

Table 3. Uncertainty in Parameters in LCT023 (Ref. 6)

Parameter	Uncertainty of Parameter	Δk_{eff}
Pitch of Fuel Rods	± 0.001 cm	± 0.0001
External Diameter of Fuel Rod Clad	± 0.002 cm	± 0.0005
Fuel Pellet Diameter	±0.009 cm	± 0.0009
Clad Mass and Composition	± 4%	± 0.0024
Fuel Mass	$\frac{\pm 1.3\%}{\sqrt{N_{fuel\ rod}}}$	± 0.0003
Enrichment	± 0.1 wt.%	± 0.0023
^{234}U and ^{236}U	±0.04 wt.%	± 0.0005
Experimental Error		±0.0004 - ±0.0020
Total Uncertainty		±0.0036 - ±0.0041

www.manaraa.com

5.2.2 a. Enrichment

The enrichment in the fuel is reported as 9.83 ±0.1 wt.% ^{235}U. The uncertainty in the enrichment was made by changing the number densities of the ^{235}U and ^{238}U in the fuel. Table 4 displays the calculated number densities for the variations in the enrichment. The mass in the system was held constant, while modifying the enrichment.

Table 4. LCT023 Enrichment Variation Number Densities

Enrichment (wt.%)	Nuclide	Number Density (atom/barn-cm)
9.83	^{234}U	1.7635E-05
	^{235}U	2.1577E-03
	^{236}U	1.5300E-05
	^{238}U	1.9510E-02
	O	4.4661E-02
9.63	^{234}U	1.7635E-05
	^{235}U	2.1138E-03
	^{236}U	1.5300E-05
	^{238}U	1.9553E-02
	O	4.4661E-02
10.03	^{234}U	1.7635E-05
	^{235}U	2.2016E-03
	^{236}U	1.5300E-05
	^{238}U	1.9467E-02
	O	4.4661E-02

The number densities were modified for the variations in the weight fractions, and the results from the SCALE 5.1 KENO V.a calculations are displayed in the following plot.

www.manaraa.com

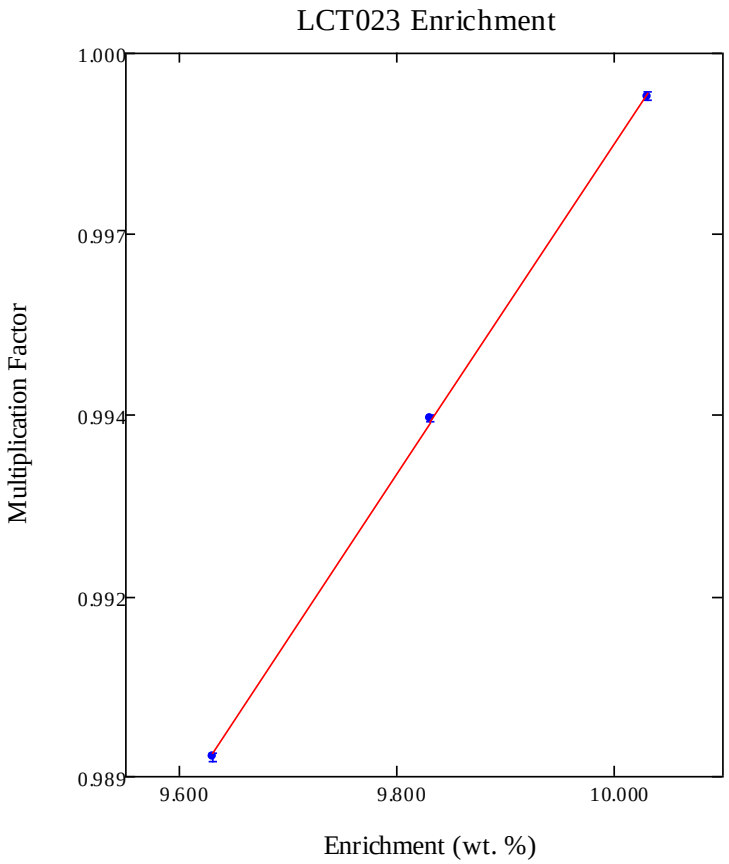

Figure 5. Fuel Enrichment LCT023

Figure 5 displays the change in the in multiplication factor versus the change uranium enrichment. The increase in the amount of uranium-235 in the system increases the multiplication factor. The density of the fuel was held constant.

5.2.2 b. Pitch – Fuel Rod Spacing

The pitch of the holes in the grid plates in the benchmark evaluation was given as 0.7 ±0.005 cm hexagonal lattice. The fuel rod pitch is given as 1.4 cm, indicating that every other fuel rod position in the grid plates was used.

www.manaraa.com

Figure 6 shows the orientation for a hexagonal pitch and the distances between fuel rods.

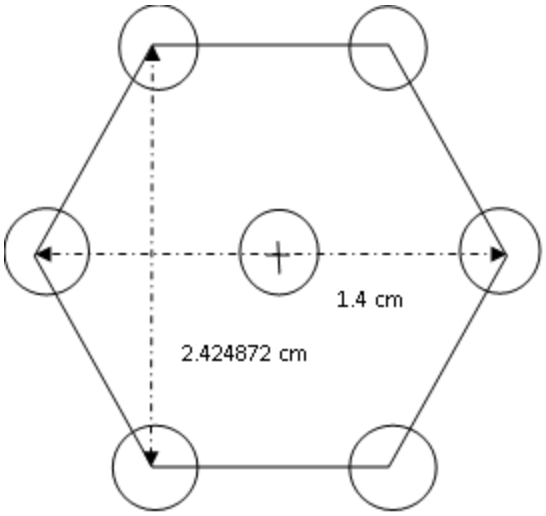

Figure 6. LCT023 Lattice Pitch Drawing

The SCALE 5.1 KENO V.a code has simple geometry inputs: rectangles, cylinders (hemi-cylinders), and spheres.

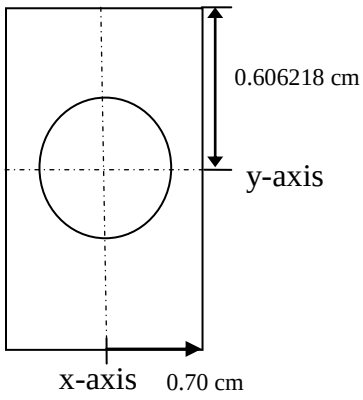

Figure 7. Unit Cell in LCT023

www.manaraa.com

Table 5. Variations in Pitch LCT023

	x-axis	y-axis
Plus 2σ	0.710	0.614878
Plus 1σ	0.705	0.610548
Nominal	0.7	0.606218
Minus 1σ	0.695	0.601888
Minus 2σ	0.690	0.597558

The process used to create a hexagonal lattice in the simple geometry is to create a unit cell shown in Figure 7 and repeat the structure to fill in the lattice.

The rectangle surrounding the fuel rod was modified for the change in the pitch. Figure 7 displays the orientation of the unit cell as defined in the input model. Table 5 displays the variation in the parameters in the input file to translate to a change in overall pitch.

The y- axis is computed as

$$y = \sqrt{\frac{(2 \times X)^2 - X^2}{4}} = \frac{\sqrt{3}}{2} \times \frac{pitch}{2} \tag{63}$$

Figure 8 displays the results of the direct uncertainty analysis.

www.manaraa.com

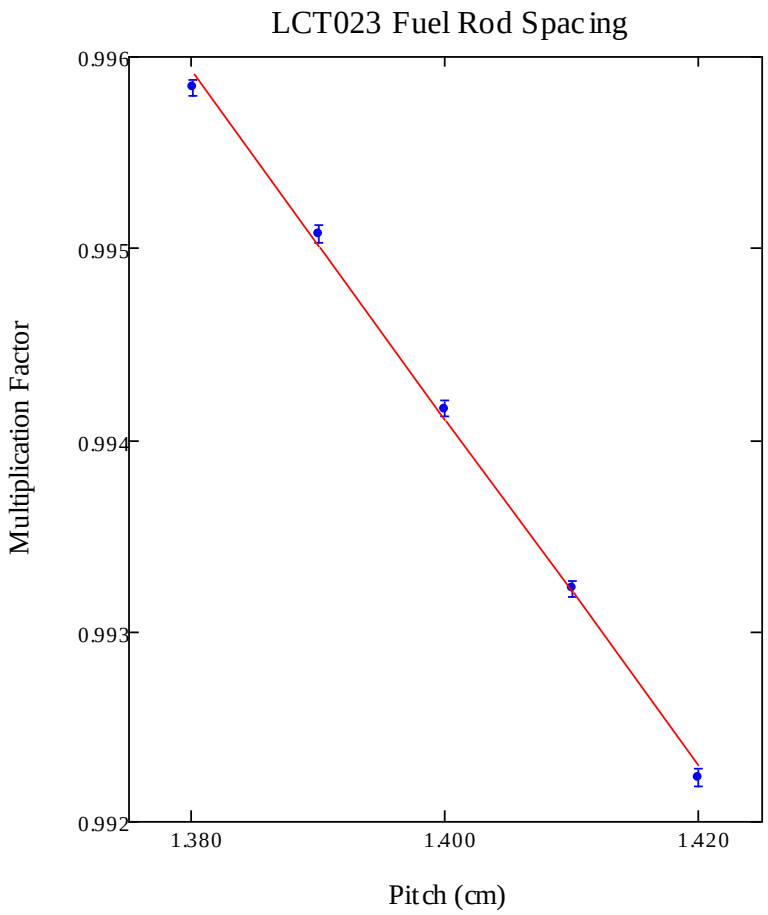

Figure 8. Fuel Rod Spacing LCT023

The error bars shown in Figure 8, as well for all future plots, are one standard deviation in the calculated value of k-effective and are reported by KENO V.a and do not include any other uncertainties. The increase in the pitch decreases the multiplication factor. This variation indicates that the system is overmoderated. The change in the physical parameter changes the amount of water that surrounds the fuel rods and changes the overall diameter of the core (fueled region). Because the system has such a small active core region, compared to the amount of fuel above the critical water height, there could be other effects resulting in the decrease of the multiplication factor, such as the axial leakage.

www.manaraa.com

5.2.2 c. Outer Clad Diameter

The outer diameter of the clad is 0.510 ± 0.002 cm. The clad outer diameter was modified for the uncertainty. The inner clad diameter was modified to maintain the volume of the clad throughout the variations. This results in a sensitivity of the clad outer diameter only. If the inner clad diameter was not modified, the result would be a sensitivity in the outer clad diameter and the cladding thickness.

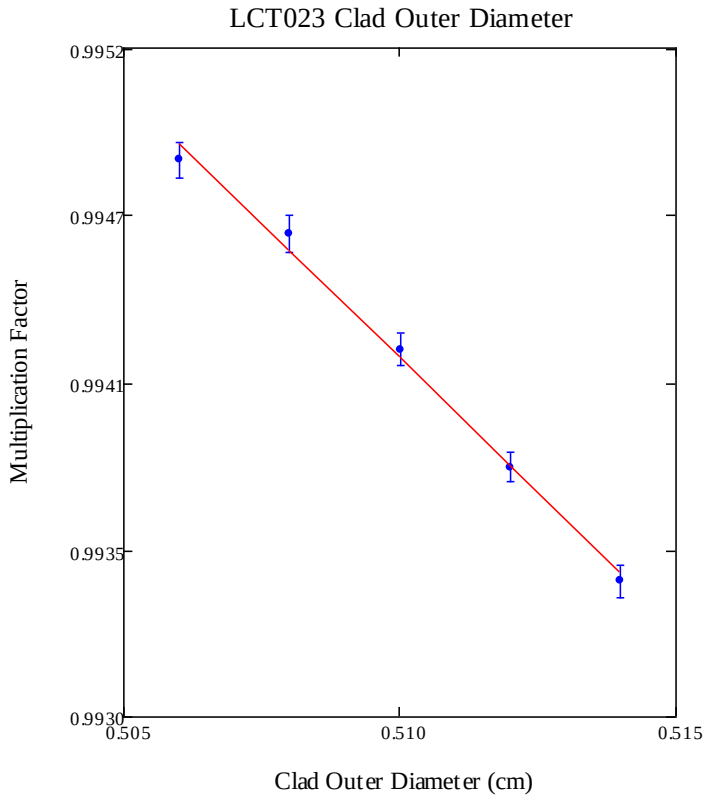

Figure 9. Clad Outer Diameter LCT023

The effect of the uncertainty in the clad outer diameter is significant, because this modification changes the amount of water that surrounds the fuel and the amount of water between the fuel rods. Changing the amount of water around the fuel rods changes

www.manaraa.com

the moderation of the system. From the variation in the pitch, it was expected that the increase in the clad outer diameter would increase the multiplication factor. Figure 9 suggests that the system is undermoderated. This result does not agree with the results from the pitch evaluation, which suggests that the system is overmoderated.

5.2.2 d. Fuel Pellet Diameter

The reported fuel pellet diameter was 0.416 ± 0.009 cm. The length of the fuel region is 85.6 ± 0.2 cm and average mass of 113.48 ± 1.5 g/fuel rod. The density of the fuel is 9.7537 ± 0.2658 g/cm^3, which is a derived value from the measured values (height, radius, mass). When the outer diameter of the fuel is either increased or decreased, it is very important to maintain the mass of the fuel such that the only variation that is made is a volume modification. The change in fuel outer diameter was made as well as changing the fuel number densities to maintain the mass of UO_2 in the system. Table 6 displays the parameters for the variations in the fuel outer diameter.

Table 6. LCT023 Fuel Outer Diameter Perturbation Parameters

Fuel OD (cm)	Volume (cm^3)	Density (g/cm^3)	Mass (g/rod)
0.406	3.52749	10.2401	113.48
0.416	3.70340	9.7537	113.48
0.426	3.88359	9.3011	113.48

www.manaraa.com

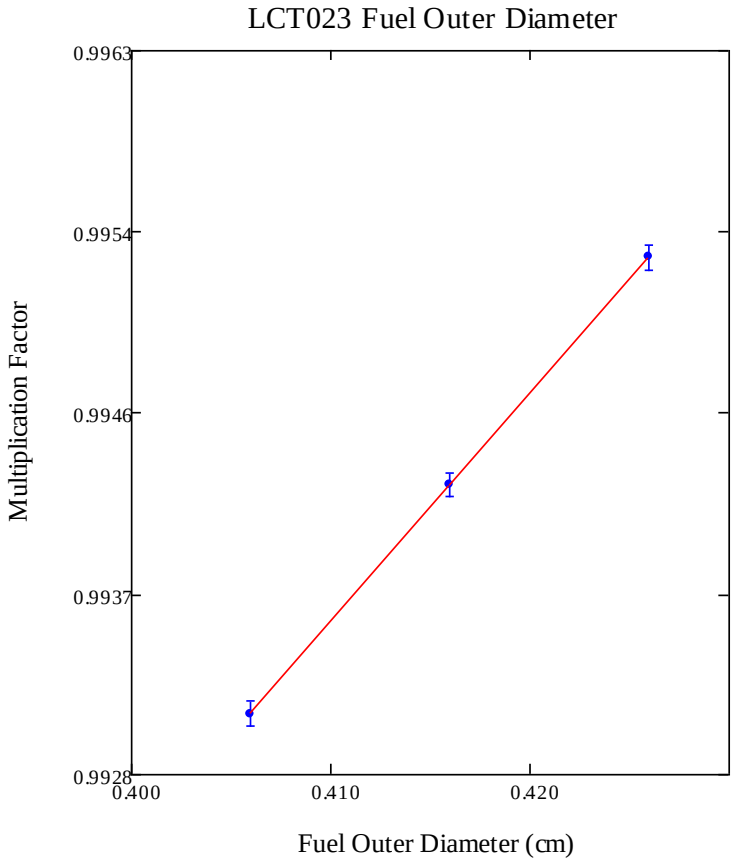

Figure 10. Fuel Outer Diameter LCT023

Figure 10 displays the results of the variation in the fuel outer diameter versus the multiplication factor. The multiplication factor increases with the increase in fuel outer diameter.

5.2.2 e. Fuel Mass

The fuel mass was reported as 113.48 g ±1.3%/$\sqrt{N_{fuel\ rod}}$, where $N_{fuel\ rod}$ is the number of fuel rods present in the given case. In reference 6 the average mass of the fuel rods is 113.48 ± 1.5 g/fuel rod. The variation for the uncertainty in the fuel mass was 113.48 ± 0.038 g/fuel rod (1503 fuel rods). The modification in the input file was made

www.manaraa.com

as a change in fuel number densities, through a UO_2 density change, while the volume of the fuel was held constant. Table 7 displays the variation in the fuel mass while the volume is held constant and the density is modified.

Table 7. LCT023 Fuel Mass Perturbation Parameters

Fuel Mass (g/rod)	Fuel OD (cm)	Volume (cm^3)	Density (g/cm^3)
112.345	0.416	11.63457	9.656137
113.48	0.416	11.63457	9.753692
114.615	0.416	11.63457	9.851246

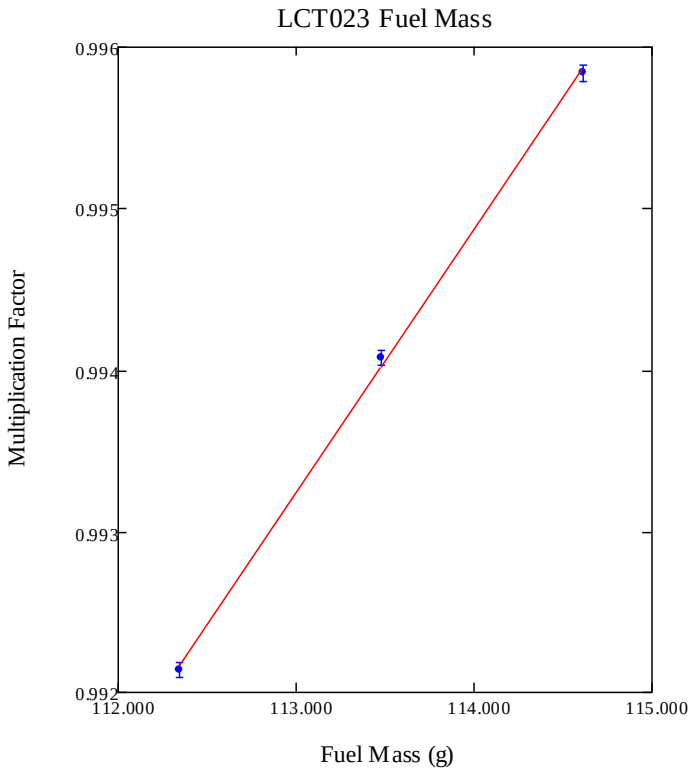

Figure 11. Fuel Rod Mass LCT023

Figure 11 displays the change in the multiplication factor versus the fuel mass. This result is expected, because increasing the fuel mass increases the amount of fissile material in the system.

www.manaraa.com

5.2.2 f. Clad Mass and Composition

The uncertainty in the clad mass and composition was reported as ± 4%. The mass of the clad in one rod was determined from the volume and density parameters provided. The mass of the clad was calculated to be 47.58 g (in one fuel rod). The change in the clad mass was represented as a change in the stainless steel density, while maintaining the same volume. This variation was translated into the input model as a change in the number density of the stainless steel material.

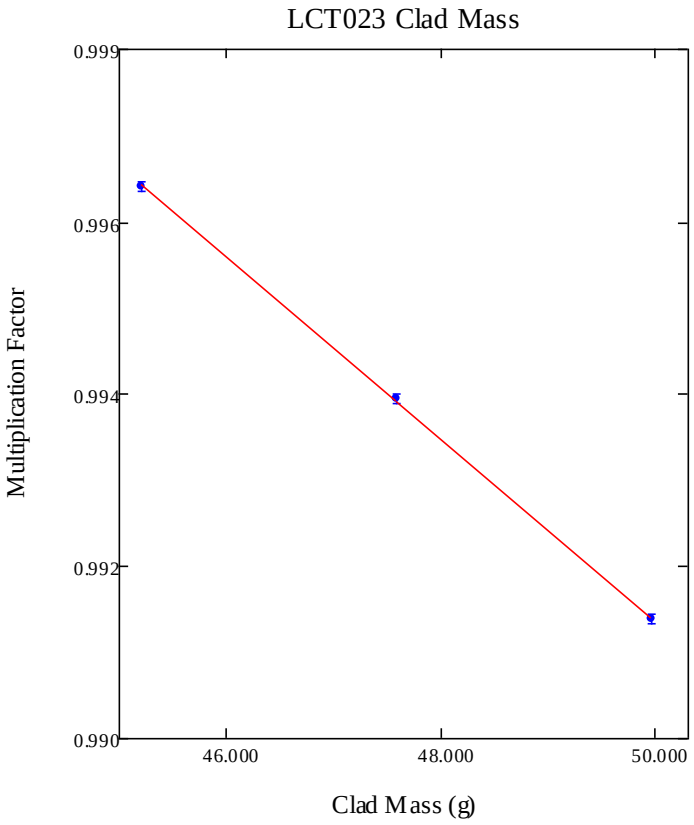

Figure 12. Clad Mass LCT023

The variation in the cladding mass has a large effect on the system because increasing the density increases the amount of absorption in that material.

www.manaraa.com

5.2.3 Direct Uncertainty Analysis for LCT023

Once each parameter was evaluated for the direct uncertainty analysis, the uncertainties in the multiplication factor for each parameter are determined individually and summed in quadrature. The sum represents the total uncertainty in the system.

Table 8 presents each parameter with the uncertainty from the benchmark, the uncertainty from the direct uncertainty analysis and the percent difference between the two values.

The uncertainty in the parameter is the value obtained from the benchmark evaluation, the Δk_{eff} is the change in k_{eff} for the change in that parameter, the sensitivity is the change in k_{eff} divided by the change in that parameter. The direct uncertainty analysis column is the analysis performed above. The sensitivity is the slope of the least squares line fit to the data and the standard deviation is the associated uncertainty with the slope of that line. The percent difference is the benchmark value minus the direct uncertainty analysis all divided by the benchmark value.

www.manaraa.com

Table 8. Sensitivity Analysis for LCT023

	From the Benchmark Evaluation			Direct Uncertainty Analysis		
Parameter	P Value	σ_P Unc.	Δk_{eff}	$\Delta k/\Delta P$	Δk_{eff}	Sensitivity
Pitch	1.4 cm	0.001 cm	0.0001	-0.1130 ± 0.0018 cm^{-1}	0.00011	-0.1591 ± 0.0025
Fuel Rod OD	0.51 cm	0.002 cm	0.0005	-0.1767 ± 0.00868 cm^{-1}	0.00035	-0.0906 ± 0.0044
Fuel OD	0.416 cm	0.009 cm	0.0009	0.1102 ± 0.0041 cm^{-1}	0.00099	0.0461 ± 0.0017
Clad Mass & Comp.	47.581	0.192	0.0024	-0.00110 ± 0.00017	0.00450	-0.0538 ± 0.0002
Fuel Mass	113.48 g	0.034 g	0.0003	0.001955 ± 0.000036 g^{-1}	0.00007	0.2232 ± 0.0057
Enrichment	0.0983	0.001	0.0023	2.400 ± 0.0021	0.0024	0.2373 ± 0.0021
Fuel Density	9.7537 g/cm^3	-	-	0.0223 ± 0.00044 cm^3/g^1	0.00002	0.2183 ± 0.0043
Fuel Height	85.6 cm	-	-	-0.002438 ± 0.000060 cm^{-1}	0.00002	-0.2099 ± 0.0051
Expt. Unc.	-	-	0.0004 to 0.0020	-	0.0004 to 0.0020	-
Sum in Quadrature			0.0036 to 0.0041		0.0035 to 0.0040	

As can be seen in Table 8, the current analysis replicates the Δk_{eff} values in the evaluation adequately. The differences can be attributed to the use of different versions of codes, as well as different versions of cross section libraries.

www.manaraa.com

5.3 LEU-COMP-THERM-070

5.3.1 Experiment Description

The title of the experiment is *VVER PHYSICS EXPERIMENTS: REGULAR HEXAGONAL (1.10-CM PITCH) LATTICES OF LOW-ENRICHED U(6.5 WT.% 235U)O_2 FUEL RODS IN LIGHT WATER AT DIFFERENT CORE CRITICAL DIMENSIONS.* The critical benchmark experiment is 6.5 wt.% ^{235}U, water moderated, hexagonal lattice system.[7]

The experiment was performed with different number of fuel rods and varying critical water heights. Twelve different cases were performed and included in the benchmark evaluation. This work only evaluates one of the twelve cases. Case 6 was chosen due to the large amount of uncertainty information documented in the benchmark evaluation. Case 6 contains 1081 fuel rods and has a critical water height of 97.83 cm, with a pitch of 1.1 cm. The fuel is uranium dioxide with an enrichment of 6.5 wt. % ^{235}U and the cladding material is 98.97 wt.% Zr, 1 wt.% Nb, and 0.03 wt.% Hf with density 6.55 g/cm^3.

www.manaraa.com

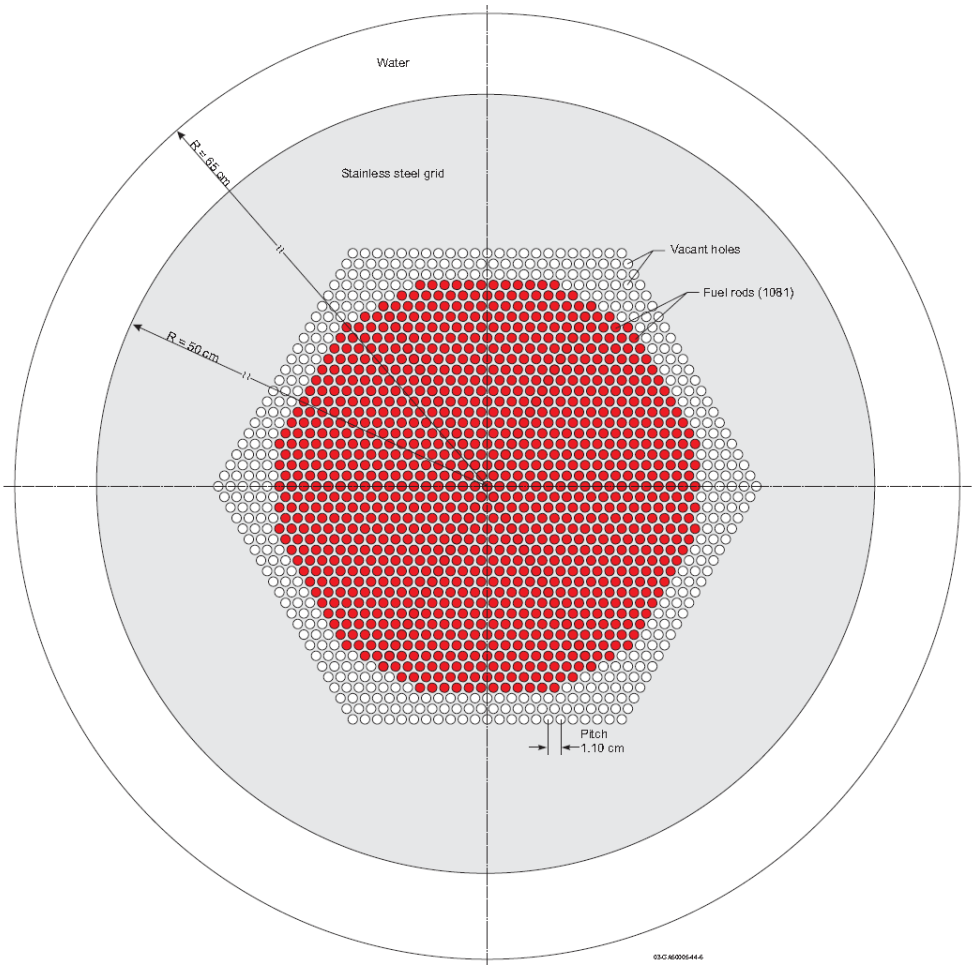

Figure 13. Horizontal Section through Lower Grid Plate, Case 6 LCT070 (Ref. 7)

Figure 13 displays the horizontal cross section view of Case 6. The red dots are the fuel rods, the white dots are water holes, the grey portion is the filled-in grid plate, and the surrounding white is the moderator/reflector. It should be noted that a portion of each fuel rod is above the water. Figure 14 below shows the side cut-through of the system model. As described above, the critical water height is below the top of the fuel rods.

www.manaraa.com

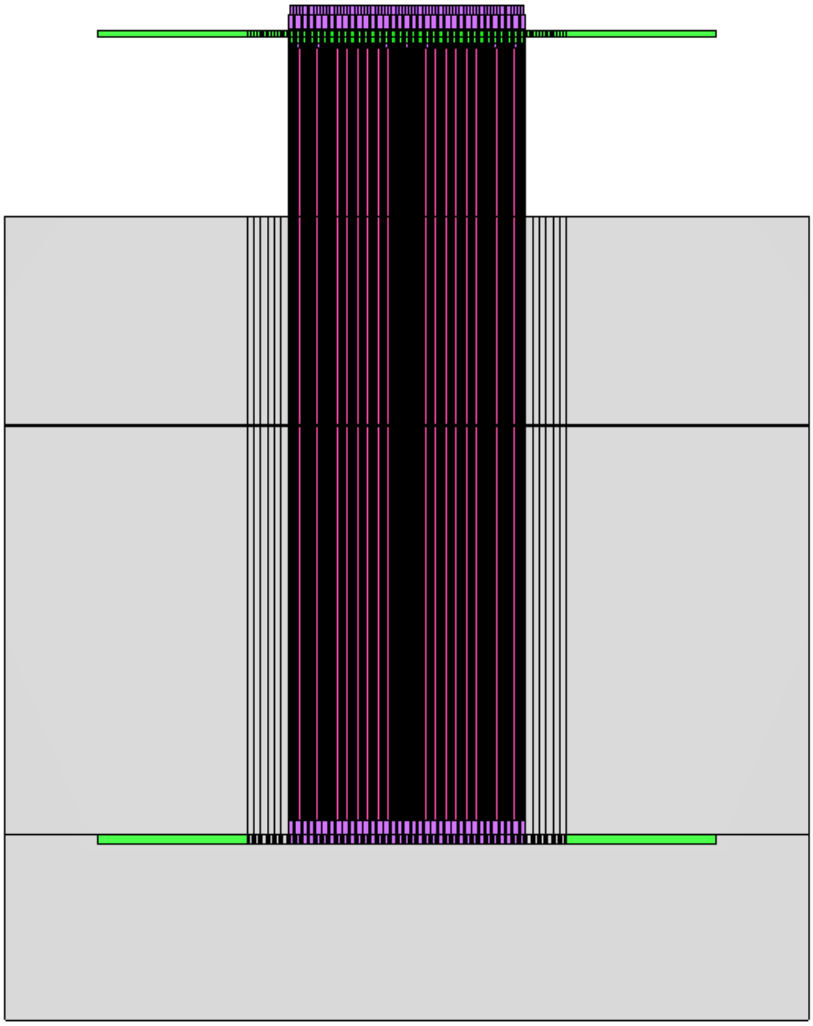

Figure 14. Vertical Section of LCT070 (KENO 3D Model)

5.3.2 Direct Uncertainty Analysis LCT070

A detailed direct uncertainty analysis was performed in the benchmark evaluation and was repeated to ensure correct modeling and uncertainty analysis approach. To have completeness for the results, the same versions of SCALE and the

www.manaraa.com

same cross section libraries were be used for all experiment evaluations performed in this work. Table 9 show the uncertainty table from the LCT070 benchmark evaluation and contains the values for the uncertainties of the various parameters in the system, the sensitivities determined from the direct uncertainty analysis and the result in uncertainty in k_{eff}.

Table 9. Uncertainty and Sensitivities of Parameters in LCT070 (Ref. 7)

Table 6. Effect on k_{eff} of Parameter Standard Uncertainties for the Core Map 6 (Number of Fuel Rods N=1081)

Parameter	Mean Value	σ_{pi}	$\sigma_{keff,i}$ 10^5
^{235}U enrichment (wt.%) [a]	6.5	$0.1/\sqrt{3}$	100
Impurities in U in boron equivalent (μg/g)	1.0	$1.0/\sqrt{3}$	20 [b]
Fuel density (g/cm^3)	10.84	$0.15/\sqrt{1081}$ [c]	2
Temperature (°C)	18	$2/\sqrt{3}$	13
Fuel-pellet diam. (cm) [d]	0.7565	$0.0035/(\sqrt{3}\cdot\sqrt{1081})$ [c]	<1
Central hole diam. (cm) [d]	0.12	$0.08/(\sqrt{3}\cdot\sqrt{1081})$ [c]	<1
Fuel rod clad outer diam. (cm) [e]	0.905	$0.002/(\sqrt{1081})$ [c]	7
Fuel rod spacing (cm)	1.10	$0.032/\sqrt{1081}$ [c]	125
Moderator height (cm)	97.83	$0.10/\sqrt{3}$	3
Combined quadratically $\sigma_{keff,total}$			162

(a) When changing the ^{235}U enrichment, the ^{238}U concentration was changed correspondingly to maintain constant mass of uranium.
(b) This result indicates that the bias on the benchmark-model k_{eff} from impurities in the fuel, estimated as equivalent to 1 μg/g of boron, is $20\cdot10^{-5}\times\sqrt{3}$ or 0.00035.
(c) The parameter p_i standard uncertainty is divided by $\sqrt{N}$, where N=1081 is the number of fuel rods in the core (assuming that uncertainties of individual fuel rods in the core are uncorrelated and the sensitivity coefficient of k_{eff} is the same for all fuel rods).
(d) Fuel mass kept constant.
(e) Clad density kept constant.

The mean value is the value evaluated in the nominal critical benchmark case, σ_{p_i} is the uncertainty in the parameter, either determined from statistical analysis or

www.manaraa.com

from a series of observations, $\sigma_{k_{eff},i}$ is the calculated uncertainty in k_{eff} of the i^{th} parameter, as a result of the direct uncertainty analysis. Equation 64 shows how the parameter $\sigma_{k_{eff},i}$ is calculated, where I_i is the sensitivity and σ_{p_i} is the uncertainty in the parameter.

$$\sigma_{k_{eff},i} = I_i \sigma_{p_i} \tag{64}$$

5.3.2 a. Uranium Enrichment

The uranium enrichment measurement was given as 6.5 ± 0.1 wt. % ^{235}U. The standard uncertainty in the uranium enrichment was evaluated as ± 0.1/√3 wt. %, because the uncertainty is considered a uniform distribution, rather than a normal (Gaussian) distribution (Appendix C). The number densities of ^{235}U and ^{238}U were changed to reflect this uncertainty. It was expected that the increase in enrichment would increase the multiplication factor. The following table contains the number densities for the three enrichments evaluated. The fuel density was held constant throughout the number density variations.

Table 10. LCT070 Number Densities for Uranium Perturbation

wt. % ^{235}U	N_O	N_{U234}	N_{U235}	N_{U238}
6.3	4.8404E-02	1.2298E-05	1.5430E-03	2.2647E-02
6.5	4.8405E-02	1.2298E-05	1.5920E-03	2.2598E-02
6.7	4.8407E-02	1.2298E-05	1.6409E-03	2.2550E-02

www.manaraa.com

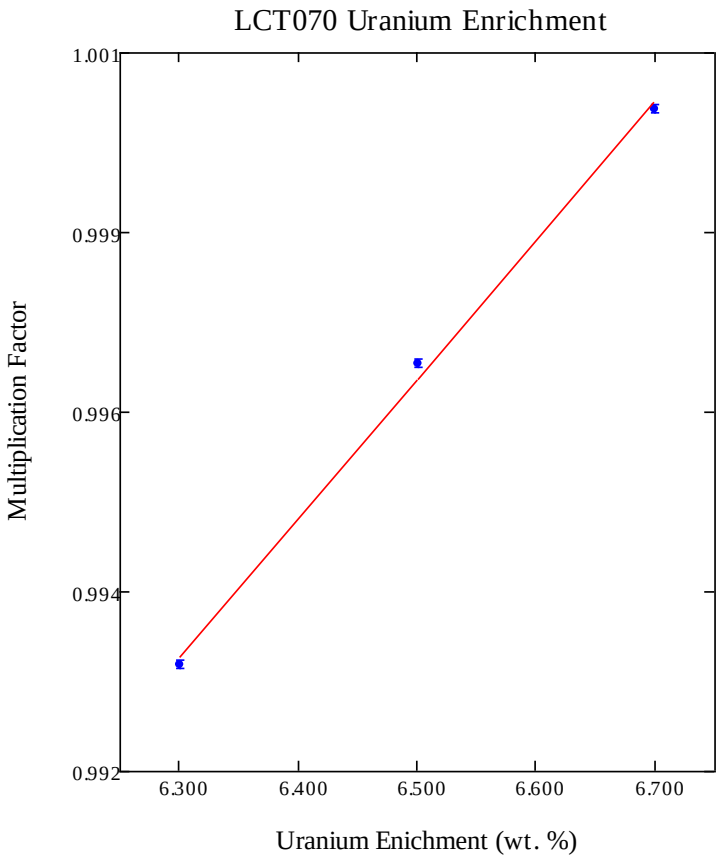

Figure 15. Uranium Enrichment LCT070

Figure 15 displays the change in uranium enrichment (wt. %) versus the change in the multiplication factor. As expected when the uranium enrichment is increased the multiplication factor increases, due to the addition of fissile material.

5.3.2 b. Fuel Rod Spacing (Pitch)

The pitch was given as 1.10 ± 0.032 cm. This small change has a large effect on the system. As the pitch is either increased or decreased, the amount of water that surrounds the fuel rod is changed. The effect of the change in the pitch can be either positive or negative effect. This effect depends on the moderation condition of the

www.manaraa.com

system, either under, optimally or over moderated. From Table 6 in the benchmark evaluation[7], the pitch is the largest sensitivity from the set of parameters.

Figure 16 displays the results of the change in lattice pitch versus the change in the multiplication factor for the LCT070 case 6 experiment.

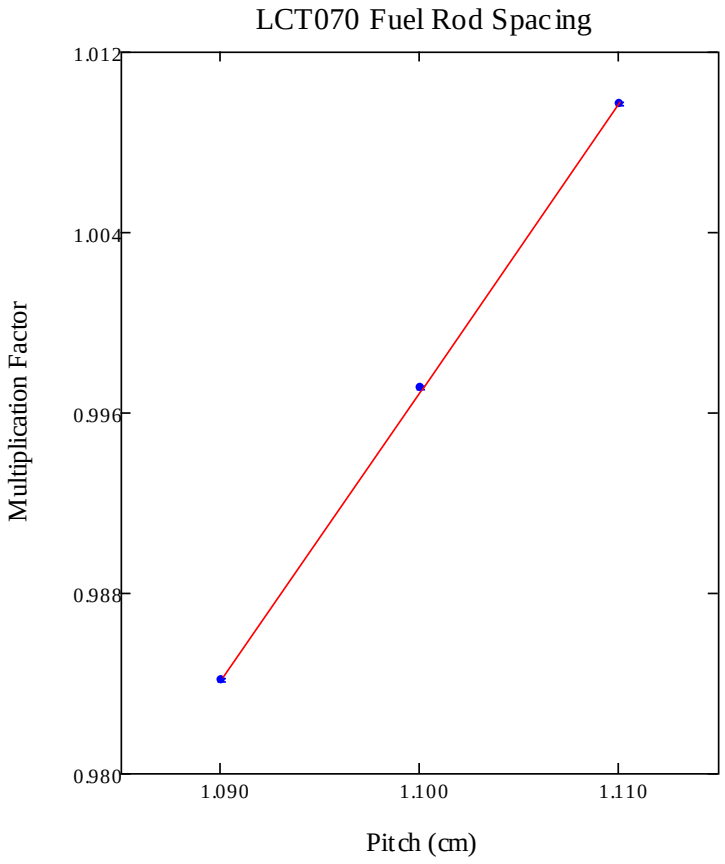

Figure 16. Fuel Rod Spacing LCT070

The increase in the pitch increases the multiplication factor, Figure 16 indicates that the system is undermoderated. The change in the pitch also changes the overall core diameter.

www.manaraa.com

5.3.2 c. Clad Outer Diameter

The clad outer diameter was reported to be 0.905 ±0.002 cm. Variation in the outer diameter of the clad has a similar but opposite effect as uncertainty in the pitch. When the diameter is the smallest, more water surrounds the fuel rods, and when the outer diameter is the largest, less water surrounds the fuel rod, when compared to the nominal case. The cladding material is Zirconium Alloy (Zr, Nb, 0.03 Hf). The impact in the variation of the clad outer diameter depends on the moderation condition of the system. If the system is over moderated then an increase in the outer clad diameter should have a positive impact while for an under moderated system, the impact would be negative.

Figure 17 displays the result of the physical perturbation of the outer diameter of the clad. The plot shows the change in the multiplication factor versus the change in clad outer diameter.

www.manaraa.com

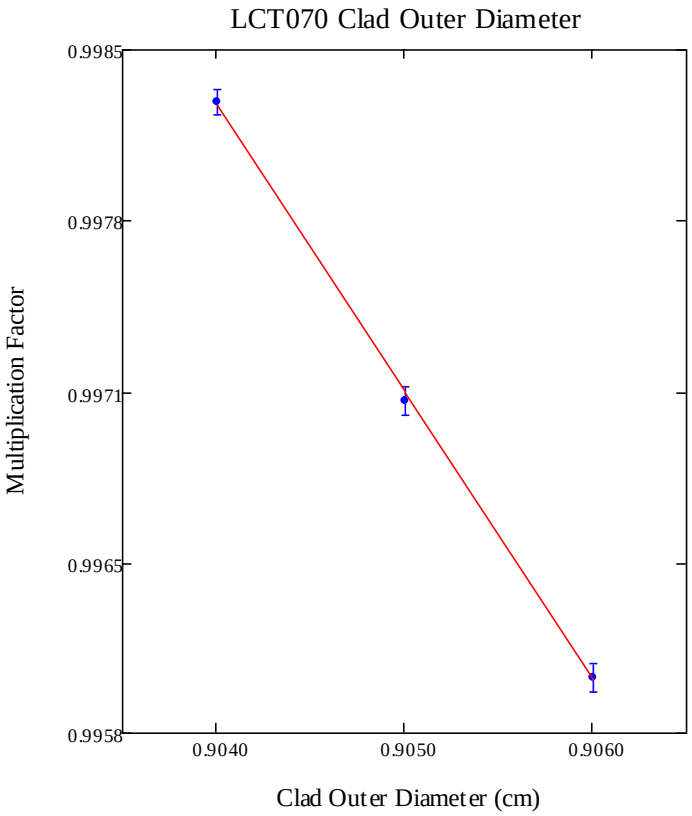

Figure 17. Clad Outer Diameter LCT070

As discussed previously changing the outer diameter of the clad changes in the amount of water that surrounds the fuel rod. This change affects the moderation of the system and as viewed in the above figure reduces the multiplication factor. The figure indicates that the system is undermoderated, as was determined when varying the pitch.

5.3.2 d. Clad Inner Diameter

The clad inner diameter was reported as 0.776 ± 0.004 cm. The standard uncertainty in the clad inner diameter was evaluated as ± 0.004/√3 cm. Changing the inner clad diameter, changes the clad thickness as well as the gap size. Changes in these parameters does not have a large effect on the multiplication factor. The effect of

www.manaraa.com

changing the clad inner diameter does change the absorption in the material, however, because the absorption cross section of the cladding material is small, the effect of increasing or decreasing the clad inner diameter is minimal. The nuclide with the greatest weight fraction present in the cladding material is zirconium, which has a small absorption cross section. Figure 18 displays the multiplication factor versus the change in the clad inner diameter.

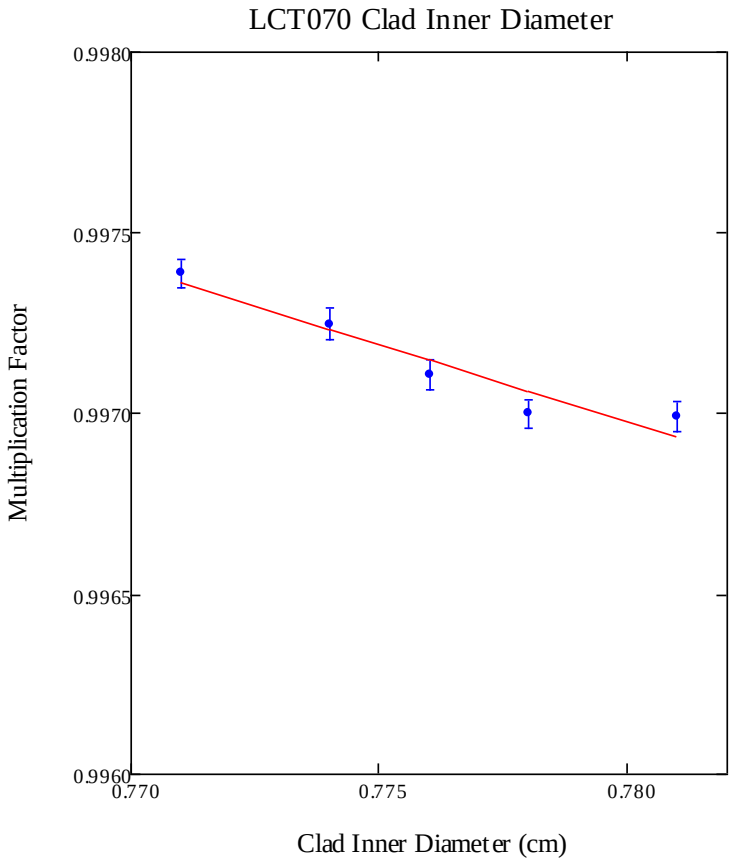

Figure 18. Clad Inner Diameter LCT070

There is a small decrease in multiplication factor for an increase in clad inner diameter. This result differs from what would be expected. The variation in the clad inner diameter does not affect the amount of water in the system, but does change the

www.manaraa.com

total thickness of the cladding and thus changes the absorption in the cladding material. It would be expected that the decrease in the clad inner diameter would increase the multiplication factor because the absorption in the cladding material is decreased; however, the effects of scattering are more prominent.

5.3.2 e. Fuel Outer Diameter

The fuel outer diameter is 0.756 ± 0.01 cm. The outer diameter of the fuel was modified for the uncertainty, and the mass of the fuel was maintained by changing the number densities of the fuel. Figure 19 displays the change in the multiplication factor as a result of the change in fuel outer diameter.

www.manaraa.com

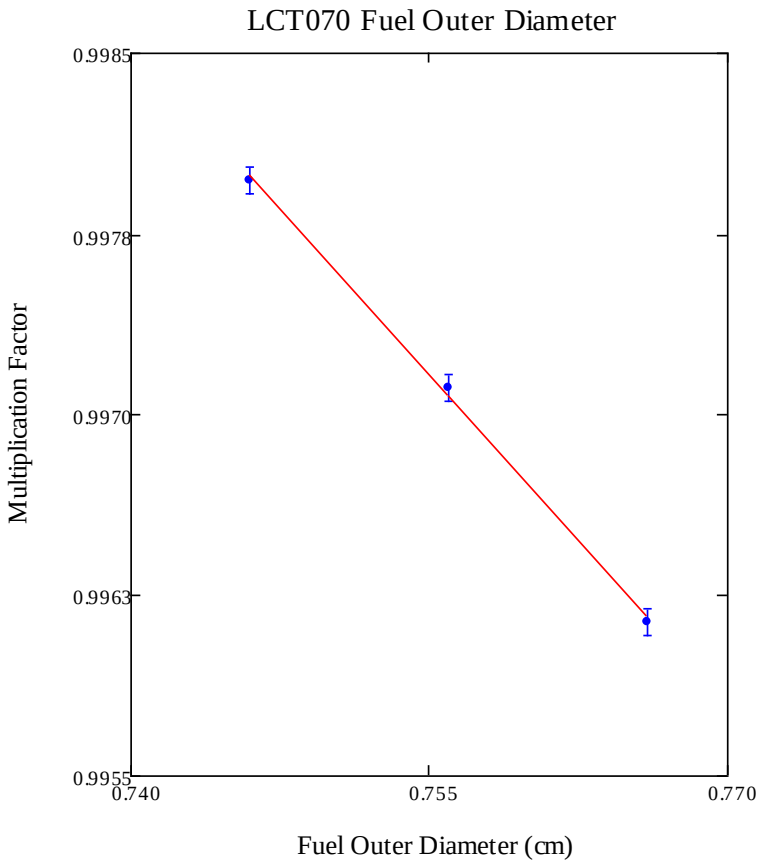

Figure 19. Fuel Outer Diameter LCT070

As the fuel outer diameter is increased the multiplication factor is decreased.

5.3.2 f. Central Hole Diameter

The fuel pellets in the critical experiment are annular with a central hole as shown in Figure 20.

www.manaraa.com

Figure 20. Central Hole Diameter Drawing LCT070

The estimated central hole diameter is 0.12 ± 0.08 cm and the standard uncertainty in the central hole diameter is ±0.08/√3 cm. When the inner diameter of the fuel is modified, the number densities were adjusted to maintain the mass of fuel mass present in the system.

www.manaraa.com

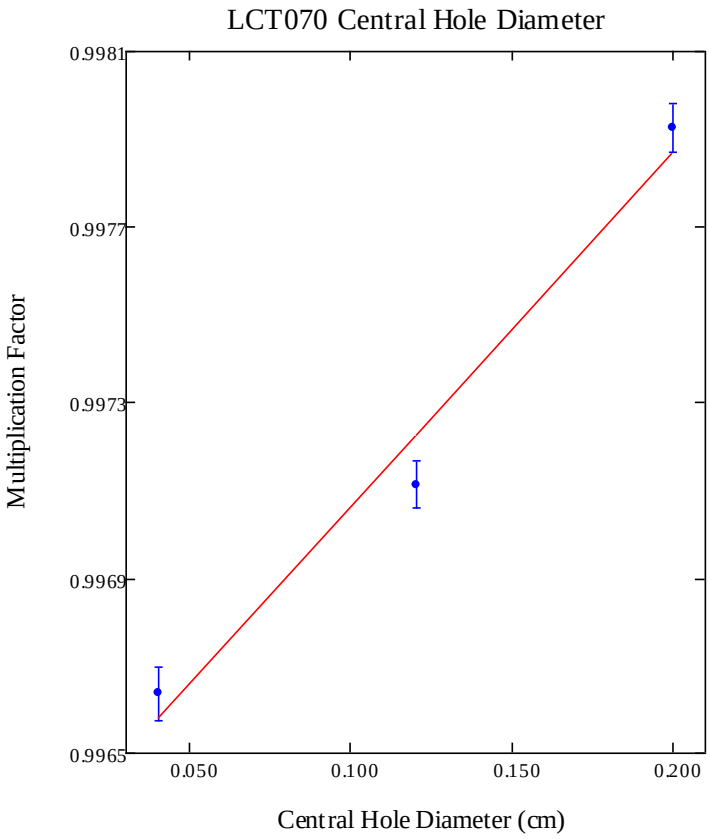

Figure 21. Central Hole Diameter LCT070

Because the fuel mass is maintained, changing the inner diameter of the fuel does not change the amount of the fissile material present in the system and the sensitivity to the inner diameter of the fuel is a function of a volume change. As the inner diameter of the fuel is increased the volume of the fuel is decreased, the multiplication factor increases.

www.manaraa.com

5.3.2 g. Uranium Dioxide Density

The fuel density was given as 10.84 ± 0.15 g/cm^3. The uncertainty in the fuel density was evaluated as a change in the uranium dioxide material number densities. The fuel mass was held constant.

Table 11. Number Densities for Fuel Density Perturbation LCT070

UO_2 Density (g/cm^3)	N_O	N_{U234}	N_{U235}	N_{U238}
10.62	4.7437E-02	1.2052E-05	1.5601E-03	2.2147E-02
10.73	4.7921E-02	1.2175E-05	1.5760E-03	2.2343E-02
10.84	4.8405E-02	1.2298E-05	1.5920E-03	2.2598E-02
10.95	4.8890E-02	1.2421E-05	1.6079E-03	2.2824E-02
11.06	4.7714E-02	1.2123E-05	1.5692E-03	2.2276E-02

www.manaraa.com

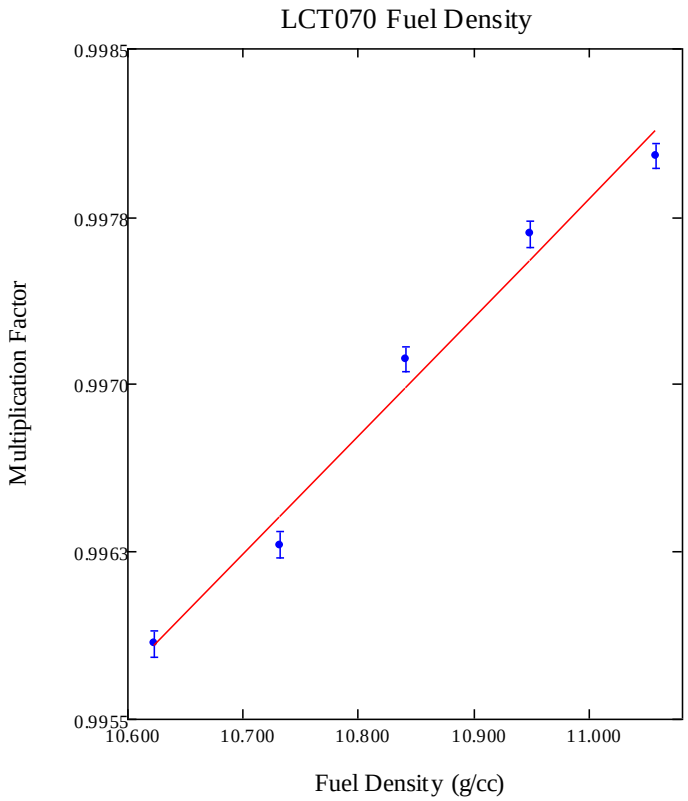

Figure 22. Fuel Density LCT070

The increase in the fuel density increases the multiplication factor.

5.3.2 h. Fissile Column Height

Reference 7 Figure 2 gives the fissile height as 125.0 ± 0.5 cm. Assuming a uniform distribution, the uncertainty in the fissile column height is ± 0.5/√3 cm. The height of the fuel was modified to reflect the uncertainty in the fissile height. The variation in the data is minimal and has a small sensitivity.

www.manaraa.com

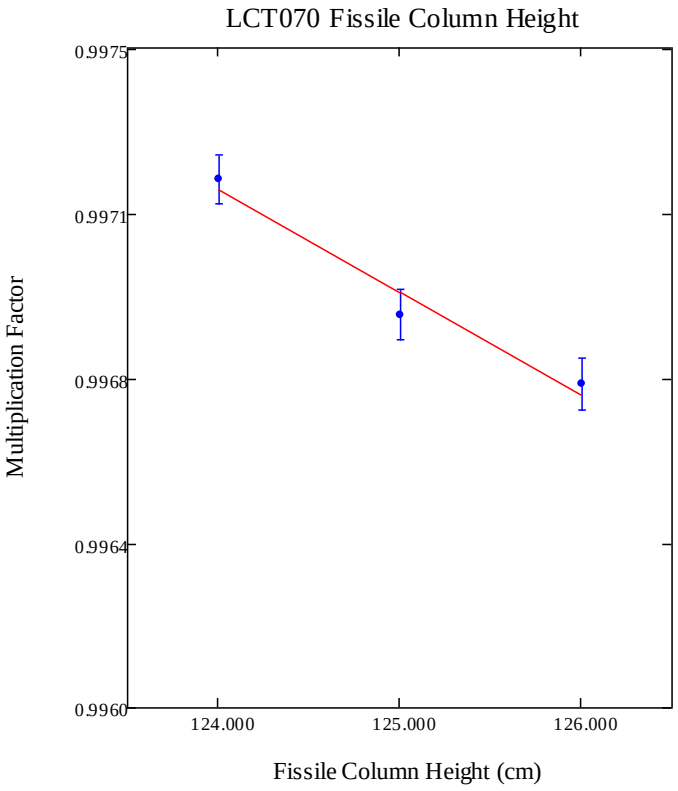

Figure 23. Fissile Column Height LCT070

As expected, due to the moderator height being much less than the fuel height, there is a minimal moderation effect of a higher fuel region. The fuel height was modified while the mass of the fuel was maintained. The number densities of the input files were modified to maintain the mass.

5.3.2 i. System Temperature

The temperature was reported to be 18 ± 2 °C. The uncertainty in the temperature was evaluated for ± 2/√3 °C. The system temperature was modified in the input file for all materials as well as the density of the moderator. The change in

www.manaraa.com

temperature has the largest effect on the water in the system as opposed to other materials present in the system.

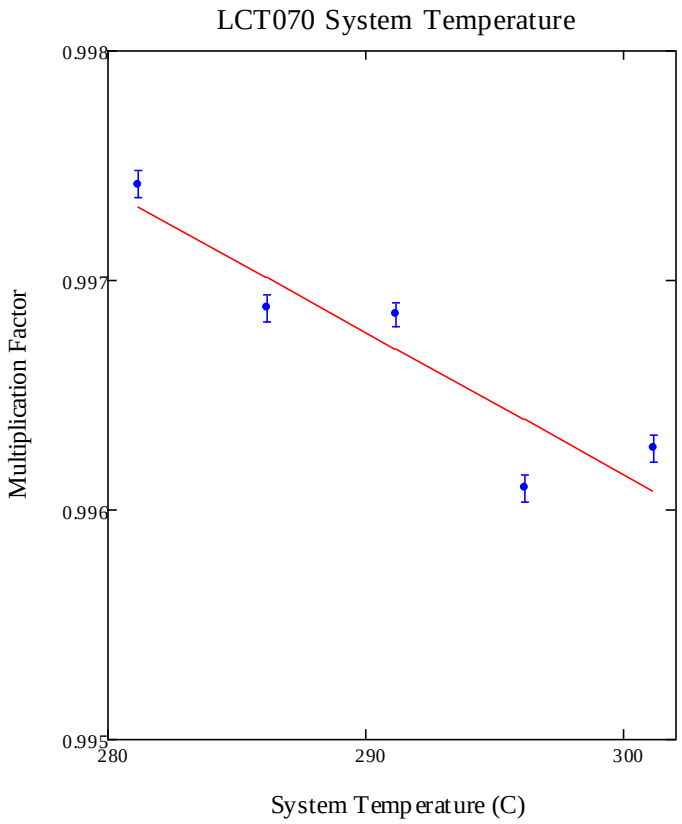

Figure 24. System Temperature LCT070

As expected the multiplication factor decreases with increasing temperature. As the temperature increases, the density of the moderator decreases and results in an increase in resonance absorption; therefore decreasing the multiplication factor.[16]

5.3.3 Direct Uncertainty Analysis LCT070

Table 12 contains the results of the direct uncertainty analysis performed for each of the parameters listed.

www.manaraa.com

Table 12. Results for Direct Uncertainty Analysis LCT070 case 6

	From the Benchmark Evaluation			Direct Uncertainty Analysis		
Parameter	P Value	σ_P Uncertainty	Δk_{eff} x10^5	$\Delta k/\Delta P$	Δk_{eff} x10^5	Sensitivity
Enrichment	0.065	0.00058	100	1.7139 ± 0.00019	101	0.11261 ± 0.00019
Pitch	1.1 cm	0.00097 cm	125	1.2772 ± 0.0042 cm^{-1}	124	1.3995 ± 0.0042
Fuel OD	0.7565 cm	0.000061 cm	<1	-0.0918 ± 0.0040 cm^{-1}	<1	-0.05859 ± 0.00403
Fuel Height	125.0 cm	0.29 cm	-	-0.000233 ± 0.000040 cm^{-1}	7*	-0.02906 ± 0.00004
Fuel Density	10.84 g/cm^{-3}	0.0046 g/cm^{-3}	2	0.00593 ± 0.00037 cm^3g^{-1}	3	0.0640 ± 0.0004
Clad OD	0.905 cm	0.000061 cm	7	-1.1390 ± 0.0378 cm^{-1}	7	-1.0269 ± 0.0378
Temp.	291 K	1.15 K	13	-0.0000647 ± 0.0000037 K^{-1}	7	-0.01889 ± 0.0000037
Clad ID	0.776 cm	0.0023 cm	-	-0.1180 ± 0.0015 cm^{-1}	27*	-0.0918 ± 0.0148
Fuel ID	0.12 cm	0.0014	<1	0.00814 ± 0.00051 cm^{-1}	1	0.000973 ± 0.00051
Sum in Quadrature			162		160	

*The Δk_{eff} were not included in the sum because they were not included in the benchmark analysis.

The results shown in the table above are for the LCT070 direct uncertainty analysis compare well to the results documented in the benchmark evaluation. The fissile column height and the clad inner diameter (clad thickness) were not included in the benchmark evaluation, however these are two parameters can have an effect on the system and were added to the direct uncertainty evaluation.

www.manaraa.com

5.4 LEU-COMP-THERM-079 BUCCX

5.4.1 Experiment Description

"The Burnup Credit Critical Experiment (BUCCX) was designed to investigate the effect of fission product materials on critical systems (LCT079 NEA/NSC/DOC/(95)03/VI)."[8] The experiment consists of 4.31 wt. % UO_2 with rhodium foils placed between the fuel pellets in some of the fuel rods. Ten different configurations were performed. Two sets of the experiments were performed with two different pitches. Four of the ten configurations contain no rhodium foils in the fuel. The remaining six configurations contain rhodium foils in various fuel rods, with three different rhodium foil thicknesses. The experiments were performed in 2002 at Sandia National Laboratories in the Sandia Pulsed Reactor Facility. Figure 25 shows the experimental setup.

www.manaraa.com

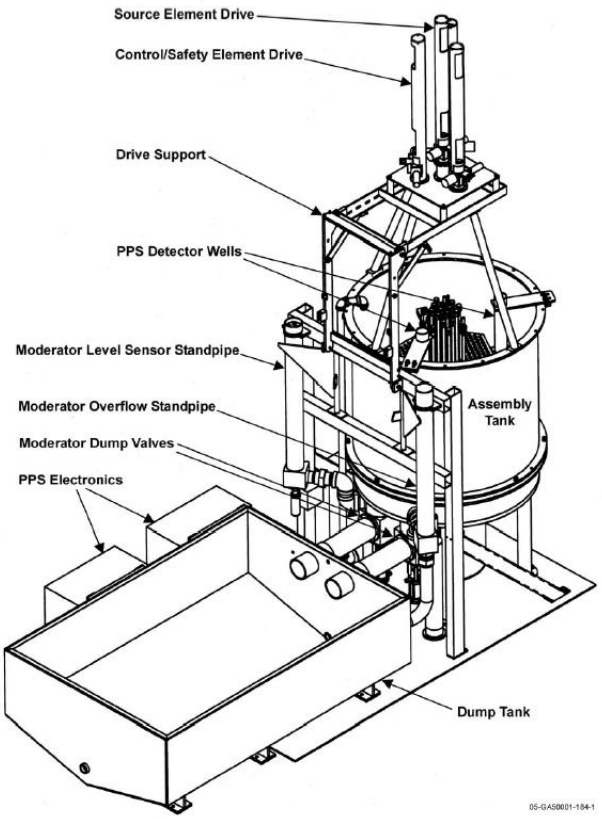

Figure 25. Experimental Setup for BUCCX (Ref. 8)

Figure 25 displays the experiment setup for the BUCCX experiment. The figure includes the core tank, external experiment equipment and the dump tank.

5.4.2 Direct Uncertainty Analysis LCT079

The LCT079 benchmark evaluation contains a very detailed uncertainty analysis. Table 13 displays the uncertainty in each parameter, the sensitivity for each parameter and the results of the evaluator's uncertainty analysis.

www.manaraa.com

Table 13. Uncertainty Analysis LCT079 2.0 cm Pitch (Ref. 8)

Table 17. Results of the Uncertainty Analysis for the Experiments with 2.0 cm Pitch.

Uncertainty Source	Type	1-σ Uncertainty in Source	k_{eff} Sensitivity to Variation[a]	1-σ k_{eff} Uncertainty
Pitch	B[b]	0.00186 cm	0.3980 ± 0.0006 cm^{-1}	0.00074
Clad OD	B	0.00293 cm	-0.419 ± 0.002 cm^{-1}	0.00123
Clad Thickness	B	0.00293 cm	-0.110 ± 0.002 cm^{-1}	0.00032
Fuel OD	A	0.0025 cm	-0.032 ± 0.001 cm^{-1}	0.00008
Upper Reflector	A	2 mm	0.000001 ± 0.000003 mm^{-1}	0.00000
Foil Diameter [c]	B	0.00440 cm	-0.0149 ± 0.0038 cm^{-1}	0.00007
Fuel Mass per Element[d]	A	0.011 cm	0.00228 ± 0.00058 cm^{-1}	0.00003
Fuel Enrichment	A	0.00013[e]	3.447 ± 0.064	0.00045
Uranium Mass Fraction	A	0.00261	-0.111 ± 0.003	0.00029
Clad Composition	B	0.577 c.u.[f]	-0.00051 ± 0.00004 $c.u.^{-1}$	0.00029
Aluminum Composition	B	0.577 c.u.	-0.00028 ± 0.00004 $c.u.^{-1}$	0.00016
Source Composition	B	0.577 c.u.	-0.000062 ± 0.000025 $c.u.^{-1}$	0.00004
Rhodium Composition [g]	A	1 c.u.	-0.000023 ± 0.000016 $c.u.^{-1}$	0.00002
Water Composition	A	1 c.u.	-0.000087 ± 0.000027 $c.u.^{-1}$	0.00009
Temperature	A	1 K	-0.0000788 ± 0.0000005 K^{-1}	0.00008
Sum in Quadrature				0.00161

(a) The sensitivity analysis was done with the code KENO V.a using the 238-group ENDF/B-V cross section set from SCALE4.4a. Also listed with the sensitivity is a 1-σ uncertainty due to the stochastic uncertainties contributed by the Monte Carlo calculations done for the sensitivity studies.

(b) The uncertainty "type" is as defined in the *ICSBEP Guide to the Expression of Uncertainties*.

(c) The value listed for the sensitivity to the foil diameter uncertainty is the value for the experiments with 100 micron foils, which gave the largest effect of the three foil thicknesses.

(d) The fuel mass per element was varied by changing the length of the fuel column.

(e) The uncertainty in the fuel enrichment is given as mass fraction rather than the more usual weight percent.

(f) The uncertainty for material compositions is given in "composition units" (c.u.) as defined in the text.

(g) The value listed for the uncertainty contribution due to the rhodium composition is the peak value for all experiments with 2.0 cm pitch which occurred for the experiment with 25 micron foils.

www.manaraa.com

5.4.2 a. Fuel Enrichment

The enrichment of the fuel is 4.306 ± 0.013 wt. % ^{235}U. The variation in the enrichment was from 4.267% to 4.345 %, giving coverage over three standard deviations. The number densities for ^{235}U and ^{238}U were modified for the change in uranium. Figure 26 displays the variation in the multiplication for the variation in the uranium enrichment. The total U mass was maintained during this analysis.

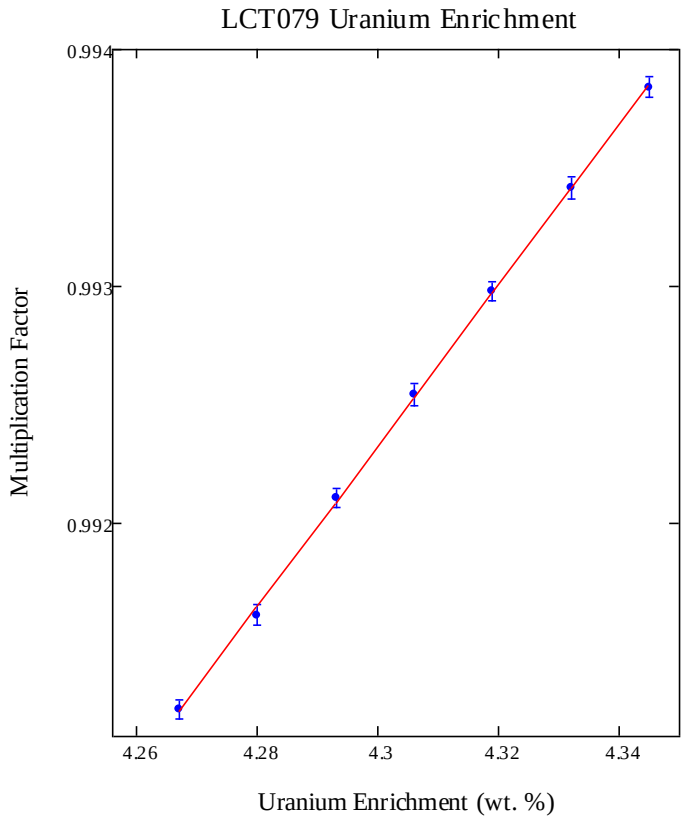

Figure 26. Uranium Enrichment LCT079

The result shown in Figure 26 is as expected; the increase in enrichment increases the multiplication factor.

www.manaraa.com

5.4.2 b. Pitch

The LCT079 experiments consist of two different pitches, 2.0 cm and 2.8 cm. Case 1 (2.0 cm pitch without rhodium foils) was evaluated in this work. This case does not include rhodium foils and has a 2.0 cm pitch. The measured pitch is 2.0 cm ± 0.00186 cm. The pitch was modified in the input model for a larger variation than provided in the uncertainty. The values for the evaluation of the pitch were 1.90 cm, 1.95 cm, 2.00 cm, 2.05 cm, and 2.10 cm.

The following figure displays the change in pitch versus the change in multiplication factor. As the pitch is increased, the spacing between fuel rods is increased; increasing the amount of water that surrounds each rod.

www.manaraa.com

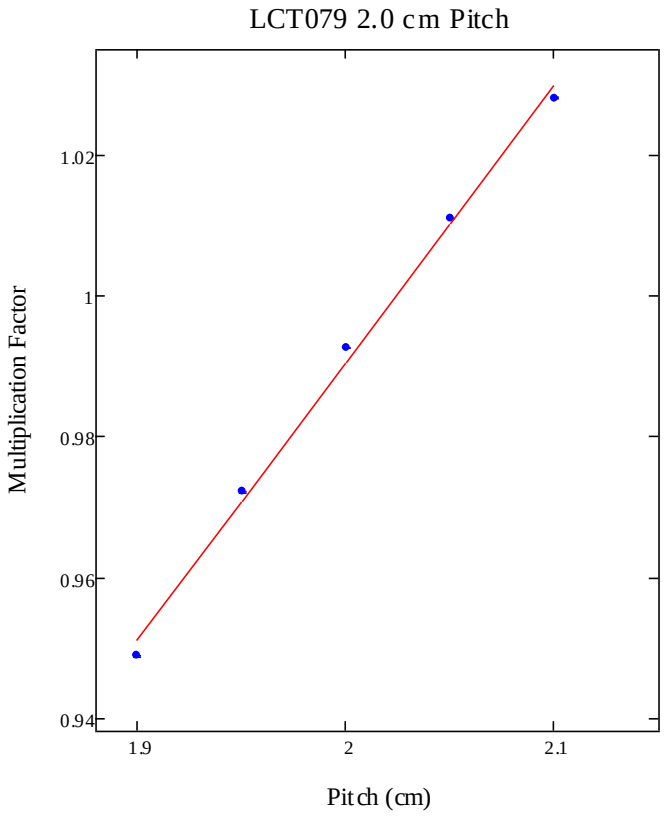

Figure 27. 2.0 cm Pitch LCT079

The increase in the pitch increases the multiplication factor, this suggests that the system is undermoderated.

5.4.2 c. Clad Outer Diameter

The outer diameter of the clad for the fuel rods is 1.38180 ± 0.00293 cm. The outer diameter of the cladding was modified to reflect the measured uncertainty. Figure 28 displays the change in the clad outer diameter versus the change in multiplication factor. As the outer diameter is increased, the amount of water that surrounds the fuel rods is decreased.

www.manaraa.com

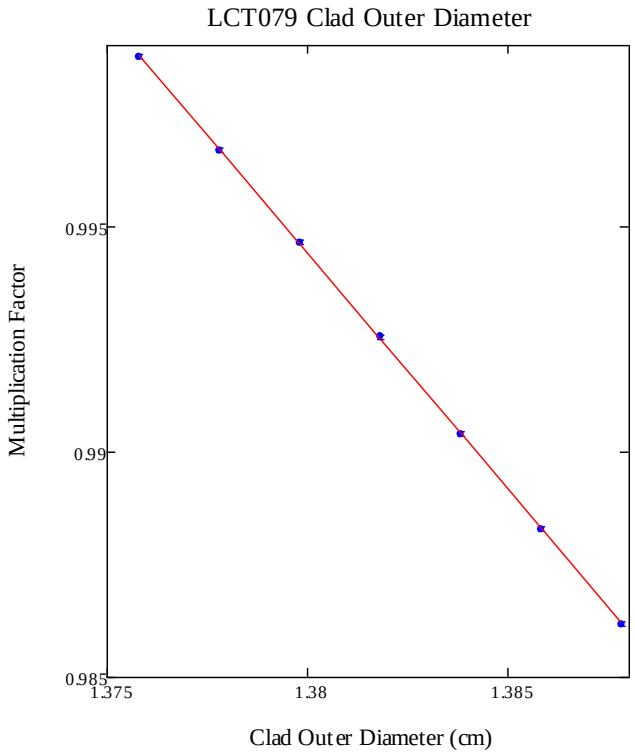

Figure 28. Outer Clad Diameter LCT079

The increase in the clad outer diameter decreases the multiplication factor. This result also suggests that the system is undermoderated, which is in agreement with the variation in the pitch.

5.4.2 d. Clad Thickness

The reported value for the clad thickness is 0.08939 ± 0.00293 cm. The clad thickness was modified by changing the inner diameter of the cladding material.

www.manaraa.com

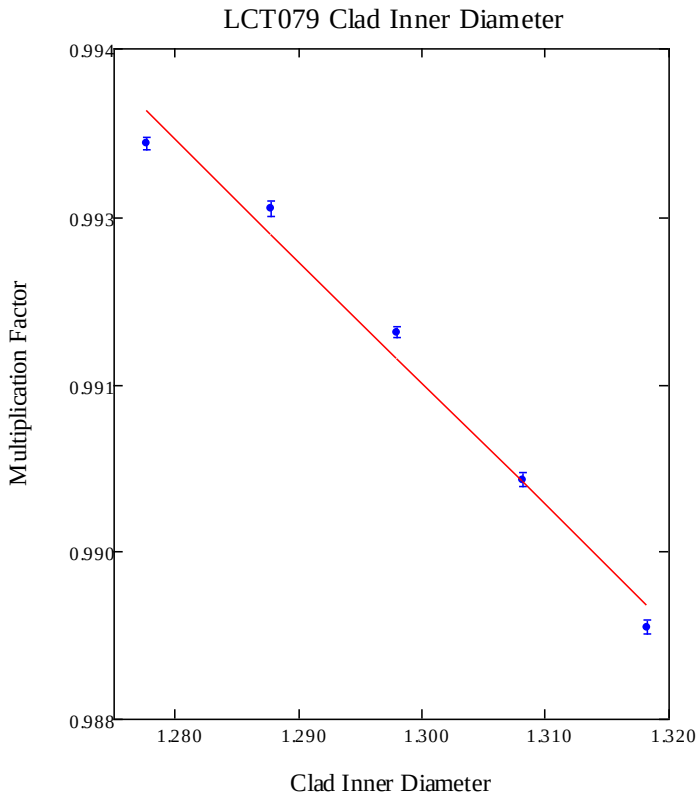

Figure 29. Clad Inner Diameter LCT079

Figure 29 displays the multiplication factor versus the change in the clad inner diameter. The change in the clad thickness is very small and has almost no effect on the system. The change that is seen in the variation in the multiplication factor is from increasing the thickness of the material.

5.4.2 e. Fuel Outer Diameter

The outer diameter of the fuel is 1.2649 ± 0.0025 cm. The fuel pellet outer diameter was modified to reflect the uncertainty. The fuel mass loading was maintained throughout the variations by changing the fuel density. The outer diameter of the fuel

www.manaraa.com

was modified as well as the uranium dioxide number densities. Table 14 below provides the parameters for each variation.

Table 14. LCT079 Fuel Outer Diameter Number Densities

Fuel Rod Diameter		
Diameter (cm)	Number Densities (atom/barn-cm)	
1.2878	N_{234}	5.3953E-06
	N_{235}	1.0515E-03
	N_{236}	5.3495E-06
	N_{238}	2.3062E-02
	N_O	4.8249E-02
1.2802	N_{234}	5.3300E-06
	N_{235}	1.0388E-03
	N_{236}	5.2847E-06
	N_{238}	2.2783E-02
	N_O	4.7665E-02
1.2725	N_{234}	5.2656E-06
	N_{235}	1.0262E-03
	N_{236}	5.2209E-06
	N_{238}	2.2508E-02
	N_O	4.7089E-02
1.2649	N_{234}	5.2022E-06
	N_{235}	1.0139E-03
	N_{236}	5.1581E-06
	N_{238}	2.2237E-02
	N_O	4.6522E-02
1.2573	N_{234}	5.1404E-06
	N_{235}	1.0018E-03
	N_{236}	5.0967E-06
	N_{238}	2.1972E-02
	N_O	4.5969E-02
1.2497	N_{234}	5.0790E-06
	N_{235}	9.8985E-04
	N_{236}	5.0359E-06
	N_{238}	2.1710E-02
	N_O	4.5420E-02
1.2421	N_{234}	5.0191E-06
	N_{235}	9.7819E-04
	N_{236}	4.9765E-06
	N_{238}	2.1454E-02
	N_O	4.4885E-02

www.manaraa.com

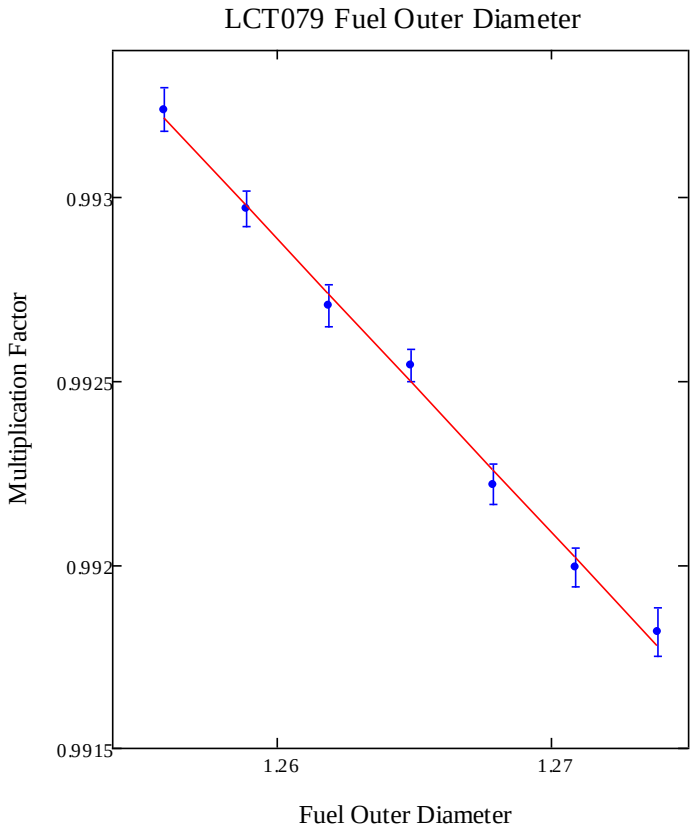

Figure 30. Fuel Outer Diameter LCT079

As the outer diameter of the fuel is modified, the mass of the fuel is maintained by varying the fuel density.

5.4.2 f. Clad Composition

The composition of the cladding material can have a very large effect on the system. If the material contains more neutron absorbing material, the multiplication factor may decrease greatly; however, given the small number of fuel rods and the low absorption cross sections of the materials present, there is a small change in the variation of the clad material.

www.manaraa.com

The change in the clad material was made by adjusting the amount of absorption in the material. The nuclide with the greatest number density is held at the average value and the nuclides with greater or less absorption cross sections are modified to reflect the change in absorption. Table 15 displays the absorption cross sections for the nuclides present in the cladding material.

Table 15. Zircaloy-4 Absorption Cross Sections (Table 14 Ref. 8)

Element	σ_a (barn)[(a)]	Element	σ_a (barn)[(a)]	Element	σ_a (barn)[(a)]
Zr	0.184				
Sn	0.61	Ca	0.43	Mo	2.5
Fe	2.56	C	0.0035	Ni	4.5
Cr	3.1	Co	37.2	Nb	1.15
Ni	4.5	Cu	3.8	N	1.89
O	0.00028	Hf	104	Si	0.168
Al	0.230	H	0.333	W	18.2
B	760	Mg	0.066	Ti	6.1
Cd	2520	Mn	13.3	U	7.57

(a) Thermal neutron (2200 m/s) absorption cross section from J. R. Parrington, et al., Nuclides and Isotopes Fifteenth Edition, General Electric, Co., 1996.

The variation in the composition was made to reflect the maximum and minimum absorption in the cladding material. The process for modifying the absorption is to modify the number densities around the nuclide with the greatest number density. For the maximum absorption case, the nuclides with absorption cross section greater than the nuclide with the greatest number density are given the maximum value of the weight fraction for the range defined. For the minimum absorption case, nuclides with the smaller absorption cross section than the nuclide with the greatest number density are given the maximum value of the weight fraction for the range defined. The nuclide with the greatest number density was zirconium. For the maximum absorption case, all

www.manaraa.com

nuclides were modified for the maximum weight fractions except nuclides O, C, Mg, and Si, which were modified to have minimum weight fractions. The opposite was performed for the minimum absorption case; all nuclides were modified for their minimum weight fractions, expect O, C, Mg, and Si, which were modified for their maximum weight fractions. The cross section, nominal weight faction, range of weight fraction are presented in the following table. The table also displays the weight fractions for the Maximum Absorption and Minimum Absorption cases.

Table 16. Weight Fraction Variation for Zircaloy-4 (Ref. 22)

		Wt. %			
Nuclide	σ_{abs}	Nominal	Range	Max Abs	Min Abs
Zr	0.184	97.597		97.318	98.069
Sn	0.61	1.45	1.2 - 1.70	1.7	1.2
Fe	2.56	0.21	0.18 - 0.24	0.24	0.18
Cr	3.1	0.1	0.07 - 0.13	0.13	0.07
Fe + Cr		0.325	0.28 - 0.37	0.37	0.28
O	0.00028	0.125	0.09 - 0.16	0.09	0.16
Al	0.23	0.0075	0.0075	0.0075	0
B	760	0.00005	0.00005	0.00005	0
Cd	2520	0.00005	0.00005	0.00005	0
Ca	0.43	0.003	0.003	0.003	0
C	0.0035	0.027	0.027	0	0.027
Co	37.2	0.002	0.002	0.002	0
Cu	3.8	0.005	0.005	0.005	0
Hf	104	0.01	0.01	0.01	0
H	0.333	0.0025	0.0025	0.0025	0
Mg	0.066	0.002	0.002	0	0.002
Mn	13.3	0.005	0.005	0.005	0
Mo	2.5	0.005	0.005	0.005	0
Ni	4.5	0.007	0.007	0.007	0
Nb	1.15	0.01	0.01	0.01	0
N	1.89	0.08	0.08	0.08	0
Si	0.168	0.012	0.012	0	0.012
W	18.2	0.01	0.01	0.01	0
Ti	6.1	0.005	0.005	0.005	0
U	7.57	0.00035	0.00035	0.00035	0

www.manaraa.com

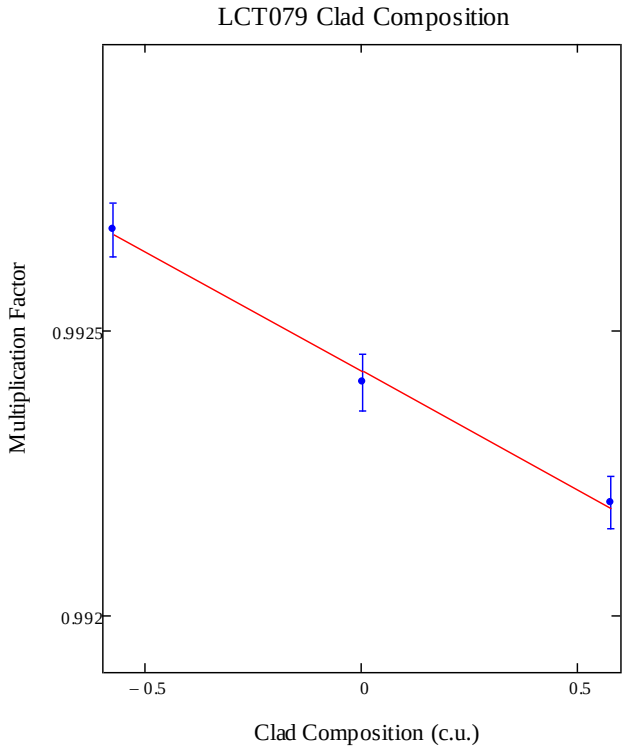

Figure 31. Clad Composition LCT079

The variable used for the composition of a material is a composition unit (c.u.). The change in the composition is specified as a limit, and one standard deviation of the composition is a "composition unit". The composition change is a uniform distribution; thus the resulting change in the parameter is divided by the square root of three, which becomes 0.577 composition units. For example when the clad composition material is modified for the maximum absorption case, the change in the material composition is translated into one composition unit.

www.manaraa.com

5.4.2 g. Aluminum Grid Plate Composition

The grid plates located in the core are composed of aluminum 6061 composition. The aluminum composition was varied in the same manner as the clad composition. Table 17 displays the nuclides present in the aluminum 6061 composition.

Table 17. Absorption Cross Sections for Aluminum 6061 Material (Ref. 8)

Element	σ_a (barn)[(a)]	Element	σ_a (barn)[(a)]	Element	σ_a (barn)[(a)]
Al	0.230				
Si	0.168	Mn	13.3	Zn	1.1
Fe	2.56	Mg	0.066	Ti	6.1
Cu	3.8	Cr	3.1		

(a) Thermal neutron (2200 m/s) absorption cross section from J. R. Parrington, et al., Nuclides and Isotopes Fifteenth Edition, General Electric, Co., 1996.

Table 18. Weight Fraction Variation for Aluminum 6061 (Ref. 23)

		Wt. %			
Nuclide	σ_{abs}	Nominal	Range	Max Abs	Min Abs
Mn	13.3	0.075	0.0-0.15	0.15	0
Ti	6.1	0.075	0.0-0.15	0.15	0
Cu	3.8	0.275	0.15-0.4	0.4	0.15
Cr	3.1	0.195	0.04-0.35	0.35	0.04
Fe	2.56	0.35	0.0-0.7	0.7	0
Zn	1.1	0.125	0.0-0.25	0.25	0
Al	0.23	97.305		96.79	97.81
Si	0.168	0.6	0.4-0.8	0.4	0.8
Mg	0.066	1	0.8-1.2	0.8	1.2

Table 18 displays the weight fractions for the nominal, maximum absorption and minimum absorption cases. The weight fractions were used to calculate the number densities for the Aluminum 6061 composition to represent the changes in absorption.

www.manaraa.com

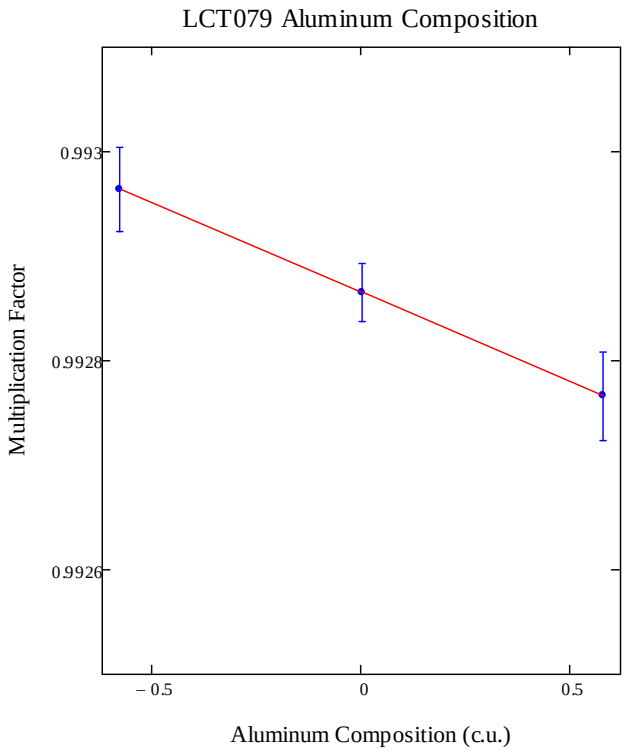

Figure 32. Aluminum Composition LCT079

Figure 32 displays the changes in the aluminum composition versus the change in the multiplication factor. The perturbation in the aluminum composition is very small, and results in a small change in the k_{eff} ($\Delta k=0.0002$). The result is as expected because the amount of material present in the system is very small, and the absorption cross section for aluminum is small.

5.4.2 h. Source Capsule Composition

When performing the experiment, a startup source was needed. The source is in a stainless steel 304 rod, which is placed in the center of the core. The variation in the source capsule composition was performed in the same approach as the Zircaloy and

www.manaraa.com

Aluminum 6061 materials. The table below displays the nuclides present in the stainless steel 304 composition, and the absorption cross sections for those nuclides.

Table 19. Stainless Steel 304 Absorption Cross Sections (Ref. 8)

Element	σ_a (barn)[(a)]	Element	σ_a (barn)[(a)]	Element	σ_a (barn)[(a)]
Fe	2.56				
C	0.0035	S	0.52	Ni	4.5
Mn	13.3	Si	0.168		
P	0.17	Cr	3.1		

(a) Thermal neutron (2200 m/s) absorption cross section from J. R. Parrington, et al., Nuclides and Isotopes Fifteenth Edition, General Electric, Co., 1996.

Table 20. Weight Fraction Variation in Stainless Steel 304 (Ref. 24)

	σ_{abs}	Nominal	Range	Max Abs	Min Abs
Fe	2.56	88.7325		67	72.845
C	0.0035	0.04	0.08	0	0.08
Mn	13.3	1	2	2	0
P	0.17	0.0225	0.045	0	0.045
S	0.52	0.015	0.03	0	0.03
Si	0.168	0.5	1	0	1
Cr	3.1	0.19	18.0 - 20.0	20	18
Ni	4.5	9.5	8.0 - 11.0	11	8

The change in the multiplication factor is very small for the change in the stainless steel composition in the system. Figure 33 displays the change in the clad material versus the change in the multiplication factor.

www.manaraa.com

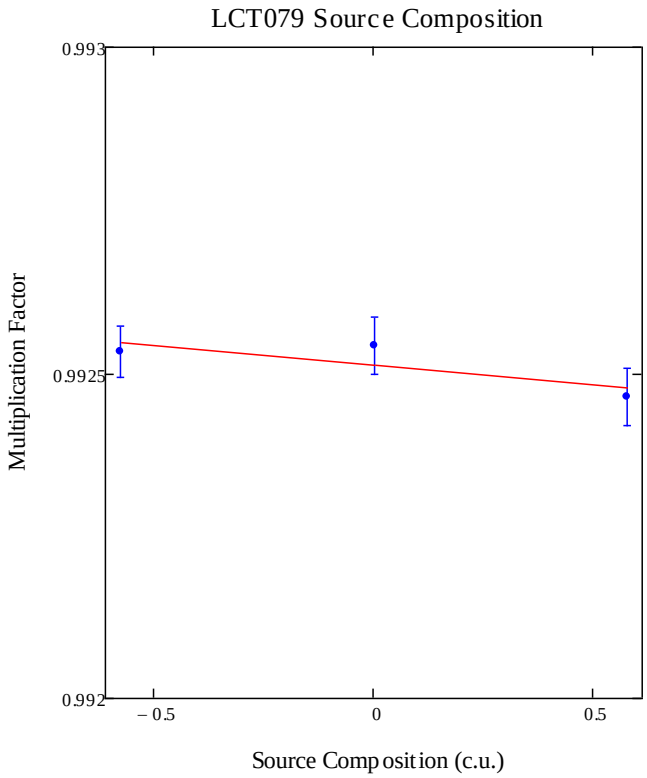

Figure 33. Source Composition LCT079

The change in the multiplication factor is expected because there is only one rod present in the system.

5.4.2 i. Temperature

The nominal temperature in the system was reported as 300 K. The variation in the temperature for the system model was from 283 K to 308 K with increments of 5 K. The system model was modified for temperature effects on cross sections as well as the moderator density.

www.manaraa.com

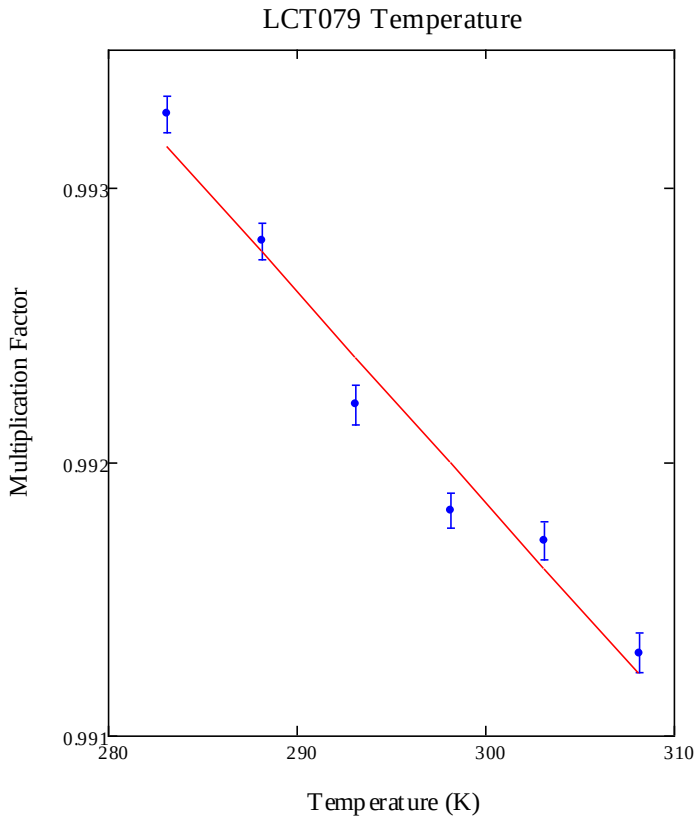

Figure 34. System Temperature LCT079

The variation in the temperature change is a result of the change in the water density. When the temperature in the system is increased, the density of the water decreases which effects the moderation of the system.

www.manaraa.com

5.3.4 Direct Uncertainty Analysis LCT079

Table 21 contains the results of the direct uncertainty analysis performed for the LCT079 Case 1 experiment. The Benchmark column contains the values provided in the benchmark evaluation. The Direct Uncertainty Analysis column contains the values obtained from the analysis described in the previous sections.

Table 21. Direct Uncertainty Analysis Results LCT079

	From the Benchmark Evaluation			Direct Uncertainty Analysis		
Parameter	P Value	σ_P Unc.	Δk_{eff}	$\Delta k/\Delta P$	Δk_{eff}	Sensitivity
Pitch	2.0 cm	0.00186 cm	0.00074	0.3963 ± 0.0038 cm^{-1}	0.00074	0.7995 ± 0.0076
Clad OD	1.3818 cm	0.00293 cm	0.00123	-0.4038 ± 0.0020 cm^{-1}	0.00120	-0.5628 ± 0.0027
Clad ID	1.2979 cm	0.00293 cm	0.00032	-0.0985 ± 0.0017 cm^{-1}	0.00029	-0.1289 ± 0.0021
Fuel OD	1.2649 cm	0.0025 cm	0.00008	-0.02357 ± 0.00203 cm^{-1}	0.00006	-0.0301 ± 0.0026
Enrichment	0.04306	0.00013	0.00045	3.415 ± 0.010	0.00044	0.14830 ± 0.00043
Clad Comp.	1 c.u.	0.577 c.u.	0.00029	-0.000369 ± 0.000070 $c.u.^{-1}$	0.00021	-0.000370 ± 0.00007
Aluminum Comp.	1 c.u.	0.577 c.u.	0.00016	-0.00019 ± 0.000070 $c.u.^{-1}$	0.00011	-0.00019 ± 0.00007
Source Comp.	1 c.u.	0.577 c.u.	0.00004	-0.000081 ± 0.000050 $c.u.^{-1}$	0.00005	-0.000080 ± 0.000047
Temp.	300 K	1 K	0.00008	-0.0000593 ± 0.0000019 K^{-1}	0.00006	-0.01796 ± 0.00057
Sum in Quadrature			0.00157		0.00151	

The overall results compare well with the benchmark evaluations. The difference in the sum in quadrature is small.

www.manaraa.com

5.5 7uPCX Experiment

5.5.1 Description

The Seven Percent Critical Experiment (7uPCX) is square-pitched array, water moderated, and nominally seven percent enriched uranium dioxide fuel with aluminum cladding. Each fuel rod is individually loaded into the array. Once the desired amount of fuel is loaded, water is added to the system to start a multiplication measurement. The fuel rods contain ~50 cm of active fuel height with 15.24 cm of poly above the fuel to ensure that the fuel will only see moderating material. The dimensions and the characteristics of the experimental setup are given in the following tables.

Table 22. Characteristics of 7uPCX Core

Fuel	**UO_2**
Uranium Enrichment (wt. %)	6.90
Fuel Pellet Diameter (cm)	0.5258
Fuel Pellet Stack Mass (g)	108.72
Cladding Material	3003 Aluminum
Clad OD (cm)	0.6376
Clad Thickness (cm)	0.036
Grid Plate Material	6061 Aluminum
Grid Plate Thickness (cm)	2.54
Grid Plate Pitch (cm)	0.8001

www.manaraa.com

Table 23. Axial Dimensions 7uPCX

Location	Axial Position (cm)
Top of Tank	82.55
Top of Guide Plate	71.76
Water Surface	68.26
Top of Top Grid Plate	53.02
Top of Fuel	48.78
Bottom of Fuel	0
Top of Lower Grid Plate	0
Bottom of Water	-19.05

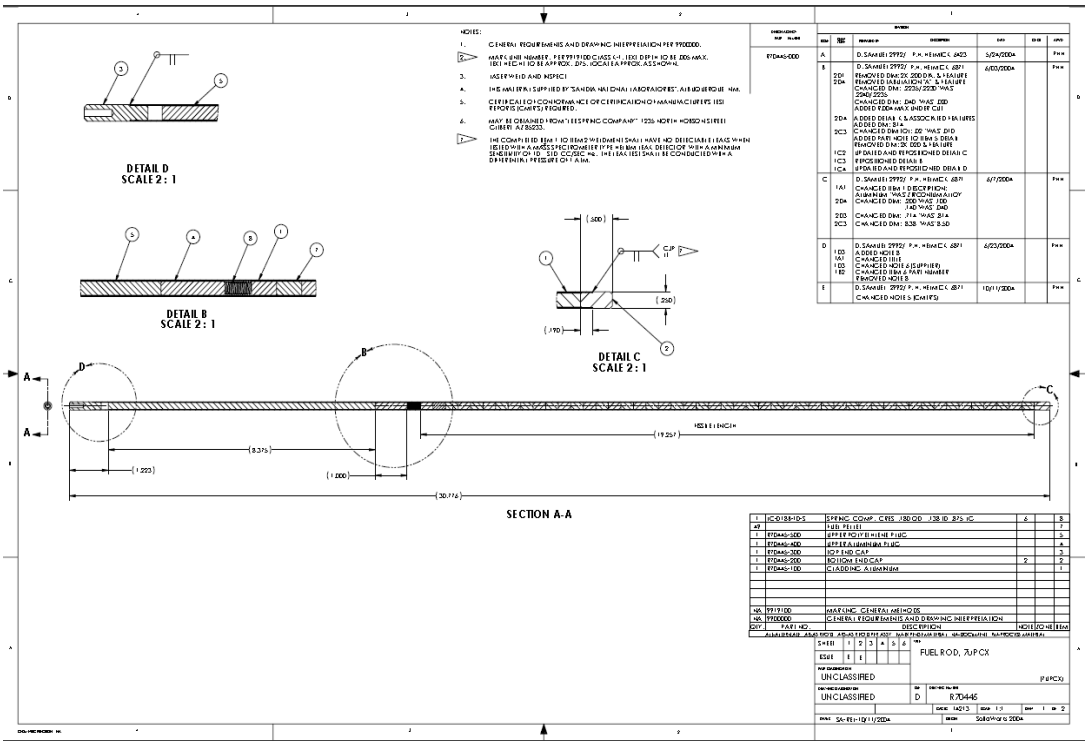

Figure 35. "Design" Drawing of Fuel Rod

Figure 35 displays the fuel rod, showing the bottom end gap, the fissile material, followed by the spring, an aluminum plug, then the 15.24 cm (6 in) of polyethylene and an end cap on the top.

www.manaraa.com

5.5.2 Direct Uncertainty Analysis 7uPCX

The 7uPCX experiments are not a published benchmark evaluation. The uncertainty analysis is performed as part of this work.

The list of uncertainties for 7uPCX is given in Table 24 and Table 25. Each uncertainty was determined to be Type A or Type B uncertainty, from the Uncertainty Guide (ICSBEP).[20] A Type A uncertainty is determined by a statistical analysis from a series of observations, and a Type B uncertainty is determined from a method or consideration other than statistical analysis.[20]

Table 24. 7uPCX List of Uncertainties for 0.800 cm Pitch

Parameter	Mean Measured Value or Design Value	Reported Uncertainty in parameter	Type of Uncertainty (A or B)	Standard Uncertainty
^{235}U enrichment (wt %)	6.9034	0.0046	A	0.0014
Temperature (K)	293.15	1	A	1
Aluminum 6061 Composition (c.u.)	1	0.577	B	0.577
Aluminum 3003 Composition (c.u.)	1	0.577	B	0.577
Water Composition (c.u.)	1	1	A	1
Source Capsule Composition (c.u.)	1	0.577	B	0.577
Pitch (cm)	0.8	0.00057	B	0.00057/√3
Fuel Diameter (cm)	0.52578	0.00127	B	0.00127
Clad Thickness (cm)	0.03556	0.001	B	0.001/√3
Clad Outer Diameter (cm)	0.637602	0.00016	A	0.00016
Water Level (cm)	69.5325	0.02	A	0.02/√3
Fissile Column Height (cm)	48.77954	0.00267	B	0.28162

www.manaraa.com

Table 25. 7uPCX List of Uncertainties for 0.855 cm Pitch

Parameter	Mean Measured Value or Design Value	Reported Uncertainty in parameter	Type of Uncertainty (A or B)	Standard Uncertainty
^{235}U enrichment (wt %)	6.9034	0.0046	A	0.0014
Temperature (K)	293.15	1	A	1
Aluminum 6061 Composition (c.u.)	1	0.577	B	0.577
Aluminum 3003 Composition (c.u.)	1	0.577	B	0.577
Water Composition (c.u.)	1	1	B	1
Source Capsule Composition (c.u.)	1	0.577	B	0.577
Pitch (cm)	0.855	0.00060	B	0.00060/√3
Fuel Diameter (cm)	0.52578	0.00127	B	0.00127
Clad Thickness (cm)	0.03556	0.001	B	0.001/√3
Clad Outer Diameter (cm)	0.637602	0.00016	A	0.00016
Water Level (cm)	69.5325	0.02	A	0.02/√3
Fissile Column Height (cm)	48.77954	0.00267	B	0.28162

A c.u. is a composition unit, which as defined in Ref. 8 is the "change from one composition to the other. Because the composition is specified as limits, the one-standard-deviation variation of the composition is assumed to be one "composition unit" divided by the square root of three or 0.577 composition units."

5.5.2 a. Enrichment

Oak Ridge National Laboratory conducted a series of enrichment measurements for the fuel to be used in 7uPCX. The measurements were performed on June 5, 2005 with the results listed in Table 26. The mass fractions determined for the 7uPCX fuel as a result of the enrichment measurements are listed in Table 27.

www.manaraa.com

Table 26. Isotopic Measurements from ORNL

Run#	Sample ID	Pellet #	234U/238U	2σ	235U/238U	2σ	236U/238U	2σ
8683	13527-1	5	0.00030846	7.076E-06	0.07525407	1.505E-04	0.00068766	1.376E-05
8686	13527-2	20	0.00030900	5.026E-06	0.07520989	1.504E-04	0.00068845	1.378E-05
8701	13527-3	164	0.00030880	2.569E-06	0.07521708	1.504E-04	0.00068727	1.375E-05
8704	13527-4	198	0.00030872	2.039E-06	0.07510904	1.502E-04	0.00068523	1.371E-05
8710	13527-5	264	0.00030752	2.347E-06	0.07522744	1.505E-04	0.00068735	1.376E-05
8713	13527-6	311	0.00030709	2.091E-06	0.07514940	1.503E-04	0.00068858	1.378E-05
8728	13527-7	328	0.00030730	1.863E-06	0.07509191	1.502E-04	0.00068601	1.373E-05
8731	13527-8	363	0.00030743	2.324E-06	0.07516269	1.503E-04	0.00068498	1.371E-05
8737	13527-9	428	0.00030708	1.735E-06	0.07513969	1.503E-04	0.00068636	1.374E-05
8740	13527-10	444	0.00030636	1.873E-06	0.07519370	1.504E-04	0.00068804	1.377E-05

Table 27. Mass Fractions of Fuel

	Mass Fractions			
	U-234	**Enrichment**	**U-236**	**U-238**
	0.0282035%	6.9100999%	0.0634122%	92.9982845%
	0.0282536%	6.9063148%	0.0634878%	93.0019437%
	0.0282355%	6.9069380%	0.0633788%	93.0014477%
	0.0282302%	6.8977152%	0.0631966%	93.0108580%
	0.0281179%	6.9078313%	0.0633856%	93.0006652%
	0.0280806%	6.9011553%	0.0635038%	93.0072604%
	0.0281014%	6.8962547%	0.0632700%	93.0123739%
	0.0281116%	6.9023122%	0.0631710%	93.0064051%
	0.0280798%	6.9003391%	0.0632990%	93.0082821%
	0.0280123%	6.9049500%	0.0634509%	93.0035868%
Average	0.02814%	6.9034%	0.06336%	93.0051%
Std Dev	0.00008%	0.0046%	0.00012%	0.0046%
# meas.	10	10	10	10
Standard Dev. Of Mean	0.00003%	0.0014%	0.00004%	0.0015%

The average of the measured values was found, and that value was used in the experimental model for the uranium enrichment of the 7uPCX fuel. The standard deviation of the mean was found in the process of the fuel enrichment analysis, and this value is the associated uncertainty in the enrichment. It was determined that the standard

www.manaraa.com

deviation of the mean was too small of a variation to yield a result outside of the statistical uncertainties in the Monte Carlo code. Thus a larger variation was evaluated. The range is 6.86 wt. % ^{235}U to 6.94 wt. % ^{235}U. Eight separate experiment models were created. The number densities for ^{235}U and ^{238}U were modified to reflect the change in uranium enrichment. Each model was run individually with 10,000 generations and 40,000 neutrons per generation, to ensure good statistics. The error bars on the plot are one standard deviation in the multiplication factor.

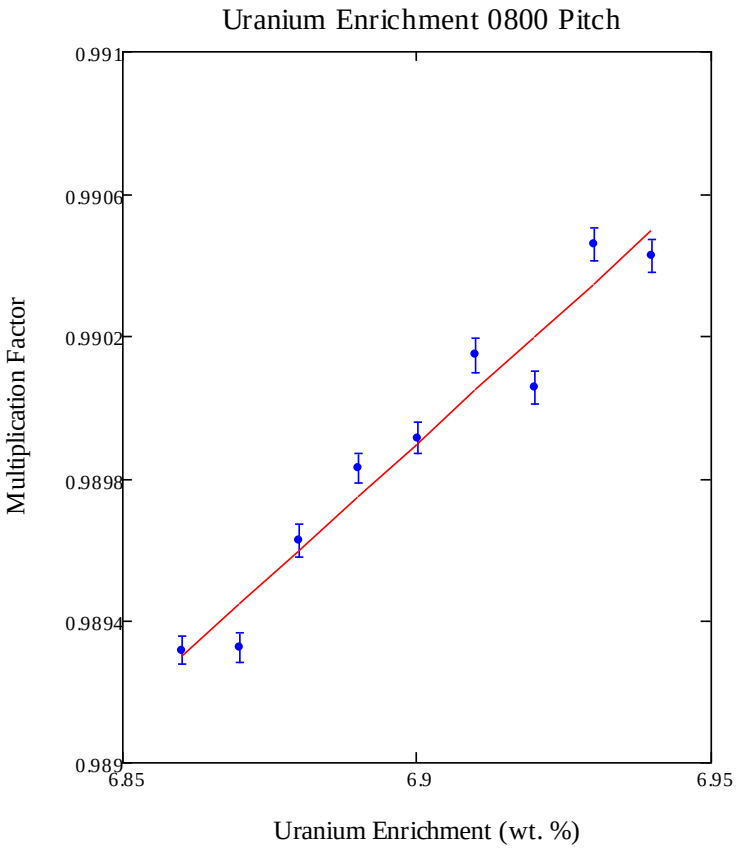

Figure 36. Uranium Enrichment 0.800 cm Pitch 7uPCX

www.manaraa.com

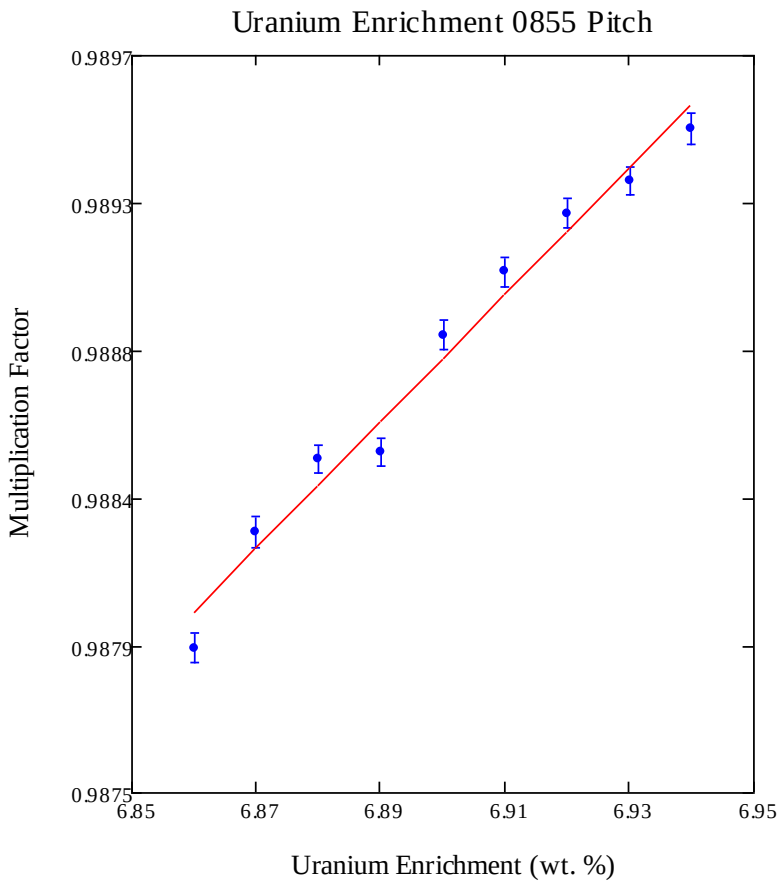

Figure 37. Uranium Enrichment 0.855 cm Pitch 7uPCX

The results in Figure 36 and Figure 37 are as expected; as the weight percent of ^{235}U increases, k_{eff} increases.

5.5.2 b. Pitch

The pitch is 0.8001 ± 0.0002 cm and 0.8549 ± 0.0002 cm, which was provided as a manufacturer's tolerance. As described in the Uncertainty Guide, the uncertainty is the manufacturer's tolerance divided by the square root of three.[20] The pitch has a large sensitivity effect on the system. When the pitch is increased, each fuel rod will be surrounded by more water and when the pitch is decreased, each fuel rod is surrounded

www.manaraa.com

by less water. When there is more or less water around the fuel rods, there is a change in the moderation of the system. When the pitch is modified the overall core diameter is modified. The experimental model was modified for this change and the results of that modification can be seen in the following plot of keff versus change in pitch.

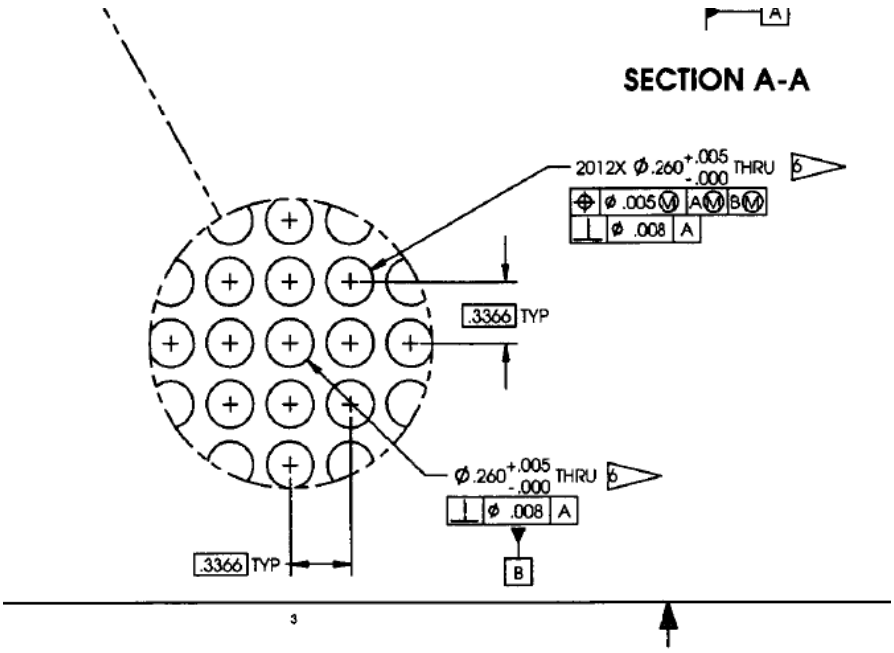

Figure 38. Drawing of Grid Plate 0.855 cm 7uPCX

Figure 38 shows the design drawing of the grid plate from the 7uPCX experiment, displaying the one-sided recorded manufactures tolerance of the hole in the grid plate as 0.005 in.

www.manaraa.com

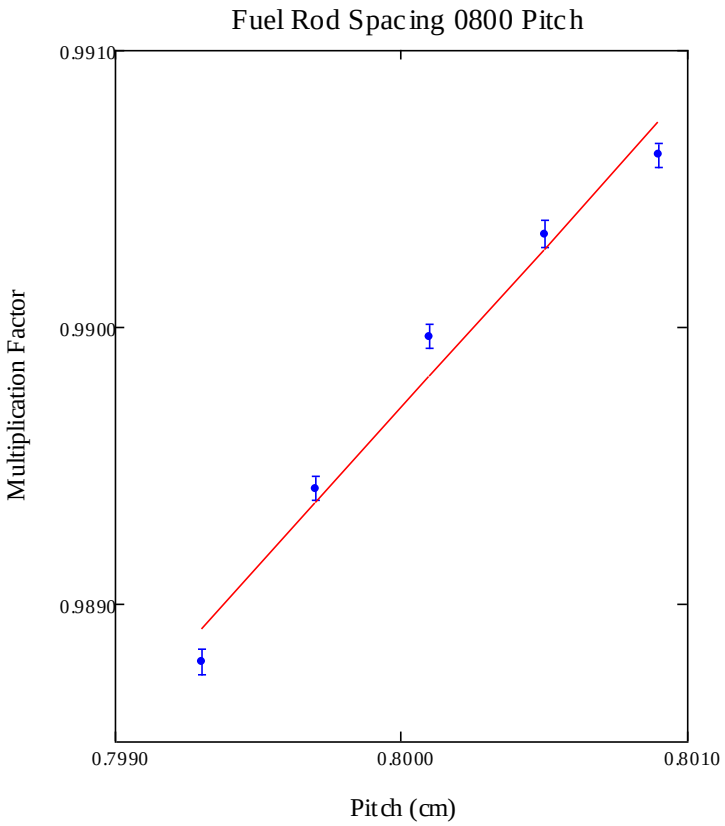

Figure 39. Fuel Rod Spacing 0.800 cm Pitch 7uPCX

www.manaraa.com

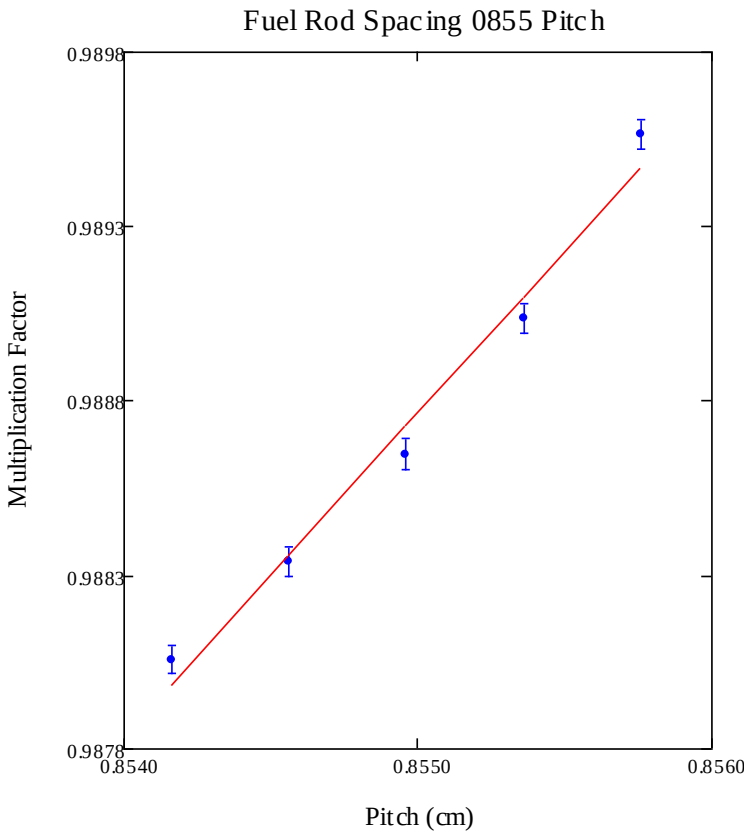

Figure 40. Fuel Rod Spacing 0.855 cm Pitch7uPCX

Figure 40 and Figure 39 clearly display a linear progression (increase), as the pitch is increased the multiplication factor increases.

5.5.2 c. Clad Outer Diameter

A series of measurements of the outer clad diameter was conducted by Ktech Corporation.[25] One hundred samples were measured. Two measurements were made for each sample. The azimuthal position of the first measurement was randomly chosen 25.7175 cm (10.125 in) from the weld plug end, then rotating the rod ninety degrees; a second measurement was taken. Table 28 displays the sample of the measurements taken.

www.manaraa.com

Table 28. Subset of the Clad Outer Diameter Measurements (Ref. 25)

TABLE 1 ELEMENT MEASUREMENTS							
	2 axis check @ 10.125				**Accuracy Check**		
	A	B		Avg 1	A2	B2	
	Meas @ 0	Meas @ 90	Delta A-B	Average	Meas @ 0	Meas @ 90	Delta A2-B2
1	0.25075	0.25035	0.00040	0.25055	0.25070	0.25065	0.00005
2	0.25075	0.25115	0.00040	0.25095			0.00000
3	0.25095	0.25100	0.00005	0.25098			0.00000
4	0.25095	0.25110	0.00015	0.25103			0.00000
5	0.25115	0.25085	0.00030	0.25100			0.00000
6	0.25110	0.25105	0.00005	0.25108			0.00000
7	0.25095	0.25060	0.00035	0.25078			0.00000
8	0.25085	0.25105	0.00020	0.25095			0.00000
9	0.25090	0.25100	0.00010	0.25095			0.00000
10	0.25120	0.25120	0.00000	0.25120			0.00000
11	0.25110	0.25115	0.00005	0.25113	0.25130	0.25110	0.00020
12	0.25070	0.25120	0.00050	0.25095			0.00000
13	0.25135	0.25100	0.00035	0.25118			0.00000
14	0.25105	0.25125	0.00020	0.25115			0.00000
15	0.25110	0.25120	0.00010	0.25115			0.00000
16	0.25125	0.25120	0.00005	0.25123			0.00000
17	0.25085	0.25120	0.00035	0.25103			0.00000
18	0.25135	0.25130	0.00005	0.25133			0.00000
19	0.25115	0.25145	0.00030	0.25130			0.00000
20	0.25125	0.25125	0.00000	0.25125			0.00000
21	0.25120	0.25130	0.00010	0.25125	0.25135	0.25120	0.00015

The conclusion of the measurements was that the clad outer diameter is 0.637602 ± 0.000157 cm (0.25102 ± 0.00062 in).

www.manaraa.com

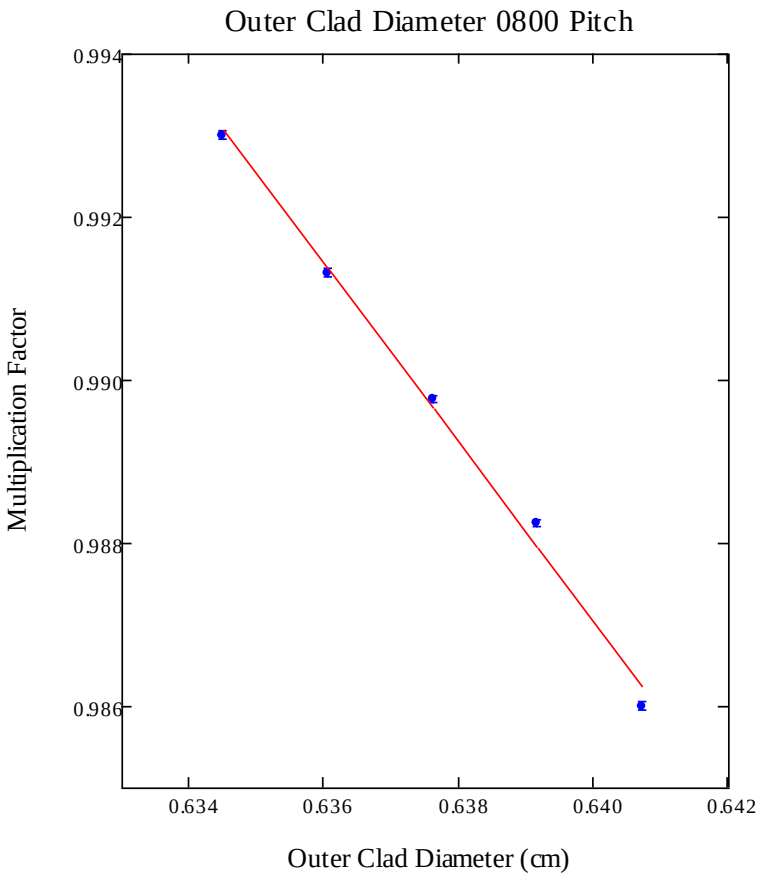

Figure 41. Outer Clad Diameter 0.800 cm Pitch 7uPCX

www.manaraa.com

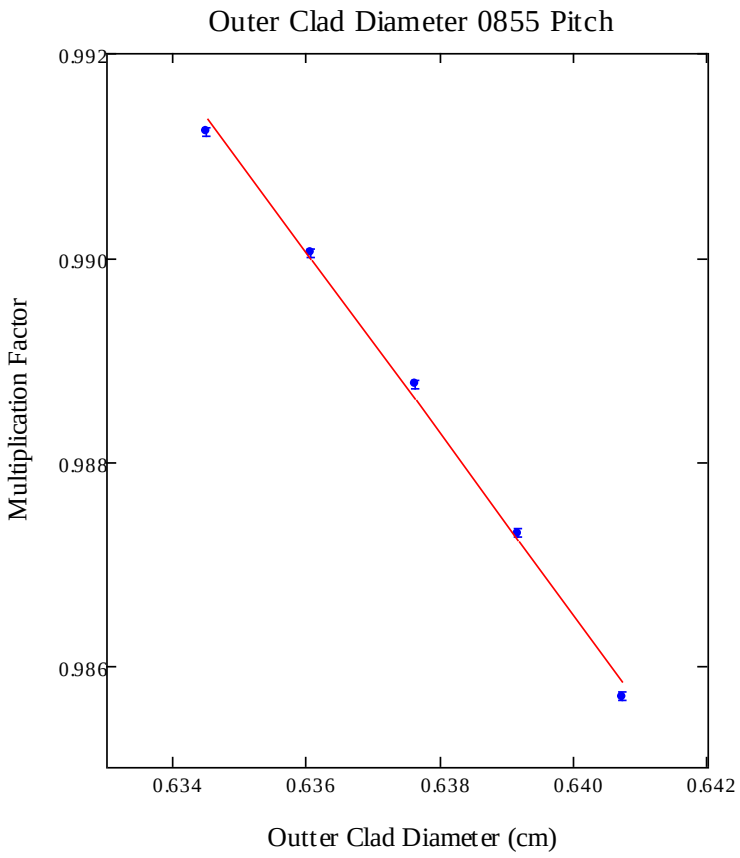

Figure 42. Outer Clad Diameter 0.855 cm Pitch 7uPCX

The increase in the clad outer diameter decreases the multiplication factor for the two systems. The outer diameter of the clad has a high sensitivity effect due to the variation in the water that surrounds the fuel rods. When the clad outer diameter is decreased, there is more water surrounding the fuel rods; when the clad outer diameter is increased, there is less water surrounding the fuel rods. Changing the amount of water that surrounds the fuel rods has a large effect on the moderation of the system and thus had an effect on the multiplication factor. Figure 42 and Figure 41 suggest that the system is under moderated; Figure 39 and Figure 40 suggest the same conclusion.

www.manaraa.com

5.5.2 d. Clad Thickness

The clad thickness has a small effect on the system, as only the inner clad diameter is modified to represent a change in the clad thickness. The uncertainty was chosen to be one percent uncertainty. No direct measurements were made for the thickness of the clad. A series of measurements was conducted for the outer diameter of the clad and the design drawings report a value of 0.014 for the thickness of the clad, without a tolerance. The assumed clad thickness is 0.035560 ± 0.000356 cm.

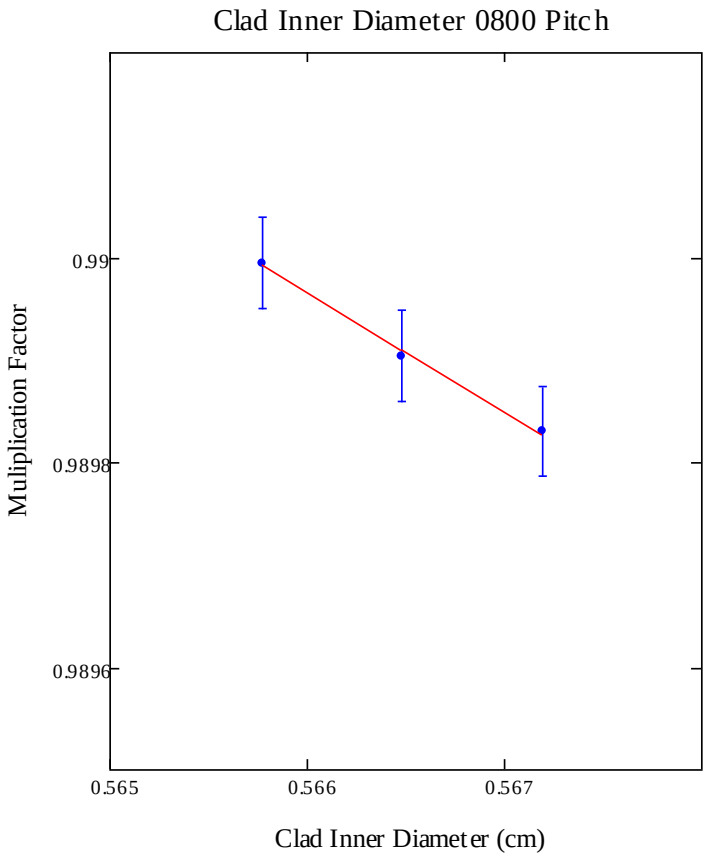

Figure 43. Clad Thickness 0.800 cm Pitch 7uPCX

www.manaraa.com

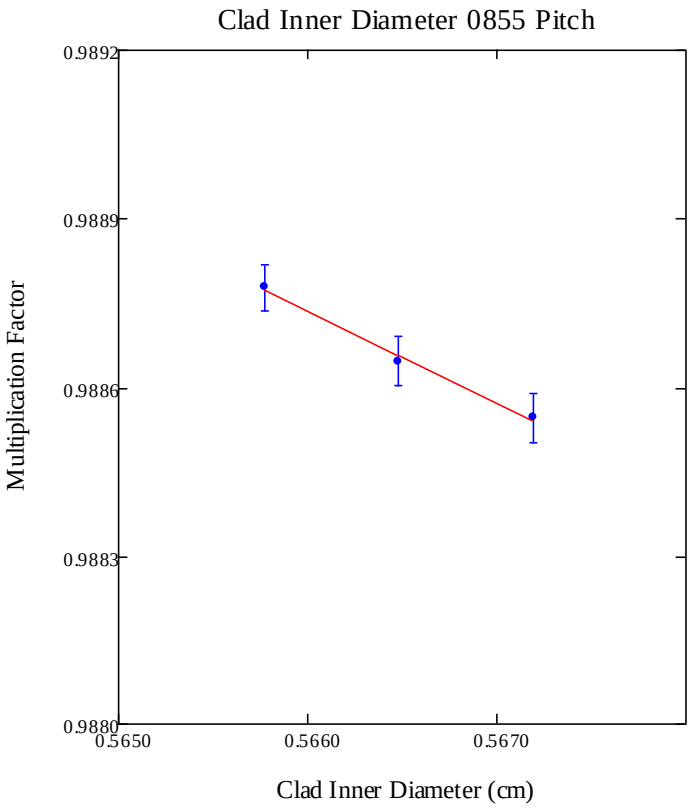

Figure 44. Clad Thickness 0.855 cm Pitch 7uPCX

The variation in the clad thickness for the two experiments is in the fourth decimal place, resulting in a very small sensitivity for both systems.

5.5.2 e. Fuel Diameter

The fuel diameter was given in a design drawing as 0.52578 ± 0.00127 cm (0.207 ± 0.0005 in). The diameter of the fuel pellet was modified for this uncertainty as well as the number densities of the fuel. The number density of the fuel composition was modified to maintain a constant uranium mass for the system. The following table contains the number densities for the perturbed fuel radii.

www.manaraa.com

Table 29. Fuel Diameter Perturbation Number Densities

Fuel Rod Diameter		
Diameter (cm)	Number Densities (atom/barn-cm)	
0.52832	N_{234}	6.487E-02
	N_{235}	1.585E-03
	N_{236}	1.448E-02
	N_{238}	2.108E-02
	N_O	4.537E-02
0.52578	N_{234}	6.550E-06
	N_{235}	1.602E-03
	N_{236}	1.462E-05
	N_{238}	2.128E-02
	N_O	4.581E-02
0.52324	N_{234}	6.614E-06
	N_{235}	1.616E-03
	N_{236}	1.477E-05
	N_{238}	2.149E-02
	N_O	4.626E-02

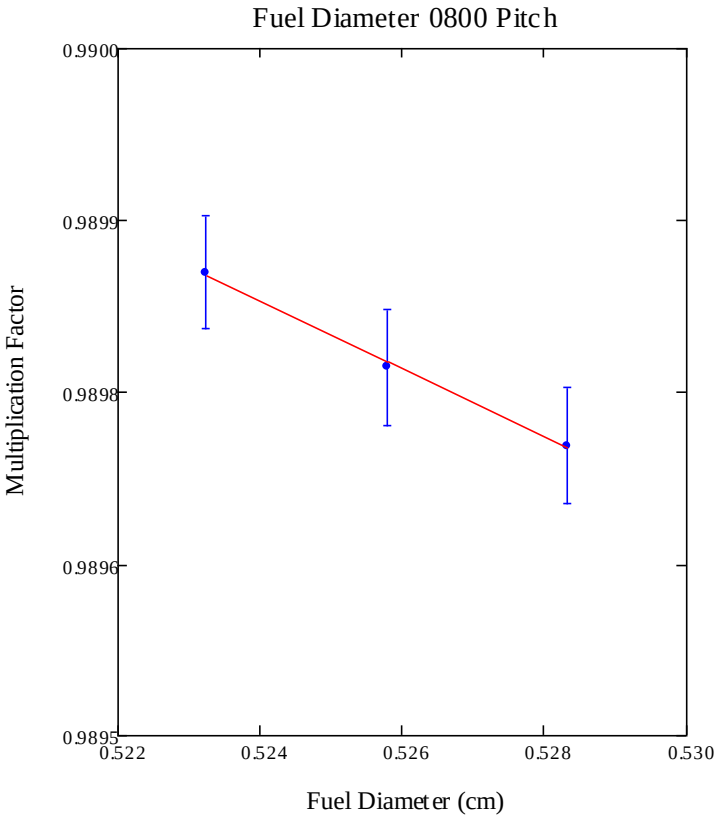

Figure 45. Fuel Pellet Diameter 0.800 cm Pitch 7uPCX

www.manaraa.com

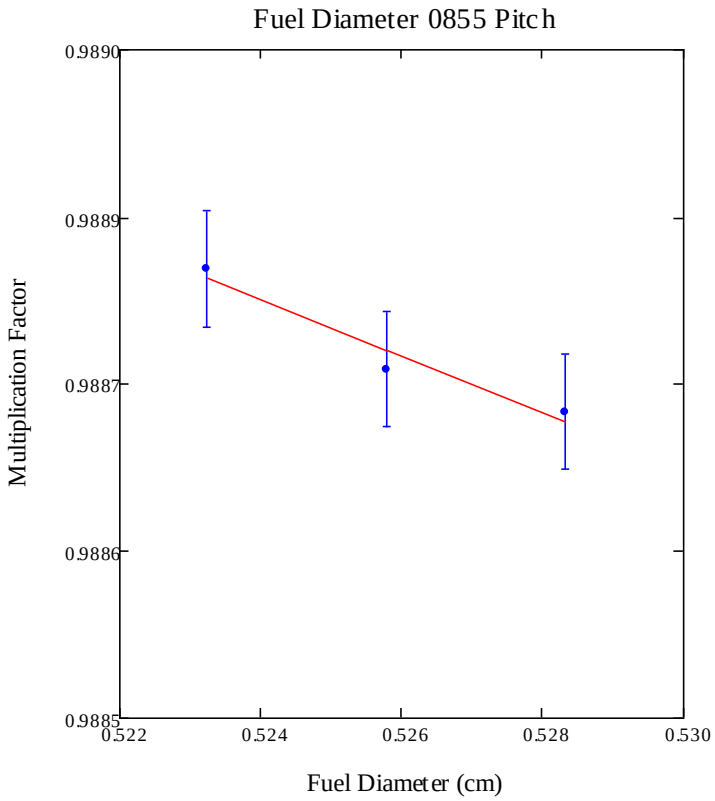

Figure 46. Fuel Pellet Diameter 0.855 cm Pitch 7uPCX

The fuel pellet diameter perturbation result is a function of the change in volume. The mass of the fuel was held constant.

5.5.2 f. Fissile Column Height

The fissile column height is reported as 48.77954 cm (19.2045 in). When the fuel rods were being fabricated, the length of the fuel was measured. The Appendix C contains a sample those measurements. A mean of the measured lengths and the standard deviation of the mean were determined. The result of that evaluation, is that the fuel height is 48.77954 ± 0.00267 cm.

www.manaraa.com

The height of the fuel was modified and the number densities were changed to maintain the mass of the fuel.

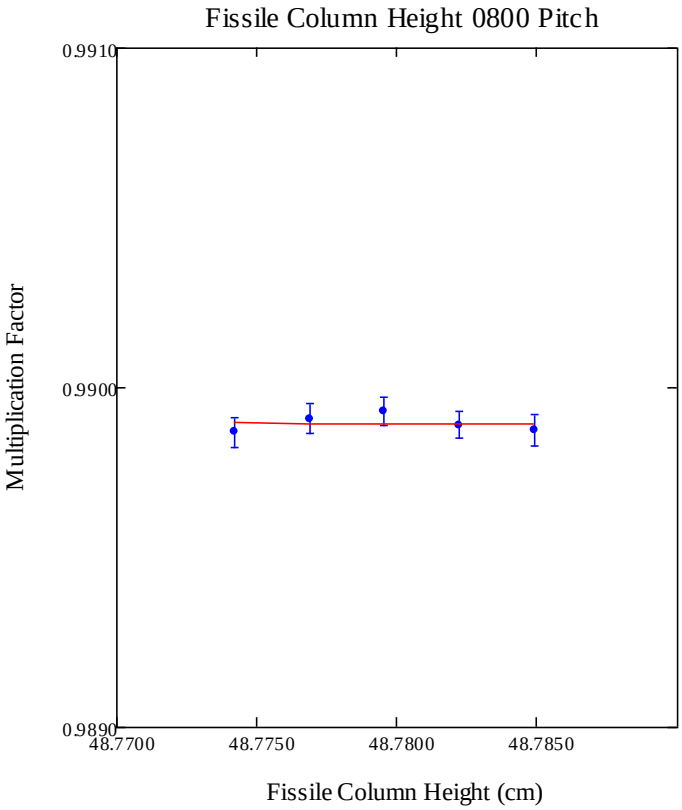

Figure 47. Fissile Column Height 0.800 cm Pitch 7uPCX

www.manaraa.com

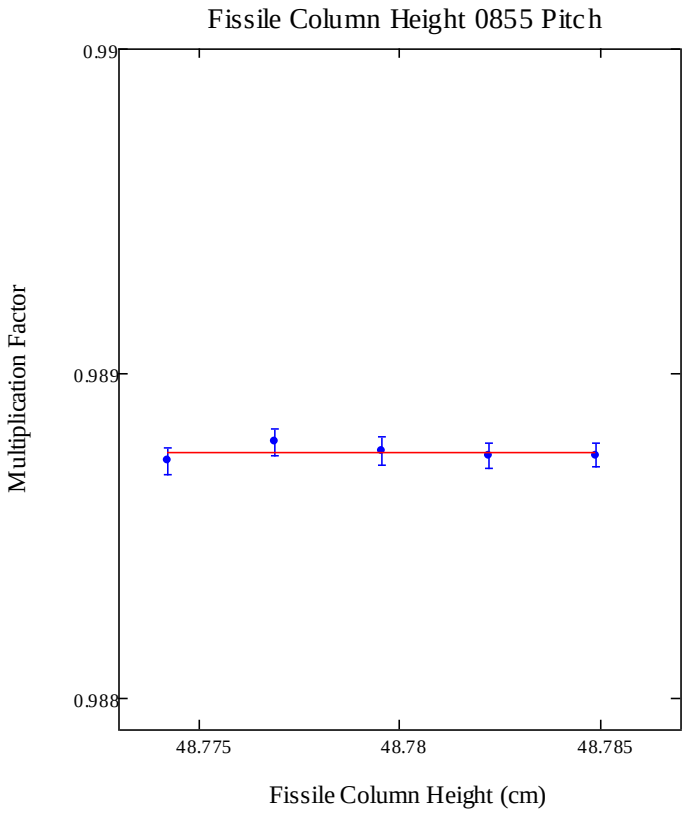

Figure 48. Fissile Column Height 0.855 cm Pitch 7uPCX

The change in the height of the fuel has a very small effect on the system. The mass of the fuel was maintained throughout the variations by changing the number densities. Figure 47 and Figure 48 shows almost no variation in the multiplication factor for the change in fuel height over the variation investigated.

5.5.2 g. Aluminum 3003 Composition – Clad

The same process performed for the grid plate and cladding material in the LCT079 experiment was performed for the Aluminum 3003 composition.

www.manaraa.com

Table 30 displays the weight fractions for the nominal, maximum absorption and minimum absorption cases. Table 31 lists the number densities for the variations in the weight fractions.

Table 30. Cross Sections and Weight Fractions for Aluminum 3003 (Ref. 26)

Nuclide	σ_{abs}	Nominal (wt. %)	Range (wt.%)	Max Abs (wt.%)	Min Abs (wt.%)
Mn	13.3	1.25	1-1.5	1.5	1
Cu	3.8	0.125	0.05-0.2	0.2	0.05
Fe	2.56	0.35	0-0.7	0.7	0
Zn	1.1	0.05	0-0.1	0.1	0
Al	0.233	97.925		97.5	98.35
Si	0.168	0.3	0-0.6	0	0.6

Table 31. Aluminum 3003 Composition Number Densities

Aluminum 3003 Composition		
Maximum Absorption	N_{Al}	5.880E-02
	N_{Cu}	5.121E-05
	N_{Fe}	2.040E-04
	N_{Mn}	4.443E-04
	N_{Si}	0
	N_{Zn}	2.488E-05
	N_{B}	3.602E-08
Nominal Absorption	N_{Al}	5.967E-02
	N_{Cu}	3.234E-05
	N_{Fe}	1.030E-04
	N_{Mn}	3.741E-04
	N_{Si}	1.756E-04
	N_{Zn}	1.257E-05
	N_{B}	1.820E-08
Minimum Absorption	N_{Al}	5.931E-02
	N_{Cu}	1.280E-05
	N_{Fe}	0
	N_{Mn}	2.962E-04
	N_{Si}	3.476E-04
	N_{Zn}	0
	N_{B}	0

The Aluminum 3003 material is used for the fuel rod cladding. Modifying the material that surrounds the fuel changes the amount of absorption that occurs within the

www.manaraa.com

fuel rod and also between the fuel rods. When the cladding material is at the maximum absorption, there is less of a probability that a neutron can leave the cladding material (this decrease in probability is small).

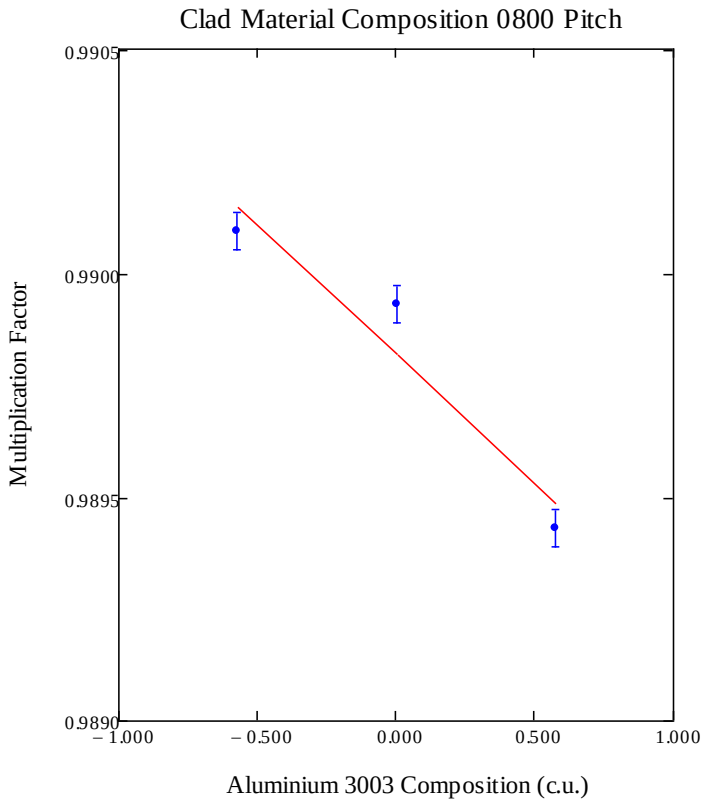

Figure 49. Aluminum 3003 0.800 cm Pitch 7uPCX

www.manaraa.com

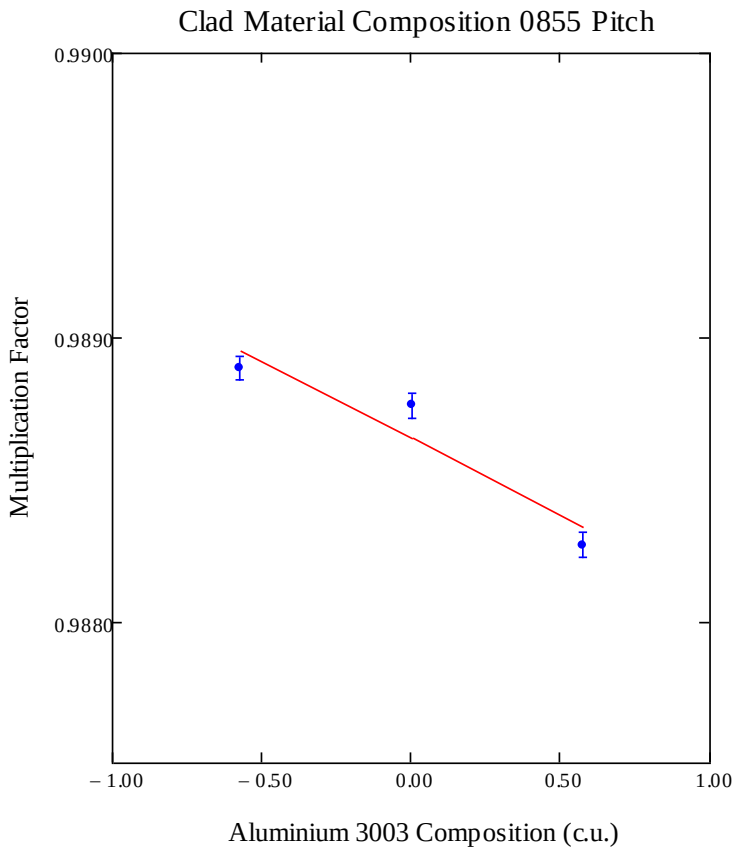

Figure 50. Aluminum 3003 0.855 cm Pitch 7uPCX

From Figure 50 and Figure 49, as the absorption in the cladding is minimized, the multiplication factor is increased due to a reduction in neutron absorption.

5.5.2 h. Aluminum 6061 Composition – grid plate

Using the analysis performed in the critical benchmark LEU-COMP-THERM-079 (Ref. 8) as an example, the material compositions are varied to represent the change in concentration. A full description of this process is provided in section 5.3.2 f.

Table 32 displays the absorption cross section for each nuclide present in the Aluminum 6061 composition. The range for the weight percent present in the 6061

www.manaraa.com

material is based upon an ASTM standard+[23], where the values are given as maximum or a range. For the nuclides Mn, Ti, V, Cu, Cr, Fe and Zn the maximum weight fraction was used for the maximum absorption while the minimum weight fractions were used for nuclides Si and Mg, and the remaining material composition was formed with Al. The opposite process was followed for the minimum absorption case. The nuclides with absorption cross sections greater than aluminum had the minimum weight fractions, while the nuclides with absorption cross section less than aluminum had maximum weight fraction specified.

Table 32. Cross section and Weight Fractions for Aluminum 6061 (Ref. 23)

Nuclide	σ_{abs}	Nominal (wt. %)	Range (wt.%)	Max Abs (wt.%)	Min Abs (wt.%)
Mn	13.3	0.075	0.0-0.15	0.15	0
Ti	6.1	0.075	0.0-0.15	0.15	0
V	5	0.01	0.0-0.01	0.01	0
Cu	3.8	0.275	0.15-0.4	0.4	0.15
Cr	3.1	0.195	0.04-0.35	0.35	0.04
Fe	2.56	0.35	0.0-0.7	0.7	0
Zn	1.1	0.125	0.0-0.25	0.25	0
Al	0.23	97.305		96.79	97.81
Si	0.168	0.6	0.4-0.8	0.4	0.8
Mg	0.066	1	0.8-1.2	0.8	1.2

www.manaraa.com

Table 33. Number Densities Aluminum 6061

Aluminum 6061 Composition		
	Number Density (atom/barn-cm)	
Maximum Absorption	N_{Al}	5.8328E-02
	N_{Si}	2.3158E-02
	N_{Fe}	2.0380E-02
	N_{Cu}	1.0235E-04
	N_{Mn}	4.4385E-05
	N_{Mg}	5.3519E-04
	N_{Cr}	1.0945E-04
	N_{Zn}	6.2174E-05
	N_{B}	8.9989E-08
	N_{Ti}	5.0918E-05
	N_{V}	6.3837E-06
Nominal Absorption	N_{Al}	5.7880E-02
	N_{Si}	4.1685E-04
	N_{Fe}	1.8051E-04
	N_{Cu}	7.9321E-05
	N_{Mn}	2.6637E-04
	N_{Mg}	6.9575E-04
	N_{Cr}	6.2542E-05
	N_{Zn}	2.9844E-05
	N_{B}	4.3195E-08
	N_{Ti}	6.7890E-06
	N_{V}	3.1919E-05
Minimum Absorption	N_{Al}	5.8943E-02
	N_{Si}	4.6315E-04
	N_{Fe}	0
	N_{Cu}	3.8381E-05
	N_{Mn}	0
	N_{Mg}	8.0279E-04
	N_{Cr}	1.2508E-05
	N_{Zn}	0
	N_{B}	0
	N_{Ti}	0
	N_{V}	0

www.manaraa.com

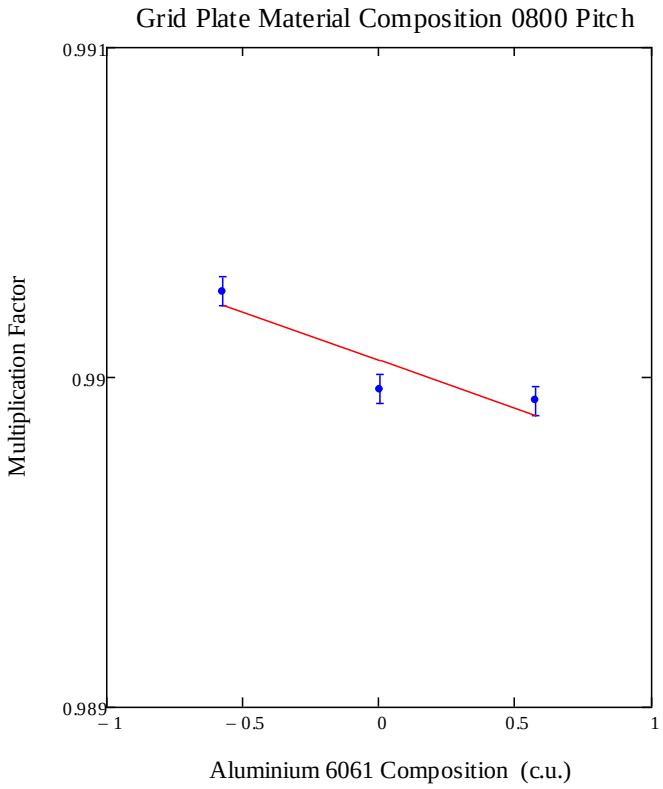

Figure 51. Aluminum 6061 Composition 0.800 cm Pitch 7uPCX

www.manaraa.com

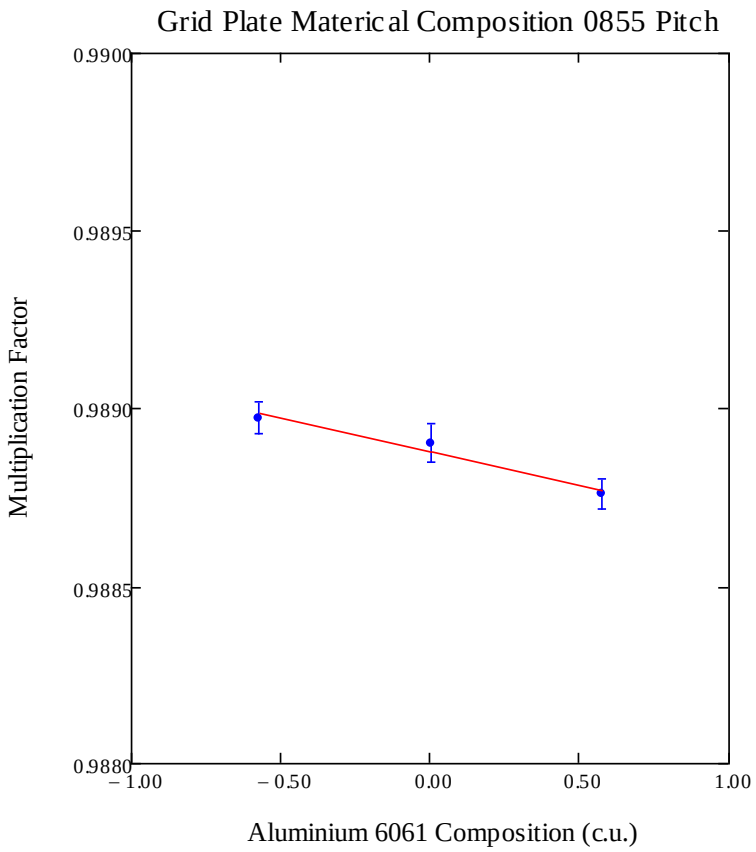

Figure 52. Aluminum 6061 Composition 0.855 cm Pitch 7uPCX

There is a small variation in the clad material sensitivity. This change in the multiplication factor is a result of the increase in absorption of the grid plate material.

5.5.2 i. Source Capsule Composition

The composition of the source capsule is composed of Stainless Steel 304. The procedure for the Aluminum compositions was implemented for the SS304 composition. Iron has the largest number density in the stainless steel 304 composition and to maximize or minimized the absorption, all other nuclides with are modified around iron. The elements with a larger cross section than iron are manganese (Mn), chromium (Cr), and nickel (Ni), and the nuclides with smaller absorption cross sections are carbon (C),

www.manaraa.com

phosphorus (P), sulfur (S) and silicon (Si). The range of weight fractions were presented in Table 19, in the previous section.

Table 34. Stainless Steel 304 Number Densities

Stainless Steel 304 Composition		
Maximum Absorption	N_{Fe}	5.780E-02
	N_{Cr}	1.853E-02
	N_{Ni}	9.029E-03
	N_{Mn}	1.754E-03
	N_{C}	0
	N_{P}	0
	N_{S}	0
	N_{Si}	0
Nominal Absorption	N_{Fe}	1.258E-02
	N_{Cr}	3.672E-03
	N_{Ni}	1.626E-03
	N_{Mn}	1.829E-04
	N_{C}	3.347E-05
	N_{P}	7.299E-06
	N_{S}	4.701E-06
	N_{Si}	1.789E-04
Minimum Absorption	N_{Fe}	6.284E-02
	N_{Cr}	1.668E-02
	N_{Ni}	6.567E-03
	N_{Mn}	0
	N_{C}	3.089E-05
	N_{P}	6.999E-05
	N_{S}	4.507E-05
	N_{Si}	1.715E-03

www.manaraa.com

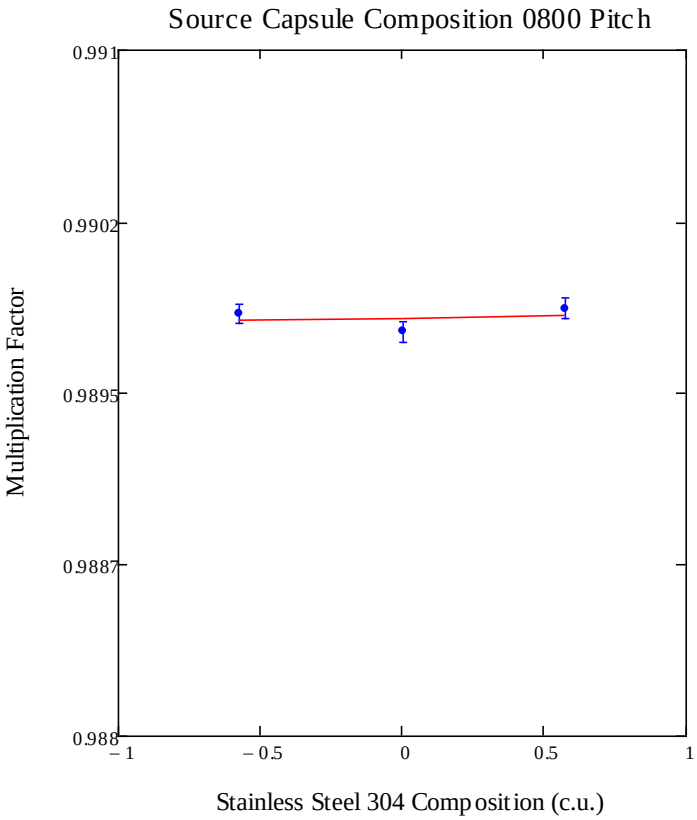

Figure 53. Stainless Steel 304 Composition 0.800 cm Pitch 7uPCX

www.manaraa.com

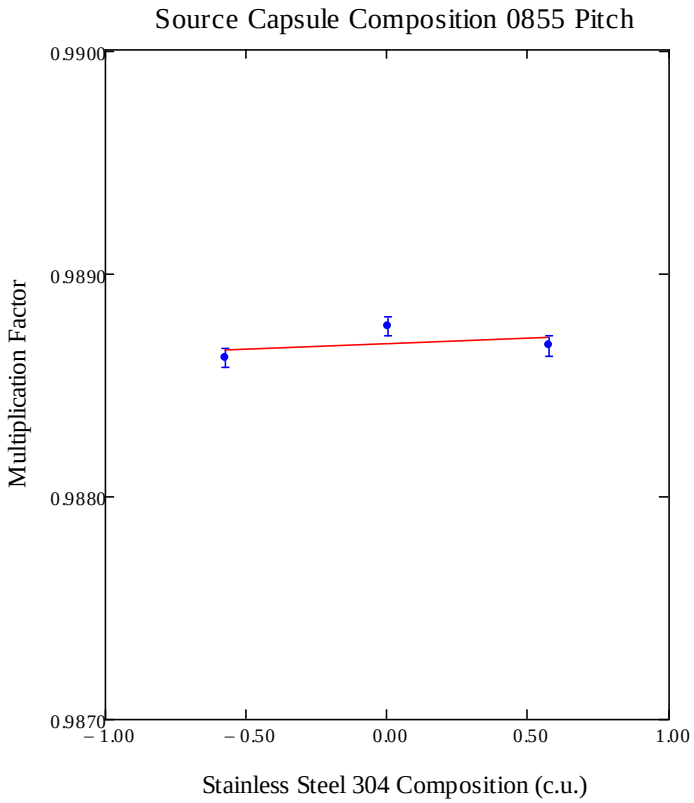

Figure 54. Stainless Steel 304 Composition 0.855 cm Pitch 7uPCX

Figure 53and Figure 54 display the effects of changing the absorption in the stainless steel 304 material. The result of the sensitivity for both experiments is very small. Because there is a small amount of stainless steel 304 in the system, changing the amount of absorption in that material has a very small effect on the overall systems.

5.5.2 j. Temperature

The temperature for 7uPCX has an estimated uncertainty of 1 K. The system temperature is approximately room temperature, 23 °C (296.15 K), and with a small uncertainty, the only effect from this variation is noticed in the water density. When the temperature of the moderator increases, the density decreases, which then decreases

www.manaraa.com

moderation and as a result, k_{eff} decreases. This trend can be seen in the following plots. The experimental model was modified for the temperature of each material as well as the number density of the moderator to reflect the change in density.

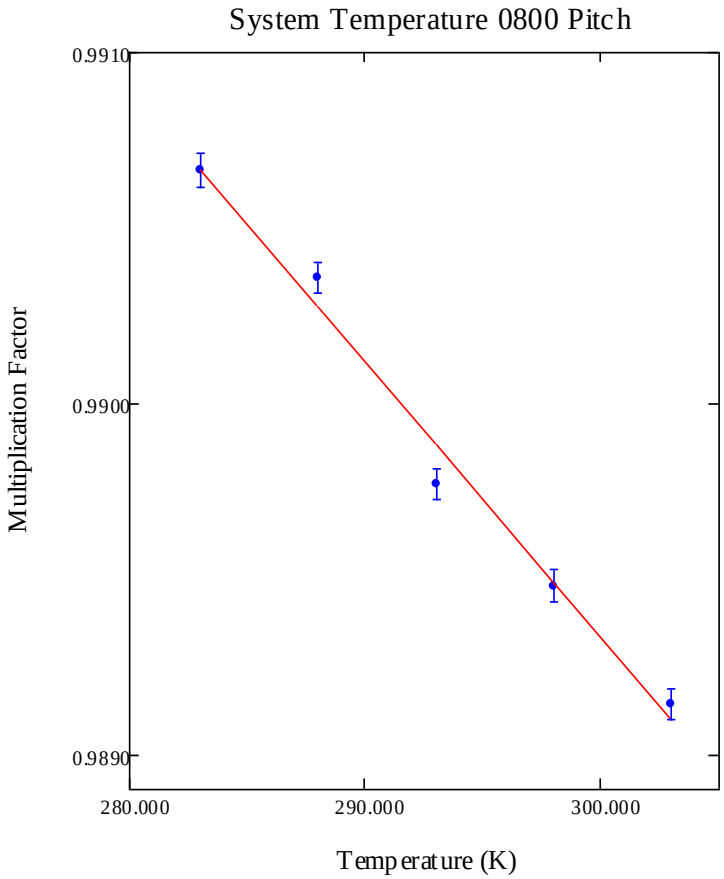

Figure 55. System Temperature 0.800 cm Pitch 7uPCX

www.manaraa.com

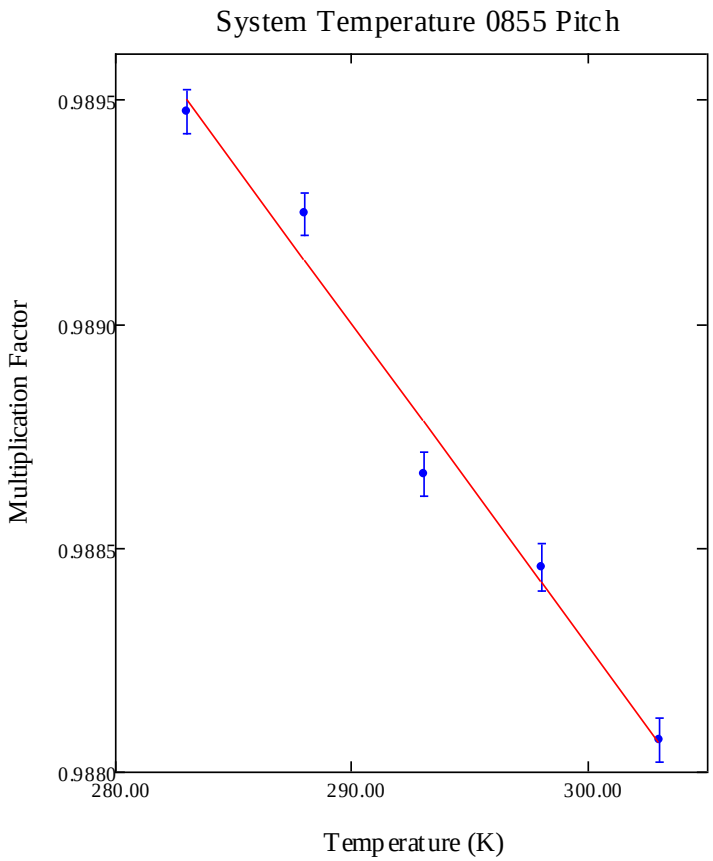

Figure 56. System Temperature 0.855 cm Pitch 7uPCX

The overall change in the temperature has a large effect on the multiplication factor. The change in multiplication factor is a result of Doppler Broadening, which occurs when temperatures are increased. From Duderstadt[16], Doppler broadening is described as the widening of resonances. When this process occurs, the resonance peak decreases and the width of resonance is widened; however, leaving the same area underneath the resonance. When the resonance is lower and wider, covering a larger interval of energies, the absorption probability increases.

www.manaraa.com

5.3.4 Direct Uncertainty Analysis Results 7uPCX

Table 35 and Table 36 display the results of the direct uncertainty analysis for the 7uPCX experiments.

Table 35. Direct Uncertainty Analysis 7uPCX 0.800 cm Pitch

	Direct Uncertainty Analysis				
Parameter	P Value	σ_P Unc.	$\Delta k/\Delta P$	Δk_{eff}	Sensitivity
Pitch	0.800 cm	0.00057 cm	1.1420 ± 0.0360 cm^{-1}	0.000651	0.9230 ± 0.0288
Clad OD	0.6376 cm	0.00016 cm	-1.0978 ± 0.0399 cm^{-1}	0.000176	-0.7071 ± 0.0254
Clad ID	0.5664 cm	0.00036 cm	-0.1152 ± 0.0036 cm^{-1}	0.000042	-0.0659 ± 0.0204
Fuel OD	0.5258 cm	0.00127 cm	-0.0248 ± 0.0115 cm^{-1}	0.000032	-0.0132 ± 0.0061
Fuel Height	48.77954 cm	0.00267 cm	-0.0018 ± 0.0052 cm^{-1}	0.000005	-0.0910 ± 0.2545
Enrichment	0.06903	0.000046	1.5006 ± 0.0564	0.000069	0.1046 ± 0.0039
Aluminum 6061 Comp.	1 c.u.	0.577 c.u.	-0.00029 ± 0.00005 $c.u.^{-1}$	0.000166	-0.000290 ± 0.000054
Aluminum 3003 Comp.	1 c.u.	0.577 c.u.	-0.00058 ± 0.00005 $c.u.^{-1}$	0.000331	-0.000580 ± 0.000051
Source Comp.	1 c.u.	0.577 c.u.	0.0000175 ± 0.0000551 $c.u.^{-1}$	0.000010	0.000018 ± 0.000055
Temp.	300 K	1 K	-0.000078 ± 0.000003 K^{-1}	0.000078	-0.02378 ± 0.00087
Sum in Quad.				0.001144	

www.manaraa.com

Table 36. Direct Uncertainty Analysis 7uPCX 0.855 cm Pitch

	Direct Uncertainty Analysis				
Parameter	P Value	σ_P Unc.	$\Delta k/\Delta P$	Δk_{eff}	Sensitivity
Pitch	0.855 cm	0.00060 cm	0.9271 ± 0.0338 cm^{-1}	0.00056	0.8014 ± 0.0289
Clad OD	0.6376 cm	0.00016 cm	-0.8842 ± 0.0174 cm^{-1}	0.000141	-0.5699 ± 0.0111
Clad ID	0.5664 cm	0.00036 cm	-0.1625 ± 0.0427 cm^{-1}	0.000059	-0.0931 ± 0.0219
Fuel OD	0.5258 cm	0.00127 cm	-0.0210 ± 0.0121 cm^{-1}	0.000027	-0.0112 ± 0.0064
Fuel Height	48.77954 cm	0.00267 cm	-0.00225 ± 0.0045	0.000006	-0.11113 ± 0.2182
Enrichment	0.06903	0.000046	1.8994 ± 0.0820	0.000087	0.1326 ± 0.0057
Aluminum 6061 Comp.	1 c.u.	0.577 c.u.	-0.000287 ± 0.000053 $c.u.^{-1}$	0.000166	-0.000290 ± 0.000053
Aluminum 3003 Comp.	1 c.u.	0.577 c.u.	-0.000529 ± 0.000053 $c.u.^{-1}$	0.000305	-0.000535 ± 0.000053
Source Comp.	1 c.u.	0.577 c.u.	0.000056 ± 0.000055 $c.u.^{-1}$	0.000032	0.000055 ± 0.000055
Temp.	300 cm	1 K	-0.000072 ± 0.0000003 K^{-1}	0.000072	-0.02183 ± 0.00093
Sum in Quad.				0.000961	

The results obtained for the direct uncertainty analysis for the seven percent experiment seem to offer a good representation of the parameters listed. These results will later be used to validate the uncertainty analysis presented in the following sections.

www.manaraa.com

CHATER 6

6.1 TSUNAMI-3D Evaluations

Each of the experiments was evaluated in the TSUNAMI-3D control module to determine the sensitivities to each of the mixtures in the system. TSUNAMI-3D was run with 10,000 generations and 10,000 neutrons per generation for the forward calculation and 2000 generations and 30,000 neutrons per generation for the adjoint calculation. The results of these calculations are displayed in tables for each experiment.

To ensure that the TSUNAMI-3D evaluations are valid, there are two suggested tests. The first is to determine the difference between the forward and the adjoint multiplication factor. It is recommended by the developers of the code that this difference be less than 0.5% for a good result. If the difference is greater than 0.5% the experiment model should be run with more generations and more neutrons per generation. The second check is to perform a direct perturbation for the nuclides that have the greatest sensitivity in the model. Both of these tests were performed here and are the results are presented below.

6.1.1 TSUNAMI-3D Check LCT023

As described above, the first test to determine the validity of the TSUNAMI-3D results is the difference between the forward and adjoint multiplication factor. The forward multiplication factor is 0.99498 ± 0.0005 and the adjoint multiplication factor is 0.99360 ± 0.0019, and the percent difference between the forward and adjoint multiplication factors is 0.14%.

www.manaraa.com

The second test was performed by individually perturbing the hydrogen (in the moderator), ^{235}U and ^{16}O (in the fuel) number densities. This determines the sensitivity to the nuclides, and a correlation to the TSUNAMI-3D sensitivity can be made to ensure that the TSUNAMI-3D results are good. Table 37 displays the results of that evaluation.

The TSUNAMI-3D Sensitivity is the sensitivity coefficient for the nuclide produced from TSUNAMI-3D, the keff is the multiplication factor for the various perturbations, the perturbation sensitivity is the calculated using Equation 65 and the relative difference is the Direct Perturbation sensitivity subtracted from the TSUNAMI-3D Sensitivity all divided by the Direct Perturbation Sensitivity.

$$S_{\alpha} = \frac{\alpha}{k}\left[\frac{k_{+} - k_{-}}{\alpha_{+} - \alpha_{-}}\right] \tag{65}$$

Table 37. LCT023 Direct Perturbation Calculations

Perturbation		TSUNAMI-3D Sensitivity	k_{eff}	Uncertainty in k_{eff}	Perturbation Sensitivity	Relative Difference
H (moderator)	6.6736E-02	2.39E-01			2.5991E-01	-8.0%
plus 2.00%	6.8071E-02		0.999729	0.000058		
minus 2.00%	6.5401E-02		0.989393	0.000048		
^{235}U	2.1577E-03	2.40E-01			2.3534E-01	2.0%
plus 2.00%	2.2009E-03		0.998756	0.000060		
minus 2.00%	2.1145E-03		0.989397	0.000058		
^{16}O (moderator)	3.3368E-02	5.58E-02			5.6026E-02	-0.40%
plus 2.00%	3.4035E-02		0.995221	0.000058		
minus 2.00%	3.2701E-02		0.992993	0.000059		
		Nominal Case	0.994182	0.000060		

www.manaraa.com

6.1.2 TSUNAMI-3D Check LCT070

The two tests were performed for the LCT070 case 6 experiment. The forward multiplication factor is 0.99732 ± 0.00049 and the adjoint multiplication factor is 0.99789 ± 0.00099, the percent difference is 0.057 %.

The direct perturbation calculations were completed and offered good results, indicating that the TSUNAMI-3D values are a good representation of the system.

Table 38. LCT070 Direct Perturbation Calculations

Perturbation		TSUNAMI-3D Sensitivity	k_{eff}	Uncertainty in k_{eff}	Perturbation Sensitivity	Relative Difference
H (moderator)	6.6762E-02	3.30E-01			3.38E-01	-2.4%
plus 2%	6.8097E-02		1.003866	0.000057		
minus 2%	6.5427E-02		0.990404	0.00084		
^{235}U	1.5920E-03	1.11E-01			1.14E-01	-2.6%
plus 1%	1.6079E-03		0.998257	0.000057		
minus 1%	1.5761E-03		0.995995	0.000056		
^{16}O (fuel)	4.8405E-02	2.12E-02			2.89E-02	-27%
plus 2%	4.9373E-02		0.997565	0.000052		
minus 2%	4.7437E-02		0.996414	0.000057		
		Nominal k_{eff}	0.996894	0.000057		

6.1.3 TSUNAMI-3D Check LCT079

The two tests were performed for the LCT079 case 1 experiment. The forward multiplication factor is 0.99146 ± 0.00018 and the adjoint multiplication factor is

www.manaraa.com

0.98990 ± 0.0013, and the percent difference is 0.16%. This shows that enough generations and neutrons per generation were run to obtain good statistics.

Table 39. Direct Perturbation Results LCT079

		TSUNAMI-3D Sensitivity	k_{eff}	Uncertainty in k_{eff}	Perturbation Sensitivity	Relative Difference
H (moderator)	6.6625E-02	3.50E-01			3.4424E-01	1.7%
plus 2%	6.7958E-02		0.998356	0.000057		
minus 2%	6.5293E-02		0.984701	0.000057		
^{235}U	1.0131E-03	1.44E-01			1.4813E-01	2.8%
plus 2%	1.0334E-03		0.994296	0.000058		
minus 2%	9.9284E-04		0.988420	0.000057		
^{16}O (fuel)	4.6888E-02	2.35E-02			2.8991E-02	-14%
plus 2%	4.7826E-02		0.992170	0.000059		
minus 2%	4.5950E-02		0.991020	0.000059		
		Nominal k_{eff}	0.991672	0.00057		

6.1.4 TSUNAMI-3D Check 7uPCX

The forward multiplication factor for the 0.800 cm pitch is 1.00340 ± 0.00049 and the adjoint multiplication factor is 1.00359 ± 0.00041, and a percent difference of 0.02%. The forward multiplication factor for the 0.855 cm pitch is 1.00082 ± 0.00047, the adjoint multiplication factor is 1.00150 ± 0.00130 and the percent difference is 0.07%.

www.manaraa.com

Table 40. 7uPCX Direct Perturbation Calculation 0.800 cm Pitch

Perturbation		TSUNAMI-3D Sensitivity	k_{eff}	Uncertainty in k_{eff}	Perturbation Sensitivity	Relative Difference
H (moderator)	6.6736E-02	3.53E-01			3.80E-01	-7.1%
plus 2%	6.8071E-02		0.996179	0.000043		
minus 2%	6.5401E-02		0.981151	0.000043		
^{235}U	1.6000E-03	1.21E-01			1.17E-01	3.4%
plus 2%	1.6320E-03		0.99102	0.000042		
minus 2%	1.5680E-03		0.986378	0.000045		
^{16}O (moderator)	3.3368E-02	3.58E-02			3.80E-02	-5.8%
plus 2%	3.4035E-02		0.989511	0.000043		
minus 2%	3.2701E-02		0.988008	0.000045		
		Nominal k_{eff}	0.988761	0.000044		

Table 41. 7uPCX Direct Perturbation Calculation 0.855 Pitch

Perturbation		TSUNAMI-3D Sensitivity	k_{eff}	Uncertainty in k_{eff}	Perturbation Sensitivity	Relative Difference
H (moderator)	6.6736E-02	3.67E-01			3.82E-01	-3.9%
plus 2%	6.8071E-02		0.997409	0.000042		
minus 2%	6.5401E-02		0.982278	0.000044		
^{235}U	1.6000E-03	1.13E-01			1.17E-01	-3.4%
plus 2%	1.6320E-03		0.99225	0.0019		
minus 2%	1.5680E-03		0.987629	0.000044		
^{16}O (moderator)	3.3368E-02	3.36E-02			3.53E-02	-4.8%
plus 2%	3.4035E-02		0.990561	0.000046		
minus 2%	3.2701E-02		0.989163	0.000043		
		Nominal k_{eff}	0.989929	0.000043		

The tests all gave good results, within the necessary percent difference to be useful. If the case had come up in which the percent difference was not sufficient, the cases were reevaluated to ensure the sensitivity coefficients are correct for the given system. This is a very important part of the process to be able to have confidence in the

www.manaraa.com

TSUNAMI-3D results. If these tests are not performed there is no way to ensure that the sensitivity coefficients adequately represent the system.

www.manaraa.com

6.2 Sensitivity Analysis with First Order Derivatives

Correlations for Direct Uncertainty Analysis to TSUNAMI Sensitivity Analysis

6.2.1. Physical Parameters

TSUNAMI-3D produces sensitivities to nuclear data. The work described below relates the sensitivities produced from TSUNAMI-3D to the physical dimension of a system to produce a sensitivity to a physical parameter, rather than just a nuclide or composition.

6.2.1 a. Fuel Diameter

The uncertainty in the fuel diameter is important due to the change in density associated with the change in diameter. The sensitivity was found by changing the fuel diameter by the uncertainty in the measured value. As described previously, TSUNAMI-3D outputs sensitivities to cross section data not physical parameters, therefore a set of equations were used and developed to correlate the sensitivities from TSUNAMI-3D to the direct uncertainty analysis.

The density of the fuel is represented by the equation below,

$$\rho_{UO_2} = \frac{m_{fuel}}{\pi\left(\frac{d_{fuel}}{2}\right)^2 h_{fuel}} \tag{66}$$

www.manaraa.com

where d_{fuel} is the diameter of the fuel, h_{fuel} is the fissile height, and m_{fuel} is the mass of the fuel.

The sensitivity of the multiplication factor to the fuel diameter is given by the following equation.

$$\frac{\frac{\partial k}{k}}{\frac{\partial d_{fuel}}{d_{fuel}}} = S_{d_{fuel}} \tag{67}$$

When the first derivative of the equation for the fuel density is taken with respect to the fuel diameter, the result is the following equation.

$$\frac{\partial \rho_{UO_2}}{\partial d_{fuel}} = -\frac{8m_{fuel}}{\pi d_{fuel}^3 h_{fuel}} \tag{68}$$

$$\partial \rho_{UO_2} = -\frac{8m_{fuel}}{\pi d_{fuel}^3 h_{fuel}} \partial d_{fuel} \tag{69}$$

$$\partial d_{fuel} = \partial \rho_{UO_2} \left(-\frac{\pi d_{fuel}^3 h_{fuel}}{8m_{fuel}} \right) \tag{70}$$

$$\frac{\frac{\partial k}{k}}{\frac{\partial d_{fuel}}{d_{fuel}}} = \frac{\frac{\partial k}{k}}{\frac{\partial \rho_{UO_2} \left(-\frac{\pi d_{fuel}^3 h_{fuel}}{8m_{fuel}} \right)}{d_{fuel}}} \tag{71}$$

www.manaraa.com

$$\frac{\frac{\partial k}{k}}{\frac{\partial d_{fuel}}{d_{fuel}}} = \frac{\frac{\partial k}{k}}{\frac{\partial \rho_{UO_2}}{\rho_{UO_2}}\left(-\frac{\pi d_{fuel}^3 h_{fuel}}{8 m_{fuel} d_{fuel}}\right)\frac{\rho_{UO_2}}{\rho_{UO_2}}}} \tag{72}$$

$$\frac{\frac{\partial k}{k}}{\frac{\partial d_{fuel}}{d_{fuel}}} = \frac{\frac{\partial k}{k}}{\frac{\partial \rho_{UO_2}}{\rho_{UO_2}}\left(-\frac{\pi d_{fuel}^2 h_{fuel}\rho_{UO_2}}{8 m_{fuel}}\right)} \tag{73}$$

$$\frac{\frac{\partial k}{k}}{\frac{\partial \rho_{UO_2}}{\rho_{UO_2}}} = S_{\rho_{UO_2}} \tag{74}$$

Equation 73 relates the sensitivity to the fuel density produced from TSUNAMI-3D to the physical parameters of the system. Equation 74 is the sensitivity to the fuel density produced from TSUNAMI-3D.

$$\frac{\frac{\partial k}{k}}{\frac{\partial d_{fuel}}{d_{fuel}}} = \frac{\frac{\partial k}{k}}{\frac{\partial \rho_{UO_2}}{\rho_{UO_2}}}\frac{-8 m_{fuel}}{\pi d_{fuel}^2 h_{fuel}\rho_{UO_2}} = S_{\rho_{UO_2}}\frac{-8 m_{fuel}}{\pi d_{fuel}^2 h_{fuel}\rho_{UO_2}} \tag{75}$$

The result of the analysis is the relationship between the change in fuel diameter and the change in the density of the fuel. Equation 75 can be further simplified by replacing the density of the fuel with Equation 66.

www.manaraa.com

$$\frac{\frac{\partial k}{k}}{\frac{\partial d_{fuel}}{d_{fuel}}} = S_{\rho_{UO_2}} \frac{-8m_{fuel}}{\pi d_{fuel}^2 h_{fuel} \left(\frac{m_{fuel}}{\pi \left(\frac{d_{fuel}}{2} \right)^2 h_{fuel}} \right)} \tag{76}$$

$$\frac{\frac{\partial k}{k}}{\frac{\partial d_{fuel}}{d_{fuel}}} = -2S_{\rho_{UO_2}} \tag{77}$$

The final result of the derivatives is a very simple relationship between the change in the outer fuel diameter and the sensitivity produced from TSUNAMI-3D evaluation. Application of Equation 77 is discussed later.

6.2.1 b. Outer Fuel Diameter with Central Hole

The fuel in the LCT070 benchmark experiment contains a central hole. This requires a different solution for the physical sensitivity to the outer fuel diameter. The first equation is the same relationship as the fuel outer diameter discussed about, except the fuel cross sectional area is for an annulus.

www.manaraa.com

$$\rho_{fuel} = \frac{m_{fuel}}{\pi\left(\frac{d_{out}^2 - d_{in}^2}{4}\right)h_{fuel}} \tag{78}$$

$$\frac{\partial \rho_{fuel}}{\partial d_{out}} = -\frac{8m_{fuel}d_{out}}{\pi\left(d_{in}^2 - d_{out}^2\right)^2 h_{fuel}} \tag{79}$$

$$\partial \rho_{fuel} = -\frac{8m_{fuel}d_{in}\partial d_{out}}{\pi\left(d_{in}^2 - d_{out}^2\right)^2 h_{fuel}} \tag{80}$$

$$\frac{\frac{\partial k}{k}}{\frac{\partial \rho_{fuel}}{\rho_{fuel}}} = \frac{\frac{\partial k}{k}}{\frac{-8m_{fuel}d_{out}\partial d_{out}\frac{d_{out}}{d_{out}}}{\pi\left(d_{in}^2 - d_{out}^2\right)^2 h_{fuel}\rho_{fuel}}} \tag{81}$$

$$\frac{\frac{\partial k}{k}}{\frac{\partial \rho_{fuel}}{\rho_{fuel}}} = \frac{\frac{\partial k}{k}}{\frac{\partial d_{out}}{d_{out}}\frac{-8m_{fuel}d_{out}^2}{\pi\left(d_{in}^2 - d_{out}^2\right)^2 h_{fuel}\rho_{fuel}}} \tag{82}$$

$$\frac{\frac{\partial k}{k}}{\frac{\partial d_{out}}{d_{out}}} = \frac{\frac{\partial k}{k}}{\frac{\partial \rho_{fuel}}{\rho_{fuel}}}\frac{-8m_{fuel}d_{out}^2}{\pi\left(d_{in}^2 - d_{out}^2\right)^2 h_{fuel}\rho_{fuel}} \tag{83}$$

$$\frac{\frac{\partial k}{k}}{\frac{\partial d_{out}}{d_{out}}} = S_{\rho_{UO_2}}\frac{-8m_{fuel}d_{out}^2}{\pi\left(d_{in}^2 - d_{out}^2\right)^2 h_{fuel}\rho_{fuel}} \tag{84}$$

www.manaraa.com

$$\frac{\frac{\partial k}{k}}{\frac{\partial d_{out}}{d_{out}}} = S_{\rho_{UO_2}} \frac{-8 m_{fuel} d_{out}^2}{\pi \left(d_{in}^2 - d_{out}^2\right)^2 h_{fuel} \left(\frac{m_{fuel}}{\pi \left(\frac{d_{out}^2 - d_{in}^2}{4} \right) h_{fuel}} \right)} \tag{85}$$

$$\frac{\frac{\partial k}{k}}{\frac{\partial d_{out}}{d_{out}}} = S_{\rho_{UO_2}} \frac{-8 m_{fuel} d_{out}^2}{\pi \left(d_{in}^2 - d_{out}^2\right)^2 h_{fuel} \left(\frac{m_{fuel}}{\pi \left(-\left(\frac{d_{in}^2 - d_{out}^2}{4} \right) \right) h_{fuel}} \right)} \tag{86}$$

$$\frac{\frac{\partial k}{k}}{\frac{\partial d_{out}}{d_{out}}} = S_{\rho_{UO_2}} \frac{2 d_{out}^2}{\left(d_{in}^2 - d_{out}^2\right)} \tag{87}$$

6.2.1 b. Fuel Inner Diameter

The variation in the central hole diameter of the fuel was made by modifying the diameter of the inner diameter of the fuel by the provided uncertainty. This modification required that the first derivative be taken with respect to the modified parameter (d_{in}).

$$\frac{\partial \rho_{fuel}}{\partial d_{in}} = \frac{d_{in} m_{fuel}}{2\pi \left(\frac{d_{in}^2 - d_{out}^2}{4} \right)^2 h_{fuel}} \tag{88}$$

$$\partial d_{in} = \frac{2\pi \left(\frac{d_{in}^2}{4} - \frac{d_{out}^2}{4} \right)^2 h_{fuel}}{d_{in} m_{fuel}} \partial \rho_{fuel} \tag{89}$$

www.manaraa.com

$$\partial d_{in}\frac{d_{in}}{d_{in}}=\frac{2\pi\left(\frac{d_{in}^2}{4}-\frac{d_{out}^2}{4}\right)^2 h_{fuel}}{d_{in}m_{fuel}}\partial\rho_{fuel}\frac{\rho_{fuel}}{\rho_{fuel}} \tag{90}$$

Equation 90 is multiplied by one on both sides, the left side is multiplied by the inner diameter of the fuel and the right side is multiplied by the density.

$$\frac{\partial d_{in}}{d_{in}}=\frac{2\pi\left(\frac{d_{in}^2}{4}-\frac{d_{out}^2}{4}\right)^2 \rho_{fuel}h_{fuel}}{d_{in}^2 m_{fuel}}\frac{\partial\rho_{fuel}}{\rho_{fuel}} \tag{91}$$

$$\frac{\frac{\partial k}{k}}{\frac{\partial d_{in}}{d_{in}}}=\frac{\frac{\partial k}{k}}{\frac{2\pi\left(\frac{d_{in}^2}{4}-\frac{d_{out}^2}{4}\right)^2 \rho_{fuel}h_{fuel}}{d_{in}^2 m_{fuel}}\frac{\partial\rho_{fuel}}{\rho_{fuel}}} \tag{92}$$

Equation 92 relates the change in the density of the fuel to the change in the inner diameter of the fuel.

$$\frac{\frac{\partial k}{k}}{\frac{\partial d_{in}}{d_{in}}}=\frac{\frac{\partial k}{k}}{\frac{\partial\rho_{fuel}}{\rho_{fuel}}}\frac{}{\frac{2\pi\left(\frac{d_{in}^2}{4}-\frac{d_{out}^2}{4}\right)^2 \rho_{fuel}h_{fuel}}{d_{in}^2 m_{fuel}}} \tag{93}$$

Equation 93 is rearranged to be in terms of the sensitivity of the fuel.

www.manaraa.com

$$\frac{\frac{\partial k}{k}}{\frac{\partial \rho_{fuel}}{\rho_{fuel}}} = S_{\rho_{fuel}} \tag{94}$$

Substituting Equation 94 into Equation 93 provides the final result to relate the physical change in the fuel inner diameter to the sensitivity that TSUNAMI-3D produces for the fuel mixture.

$$\frac{\frac{\partial k}{k}}{\frac{\partial d_{in}}{d_{in}}} = S_{\rho_{fuel}} \left[\frac{d_{in}^2 m_{fuel}}{2\pi \left(\frac{d_{in}^2}{4} - \frac{d_{out}^2}{4} \right)^2 \rho_{fuel} h_{fuel}} \right] \tag{95}$$

$$\frac{\frac{\partial k}{k}}{\frac{\partial d_{in}}{d_{in}}} = S_{\rho_{fuel}} \left[\frac{d_{in}^2 m_{fuel}}{2\pi \left(\frac{d_{in}^2}{4} - \frac{d_{out}^2}{4} \right)^2 \frac{m_{fuel}}{\pi \left(\frac{d_{out}^2 - d_{in}^2}{4} \right) h_{fuel}} h_{fuel}} \right] \tag{96}$$

$$\frac{\frac{\partial k}{k}}{\frac{\partial d_{in}}{d_{in}}} = S_{\rho_{fuel}} \frac{d_{in}^2}{2 \frac{\left(\frac{d_{in}^2}{4} - \frac{d_{out}^2}{4} \right)^2}{\left(\frac{d_{out}^2}{4} - \frac{d_{in}^2}{4} \right)}} \tag{97}$$

$$S_{d_{in}} = \frac{\frac{\partial k}{k}}{\frac{\partial d_{in}}{d_{in}}} = S_{\rho_{fuel}} \frac{d_{in}^2}{2 \left(\frac{d_{out}^2}{4} - \frac{d_{in}^2}{4} \right)} \tag{98}$$

www.manaraa.com

$$S_{d_{in}} = \frac{\frac{\partial k}{k}}{\frac{\partial d_{in}}{d_{in}}} = S_{\rho_{fuel}} \frac{-2d_{in}^2}{d_{in}^2 - d_{out}^2} \tag{99}$$

6.2.1 c. Clad Outer Diameter - Hexagonal Pitch

The variation in the clad outer diameter changes the amount of water present in the system. The derivative of the equation for the amount of water present in a unit cell is taken with respect to the density of the water and the clad outer diameter.

$$w = \left[\frac{\sqrt{3}}{2} P^2 - \pi \left(\frac{d}{2} \right)^2 \right] h \rho_{H_2O} \tag{100}$$

Equation 100 is for the amount of water in the hexagonal pitch in a unit cell, where:

w=mass of water in a triangular-pitched array cell

P=pitch

d=outer diameter of fuel element clad

h=height of fuel

ρ_{H_2O} =density of water

www.manaraa.com

The derivative of w is taken with respect to density of the water (Equation 101) and taken with respect to outer diameter of the fuel element clad (Equation 103).

$$\frac{\partial w}{\partial \rho_{H_2O}} = \left[\frac{\sqrt{3}}{2} P^2 - \pi \left(\frac{d}{2} \right)^2 \right] h \tag{101}$$

$$\partial w = \left[\frac{\sqrt{3}}{2} P^2 - \pi \left(\frac{d}{2} \right)^2 \right] h \partial \rho_{H_2O} \tag{102}$$

$$\frac{\partial w}{\partial d} = -\pi \frac{d}{2} h \rho_{H_2O} \tag{103}$$

$$\partial w = -\pi \frac{d}{2} h \rho_{H_2O} \partial d \tag{104}$$

Equation 105 is obtained by setting Equations 102 and 104 equal to one another.

$$\left[-\pi \left(\frac{d}{2} \right)^2 \right] h \rho_{H_2O} \partial d = \left[\frac{\sqrt{3}}{2} P^2 - \pi \left(\frac{d}{2} \right)^2 \right] h \partial \rho_{H_2O} \tag{105}$$

Rearranging Equation 105 in terms of the change of the water density results in Equation 106.

$$\frac{\partial \rho_{H_2O}}{\rho_{H_2O}} = \frac{-\pi \frac{d}{2} h}{\left[\frac{\sqrt{3}}{2} P^2 - \pi \left(\frac{d}{2} \right)^2 \right] h} \partial d \tag{106}$$

$$\frac{\partial \rho_{H_2O}}{\rho_{H_2O}} = \frac{-\pi}{\sqrt{3} \left(\frac{P}{d} \right)^2 - \frac{\pi}{2}} \frac{\partial d}{d} \tag{107}$$

www.manaraa.com

Finally, the equation can be formatted in terms of the change in the multiplication factor versus the change in the clad outer diameter (Equation 108).

$$\frac{\frac{\delta k}{k}}{\frac{\delta d}{d}} = \frac{\frac{\delta k}{k}}{\frac{\delta \rho_{H_2O}}{\rho_{H_2O}} \frac{\sqrt{3}\left(\frac{P}{d}\right)^2 - \frac{\pi}{2}}{-\pi}} \tag{108}$$

$$\frac{\frac{\partial k}{k}}{\frac{\partial \rho_{H_2O}}{\rho_{H_2O}}} = S_{\rho_{H_2O}} \tag{109}$$

Equation 109 is the sensitivity to the water that is determined from TSUNAMI-3D.

$$\frac{\frac{\partial k}{k}}{\frac{\partial d}{d}} = \frac{\frac{\partial k}{k}}{\frac{\partial \rho_{H_2O}}{\rho_{H_2O}}} \frac{\sqrt{3}\left(\frac{P}{d}\right)^2 - \frac{\pi}{2}}{-\pi} \tag{110}$$

$$\frac{\frac{\partial k}{k}}{\frac{\partial d}{d}} = S_{\rho_{H_2O}} \frac{-\pi}{\sqrt{3}\left(\frac{P}{d}\right)^2 - \frac{\pi}{2}} \tag{111}$$

Equation 110 is the sensitivity of the clad outer diameter on k_{eff}. Equation 111 is rearranged in terms of $S_{\rho_{H_2O}}$, such that the final relationship is the sensitivity to the clad outer diameter with respect to the sensitivity to water.

www.manaraa.com

6.2.1 c. Clad Outer Diameter - Square Pitch

The process for the derivation of the sensitivity to the clad outer diameter for a square pitched system is the same as the hexagonal pitched system, however, the equation that represents the mass of water in the system is different (Equation 112).

$$w = \left[P^2 - \pi \left(\frac{d_{clad}}{2} \right)^2 \right] h_{clad} \rho_{H_2O} \tag{112}$$

$$\frac{\partial w}{\partial \rho_{H_2O}} = \left[P^2 - \pi \left(\frac{d_{clad}}{2} \right)^2 \right] h_{clad} \tag{113}$$

$$\partial w = \left[P^2 - \pi \left(\frac{d_{clad}}{2} \right)^2 \right] h_{clad} \partial \rho_{H_2O} \tag{114}$$

$$\frac{\partial w}{\partial d_{clad}} = \frac{-\pi d_{clad} h_{clad} \rho_{H_2O}}{2} \tag{115}$$

$$\partial w = \frac{-\pi d_{clad} h_{clad} \rho_{H_2O}}{2} \partial d_{clad} \tag{116}$$

$$\left[P^2 - \pi \left(\frac{d_{clad}}{2} \right)^2 \right] h_{clad} \partial \rho_{H_2O} = \frac{-\pi d_{clad} h_{clad} \rho_{H_2O}}{2} \partial d_{clad} \tag{117}$$

$$\frac{\partial \rho_{H_2O}}{\rho_{H_2O}} = \frac{\frac{-\pi d_{clad} h_{clad}}{2}}{\left[P^2 - \pi \left(\frac{d_{clad}}{2} \right)^2 \right] h_{clad}} \partial d_{clad} \tag{118}$$

www.manaraa.com

$$\frac{\partial \rho_{H_2O}}{\rho_{H_2O}} = \frac{\frac{-\pi d_{clad}}{2}}{\left[P^2 - \pi\left(\frac{d_{clad}}{2}\right)^2\right]} \partial d_{clad} \frac{d_{clad}}{d_{clad}} \tag{119}$$

$$\frac{\partial \rho_{H_2O}}{\rho_{H_2O}} = \frac{-\pi d_{clad}^2}{2\left[P^2 - \pi\left(\frac{d_{clad}}{2}\right)^2\right]} \frac{\partial d_{clad}}{d_{clad}} \tag{120}$$

$$\frac{\frac{\partial k}{k}}{\frac{\partial d_{clad}}{d_{clad}}} = \frac{\frac{\partial k}{k}}{\frac{\partial \rho_{H_2O}}{\rho_{H_2O}}} \left[\frac{\left[P^2 - \pi\left(\frac{d_{clad}}{2}\right)^2\right]}{-\pi d_{clad}^2}\right] \tag{121}$$

$$\frac{\frac{\partial k}{k}}{\frac{\partial d_{clad}}{d_{clad}}} = S_{\rho_{H_2O}} \left[\frac{-\pi d_{clad}^2}{\left[P^2 - \pi\left(\frac{d_{clad}}{2}\right)^2\right]}\right] \tag{122}$$

6.2.1 d. Clad Thickness

The sensitivity to the clad thickness depends mostly on the cladding material. Cladding material composed of Aluminum or Zircaloy have little effect on the system because the absorption cross sections are small, however, cladding material composed of stainless steel has a larger effect given that the absorption cross section is larger. The effect that is seen with changing the clad thickness is the absorption of neutrons with a thicker/thinner material between fuel rods.

www.manaraa.com

Relating the change in the inner clad diameter with the change in clad density is shown below.

$$\rho_{clad} = \frac{4m_{clad}}{\pi\left(d_{out}{}^2 - d_{in}{}^2\right)l_{clad}} \tag{123}$$

$$\frac{\partial\rho_{clad}}{\partial d_{in}} = \frac{8m_{clad}d_{in}}{\pi\left(d_{out}{}^2 - d_{in}{}^2\right)^2 l_{clad}} \tag{124}$$

$$\frac{\frac{\partial k}{k}}{\frac{\partial d_{in}}{d_{in}}} = \frac{\frac{\partial k}{k}}{\frac{\partial\rho_{clad}}{\rho_{clad}}\frac{l_{clad}\pi\left(d_{in}{}^2 - d_{out}{}^2\right)^2\rho_{clad}}{8m_{clad}d_{in}{}^2}} \tag{125}$$

$$\frac{\frac{\partial k}{k}}{\frac{\partial d_{in}}{d_{in}}} = \frac{\frac{\partial k}{k}}{\frac{\partial\rho_{clad}}{\rho_{clad}}\frac{l_{clad}\pi\left(d_{in}{}^2 - d_{out}{}^2\right)^2\rho_{clad}}{8m_{clad}d_{in}{}^2}} \tag{126}$$

$$\frac{\frac{\partial k}{k}}{\frac{\partial d_{in}}{d_{in}}} = \frac{\frac{\partial k}{k}}{\frac{\partial\rho_{clad}}{\rho_{clad}}}\frac{}{\frac{l_{clad}\pi\left(d_{in}{}^2 - d_{out}{}^2\right)^2\rho_{clad}}{8m_{clad}d_{in}{}^2}} \tag{127}$$

$$\frac{\frac{\partial k}{k}}{\frac{\partial d_{in}}{d_{in}}} = S_{\rho_{clad}}\frac{8m_{clad}d_{in}{}^2}{l_{clad}\pi\left(d_{in}{}^2 - d_{out}{}^2\right)^2\rho_{clad}} \tag{128}$$

$$\frac{\frac{\partial k}{k}}{\frac{\partial d_{in}}{d_{in}}} = S_{\rho_{clad}}\frac{8m_{clad}d_{in}{}^2}{l_{clad}\pi\left(d_{in}{}^2 - d_{out}{}^2\right)^2\frac{m_{clad}}{\pi\left(\frac{d_{out}^2 - d_{in}^2}{4}\right)l_{clad}}} \tag{129}$$

www.manaraa.com

$$\frac{\frac{\partial k}{k}}{\frac{\partial d_{in}}{d_{in}}} = S_{\rho_{clad}} \frac{2{d_{in}}^2}{\frac{\left({d_{in}}^2 - {d_{out}}^2\right)^2}{-\left(d_{in}^2 - d_{out}^2\right)}} \tag{130}$$

$$\frac{\frac{\partial k}{k}}{\frac{\partial d_{in}}{d_{in}}} = S_{\rho_{clad}} \frac{-2{d_{in}}^2}{\left({d_{out}}^2 - {d_{in}}^2\right)} \tag{131}$$

The result shows that the sensitivity of the clad material from TSUNAMI-3D, $S_{\rho clad}$, can be related with the physical quantities.

6.2.1 e. Hexagonal Pitch

The change in pitch changes the amount of water that is present in a unit cell. Starting with the equation for the mass of water in a unit cell (Equation 100) and taking the derivative with respect to density and taking the derivative with respect to the pitch, allows for a correlation with the sensitivity to the water. After taking the derivatives the two equations are set equal to one another (Equation 134).

$$\frac{\partial w}{\partial \rho_{H_2O}} = \left[\frac{\sqrt{3}}{2}P^2 - \pi\left(\frac{d_{clad}}{2}\right)^2\right]h \tag{132}$$

$$\frac{\partial w}{\partial P} = \sqrt{3}Ph\rho_{H_2O} \tag{133}$$

$$\frac{\partial w}{\partial \rho_{H_2O}} = \frac{\partial w}{\partial P} \tag{134}$$

www.manaraa.com

$$\frac{\frac{\partial k}{k}}{\frac{\partial P}{P}} = \frac{\frac{\partial k}{k}}{\frac{\partial \rho_{H_2O}}{\rho_{H_2O}}\left[\frac{\frac{\sqrt{3}}{2}P^2 - \pi\left(\frac{d_{clad}}{2}\right)^2 h}{P^2 h\sqrt{3}}\right]} \tag{135}$$

$$\frac{\frac{\partial k}{k}}{\frac{\partial P}{P}} = S_{\rho_{H_2O}} \frac{\sqrt{3}P^2}{\frac{\sqrt{3}}{2}P^2 - \pi\left(\frac{d_{clad}}{2}\right)^2} \tag{136}$$

The sensitivity of the pitch is related to the sensitivity to the water in the system, given the physical parameters of the system.

6.2.1 f. Square Pitch

The same process is performed for a square pitch; the only difference is the equation the represents the mass of water in the unit cell. The following equation is for the square pitch.

$$\frac{\partial w}{\partial \rho_{H_2O}} = \left[P^2 - \pi\left(\frac{d_{clad}}{2}\right)^2\right] h \tag{137}$$

$$\frac{\partial w}{\partial P} = 2Ph\rho_{H_2O} \tag{138}$$

$$\frac{\partial w}{\partial \rho_{H_2O}} = \frac{\partial w}{\partial P} \tag{139}$$

www.manaraa.com

$$\frac{\frac{\partial k}{k}}{\frac{\partial P}{P}} = \frac{\frac{\partial k}{k}}{\frac{\partial \rho_{H_2O}}{\rho_{H_2O}} \frac{\left[P^2 - \pi\left(\frac{d_{clad}}{2}\right)^2\right]h}{2Ph\rho_{H_2O}}} \tag{140}$$

$$\frac{\frac{\partial k}{k}}{\frac{\partial P}{P}} = \frac{\frac{\partial k}{k}}{\frac{\partial \rho_{H_2O}}{\rho_{H_2O}} \frac{\left[P^2 - \pi\left(\frac{d_{clad}}{2}\right)^2\right]h}{2P^2h}} \tag{141}$$

$$\frac{\frac{\partial k}{k}}{\frac{\partial P}{P}} = S_{\rho_{H_2O}} \frac{\left[P^2 - \pi\left(\frac{d_{clad}}{2}\right)^2\right]}{2P^2} \tag{142}$$

$$\frac{\frac{\partial k}{k}}{\frac{\partial P}{P}} = S_{\rho_{H_2O}} \frac{2P^2}{P^2 - \pi\left(\frac{d_{clad}}{2}\right)^2} \tag{143}$$

6.2.1 g. Fissile Column Height

The sensitivity to the height of the fuel depends on the type of system and the relationship between the level of the moderator and the fuel height. If the moderator is below the height of the fuel, adding material to the top of the fuel will have very small (if any) effect on the system. For the opposite case, in which the height of the moderator is above the fuel, adding material, adds fissile material to the core where the neutron

www.manaraa.com

production can be increased, having a large effect on the system. Equation 144 is the density for the fuel in one rod.

$$\rho_{fuel} = \frac{m_{fuel}}{\pi\left(\frac{d_{fuel}}{2}\right)^2 h_{fuel}} \tag{144}$$

$$\frac{\partial \rho_{fuel}}{\partial h_{fuel}} = \frac{-4m_{fuel}}{\pi d_{fuel}^2 h_{fuel}^2} \tag{145}$$

$$\partial h_{fuel} = \frac{\pi d_{fuel}^2 h_{fuel}^2}{-4m_{fuel}} \partial \rho_{fuel} \tag{146}$$

$$\frac{\frac{\partial k}{k}}{\frac{\partial h_{fuel}}{h_{fuel}}} = \frac{\frac{\partial k}{k}}{\frac{\partial \rho_{fuel}}{\rho_{fuel}} \frac{\pi d_{fuel}^2 h_{fuel} \rho_{fuel}}{-4m_{fuel}}} \tag{147}$$

$$\frac{\frac{\partial k}{k}}{\frac{\partial h_{fuel}}{h_{fuel}}} = \frac{\frac{\partial k}{k}}{\frac{\partial \rho_{fuel}}{\rho_{fuel}}} \frac{-4m_{fuel}}{\pi d_{fuel}^2 h_{fuel} \rho_{fuel}} \tag{148}$$

$$\frac{\frac{\partial k}{k}}{\frac{\partial h_{fuel}}{h_{fuel}}} = \frac{\frac{\partial k}{k}}{\frac{\partial \rho_{fuel}}{\rho_{fuel}}} \frac{-4m_{fuel}}{\pi d_{fuel}^2 h_{fuel} \frac{m_{fuel}}{\pi\left(\frac{d_{fuel}}{2}\right)^2 h_{fuel}}} \tag{149}$$

$$\frac{\frac{\partial k}{k}}{\frac{\partial h_{fuel}}{h_{fuel}}} = \frac{\frac{\partial k}{k}}{\frac{\partial \rho_{fuel}}{\rho_{fuel}}} (-1) \tag{150}$$

www.manaraa.com

$$\frac{\frac{\partial k}{k}}{\frac{\partial h_{fuel}}{h_{fuel}}} = -1S_{\rho_{fuel}} \tag{151}$$

6.2.2. Material Parameters

6.2.2 a. Enrichment

The enrichment was expected to be a direct correlation between the individual sensitivity analysis and the TSUNAMI-3D sensitivity analysis.

The same method that was applied for the physical parameters was applied for the enrichment. Below are the two equations for the number densities of ^{235}U and ^{238}U.

$$N_{235} = \frac{\rho_{mix} wt.\%_{235} N_A}{A_{235}} \tag{152}$$

$$N_{238} = \frac{\rho_{mix} wt.\%_{238} N_A}{A_{238}} \tag{153}$$

The ^{235}U and ^{238}U are the two number densities in the fuel being evaluated because they are the only two number densities that are modified in the direct uncertainty analysis process. The sensitivity to the enrichment (from TSUNAMI-3D) is represented by the following equation

$$\frac{\frac{\partial k}{k}}{\frac{\partial N_{Enrich}}{N_{Enrich}}} = S_{Enrich} = \frac{\frac{\partial k}{k}}{\frac{\partial N_{235}}{N_{235}}} = S_{235} \tag{154}$$

www.manaraa.com

$$\Delta N_{235} A_{235} + \Delta N_{238} A_{238} = 0. \tag{155}$$

Equation 159 is the mass relationship for the change in the enrichment, the equation maintains a constant mass.

Equation 160 is Equation 159 rearranged in terms of the change in the ^{235}U number density.

$$\Delta N_{238} = -\Delta N_{235} \frac{A_{235}}{A_{238}} \tag{156}$$

Equation 161 is equation 157 divided by Equation 157.

$$\frac{N_{238}}{N_{235}} = \frac{\frac{w_{238}\rho_U N_A}{A_{238}}}{\frac{w_{235}\rho_U N_A}{A_{235}}} \frac{w_{238}}{w_{235}} \frac{A_{235}}{A_{238}} \tag{157}$$

Equation 162 simplifies Equation 161.

$$N_{238} = N_{235} \frac{w_{238}}{w_{235}} \frac{A_{235}}{A_{238}} \tag{158}$$

The next step is to take Equation 160 and divide both sides by the number density of ^{238}U, and then replace that variable with the equation for the number density of ^{238}U (Equation 164).

www.manaraa.com

$$\frac{\Delta N_{238}}{N_{238}} = \frac{-\Delta N_{235}}{N_{238}} \frac{A_{235}}{A_{238}} \tag{159}$$

$$\frac{\Delta N_{238}}{N_{238}} = \frac{-\Delta N_{235}}{N_{235} \frac{w_{238}}{w_{235}} \frac{A_{235}}{A_{238}}} \frac{A_{235}}{A_{238}} = \frac{-\Delta N_{235}}{N_{235}} \frac{w_{235}}{w_{238}} \tag{160}$$

The relationship between the change in the enrichment is represented by the following equation.

$$\frac{\Delta k}{k} = \frac{\Delta k_{235}}{k} + \frac{\Delta k_{238}}{k} \tag{161}$$

The sensitivity produced from TSUNAMI-3D for the enrichment (or ^{235}U number density) is given by Equation 166 and Equation 167 is the sensitivity for the ^{238}U number density.

$$S_{235} = \frac{\frac{\Delta k_{235}}{k}}{\frac{\Delta N_{235}}{N_{235}}} \tag{162}$$

$$S_{238} = \frac{\frac{\Delta k_{238}}{k}}{\frac{\Delta N_{238}}{N_{238}}} \tag{163}$$

Equations 167 and 166 are then rearranged and substituted into Equation 165.

www.manaraa.com

$$\frac{\Delta k}{k} = S_{235}\frac{\Delta N_{235}}{N_{235}} + S_{238}\frac{\Delta N_{238}}{N_{238}} \tag{164}$$

Next replacing the relationship shown earlier (Equation 164), the sensitivity to the enrichment is obtained.

$$\frac{\Delta k}{k} = S_{235}\frac{\Delta N_{235}}{N_{235}} + S_{238}\left(\frac{-\Delta N_{235}}{N_{235}}\frac{w_{235}}{w_{238}}\right) \tag{165}$$

$$\frac{\frac{\Delta k}{k}}{\frac{\Delta N_{235}}{N_{235}}} = S_{235} - S_{238}\frac{w_{235}}{w_{238}} \tag{166}$$

Equation 170 is the final result for the sensitivity to the enrichment given the weight fractions of ^{235}U and ^{238}U and the sensitivities produced from TSUNAMI-3D. Precaution should be taken when using the above relationship. The weight fractions of the ^{235}U and ^{238}U nuclide should be entered in the same form that they would be perturbed in the direct uncertainty analysis (either as percent or as decimal).

6.2.2 b. Temperature

The change in temperature is related to the change in density of the water. Equation 158 was determined from fitting a second order polynomial to a large set of data for the properties of water from the NIST WebBook website. Figure 57 displays the plot that was produced to obtain Equation 167.

www.manaraa.com

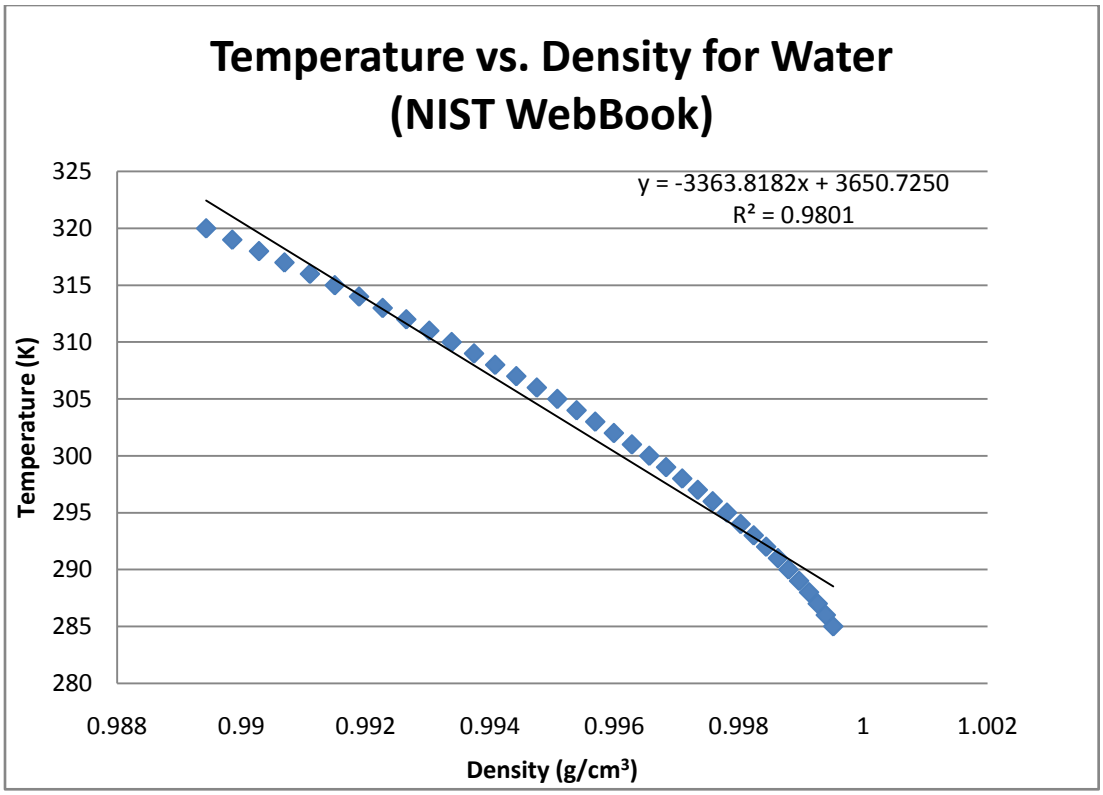

Figure 57. Plot of Water Density and Temperature Values

$$T = -3363.8182\rho_{H_2O} + 3650.7250 \tag{167}$$

This equation had an R^2 value of 0.9801. In the above equation, T is the temperature in units of Kelvin and ρ_{H_2O} is the density in units of g/cm^3. This derivative of this equation was taken with respect to density, and the following relationship was found.

www.manaraa.com

$$\frac{\partial T}{\partial \rho_{H_2O}} = -3363.8182 \tag{168}$$

$$\partial T = -3363.8282 \partial \rho_{H_2O} \tag{169}$$

$$\frac{\frac{\partial k}{k}}{\frac{\partial T}{T}} = \frac{\frac{\partial k}{k}}{\frac{\partial \rho_{H_2O}}{\rho_{H_2O}}\left(-3363.8182\right)\frac{\rho_{H_2O}}{T}} \tag{170}$$

$$\frac{\frac{\partial k}{k}}{\frac{\partial T}{T}} = \frac{S_{\rho_{H_2O}}}{-3363.8182\,\frac{\rho_{H_2O}}{T}} \tag{171}$$

Equation 171 is the sensitivity to the temperature in terms of the sensitivity produced from TSUNAMI-3D.

6.2.2 c. Grid Plate Material Composition

The grid plates that hold the fuel rods in place are usually made out of aluminum or a steel material. The process to determine the sensitivity of that material in the systems is to change the amount of absorption in that material. This is accomplished by determining the range of the weight fractions for the nuclides in the material and adjusting those weight fractions based upon the absorption cross sections in that material. A more detailed discussion is in section 5.4.2 c, d and e.

www.manaraa.com

6.2.2 d. Clad Material Composition

The cladding material can be a very important factor in the overall multiplication factor of the system. If the material should contain a greater weight fraction of a material with a larger absorption cross section, this can greatly affect the system.

6.2.2 e. Source Capsule Material Composition

When performing a critical experiment, a start up source is needed. Although the amount of material present in the system is very small, (i.e., one source rod versus thousands of fuel rods), the sensitivity of that rod being present in the system should still be analyzed. The process is the same as described above for the grid plate and the clad material.

www.manaraa.com

6.3 LCT023 TSUNAMI Correlation

The TSUNAMI-3D correlations allow for the equations developed in the previous sections and the sensitivity analysis performed by the code TSUNAMI-3D to be utilized to obtain the sensitivities for each parameter for an experiment. The following tables display the sensitivities obtained from the TSUNAMI-3D analysis for LCT023.

Table 42. LCT023 Sensitivity Coefficients from TSUNAMI-3D

LCT023 Case1	Mixture	Sensitivity	Standard Dev.	% Std. Dev.
Fuel	1	2.24E-01	3.54E-04	0.16
SS (clad)	2	-5.21E-02	8.08E-05	0.23
Water	3	2.95E-01	6.66E-03	0.27
Duralumin (Grid Plates)	4	2.74E-03	3.60E-05	0.58
Water (reflector)	5	9.30E-03	3.30E-03	7.00
^{235}U	1	2.40E-01	3.43E-04	0.14
^{238}U	1	-2.48E-02	6.06E-05	0.24

Table 43 displays the values for the sensitivity analysis performed with SCALE 5.1 KENO V.a 238 groupndf5. The purpose of performing this analysis individually is to ensure that the process for determining the sensitivities is well understood while also ensuring that the computer model compares well with the benchmark evaluations. Slight variations might occur with a newer cross section set but the multiplication factor should still be with the standard uncertainty or bias.

www.manaraa.com

Table 43. Direct Uncertainty Analysis with SAFOD LCT023

	Direct Analysis		SAFOD		
Parameter	Sensitivity	Uncertainty in Sensitivity	Sensitivity	Uncertainty in Sensitivity	Relative Difference
Pitch of Fuel Rods	-0.1591	0.0025	0.6674	0.0151	-520%
External Diameter of Fuel Rod Clad	-0.0906	0.0044	-0.0806	0.0018	-11%
Fuel Pellet Diameter	0.0461	0.0017	-0.2242	0.0004	-586%
Clad Mass and Composition	-0.0538	0.0002	-0.0522	0.0001	-3%
Fuel Mass	0.2232	0.0057	0.2242	0.0004	0%
Enrichment	0.2373	0.0021	0.2430	0.0003	2%
Fuel Density	0.2183	0.0043	0.2242	0.0004	3%
Fuel Height	-0.2099	0.0051	-0.2242	0.0004	7%

Table 43 also displays the values obtained from the SAFOD Analysis, using the equations developed in Chapter 6. The sensitivity is the change in the multiplication factor divided by the change in the parameter, multiplied by the parameter divided by the nominal multiplication.

The relative difference column was determined using a standard relative difference equation.

$$relative\_diff = \frac{calculated\_result - \exp ected\_result}{\exp ected\_result} \quad (172)$$

The expected result is the direct uncertainty analysis results and the calculated result is the SAFOD analysis result.

The results work well for some parameters, rod outer diameter, clad mass and composition, enrichment, and fuel density. The results are poor for the pitch, and fuel

www.manaraa.com

pellet diameter. A possible answer for this is that this particular system inhibits the ability to adequately represent particular parameters for the sensitivity analysis. TSUNAMI-3D should be able to give a good approximation for the sensitivity to the water in the system but because the system has such a low critical water height compared to fuel height or width of the reactor, this might cause a discrepancy in the results from TSUNAMI-3D.

This particular experiment is rather different than the other experiments explored in this analysis. The small pancake reactor design makes for a different analysis. From the Thesis Analysis, the parameters related to the amount of water in the system have the largest percent errors from the benchmark evaluation. This could be attributed to the moderation condition of the system. Specifically, the pitch suggests that the system is over moderated while the clad outer diameter suggests that the system is under moderated.

www.manaraa.com

6.4 LCT070 TSUNAMI Correlation

The following table displays the sensitivities obtained from TSUNAMI-3D for each mixture present in the system.

Table 44. Sensitivities from TSUNAMI-3D for LCT070

Mixture Name	Mixture Number	Sensitivity	Standard Deviation	% Standard Deviation
Fuel	1	4.87080E-02	4.59400E-04	0.94
Clad, Plugs, and Ends	2	8.36010E-03	9.98140E-05	1.19
Moderator and Reflector	3	3.48250E-01	1.61250E-03	0.46
Grid Plate Stainless Steel	4	5.15270E-05	1.25260E-05	24.31
Aluminum Alloy	5	8.10490E-05	1.26200E-05	15.57
Oxygen	6	-9.52890E-06	4.57650E-08	0.48
Clad, Plugs, and Ends	7	5.35280E-04	1.08340E-05	2.02
Reflector	8	2.63120E-02	1.36420E-02	51.85
Aluminum Alloy	9	7.10620E-05	7.98660E-06	11.24
^{235}U	1	1.11E-01	2.61960E-04	0.25
^{238}U	1	-8.04E-02	2.01730E-04	0.24

Table 45 displays the results of the equations developed in Chapter 6. The percent difference column is the difference between the direct uncertainty analysis benchmark evaluation sensitivity and the thesis analysis evaluation, divided by the benchmark evaluation sensitivity. The enrichment, fuel diameter, and clad outer diameter match the best.

www.manaraa.com

Table 45. Direct Uncertainty Analysis with SAFOD LCT070 Case 6

	Direct Analysis		SAFOD		
Parameter	Sensitivity	Uncertainty in Sensitivity	Sensitivity	Uncertainty in Sensitivity	Relative Difference
Enrichment (wt. %)	0.11261	0.00019	0.1164	0.0002	3%
Pitch (cm)	1.39955	0.00424	1.8012	0.0083	29%
Fuel Diameter (cm)	-0.05859	0.00403	-0.0512	0.0005	-13%
Fissile Column Height (cm)	-0.02906	0.00004	-0.0487	0.0005	68%
Fuel Density (g/cc)	0.06400	0.00037	0.0487	0.0005	-24%
Clad OD (cm)	-1.02687	0.03780	-1.1073	0.0051	8%
Temperature (K)	-0.01889	0.00007	-0.0302	0.0001	60%
Clad Inner Diameter	-0.09182	0.01484	-0.0030	0.0001	-97%
Central Hole Diameter	0.000973	0.000510	0.00251	0.00002	158%

www.manaraa.com

6.5 LCT079 TSUNAMI Correlation

Table 46 presents the results of the TSUNAMI-3D sensitivity analysis. The sensitivity is for the corresponding mixture.

Table 46. LCT079 Sensitivity Coefficients from TSUNAMI-3D

	Sensitivity	Std. Dev	% Std. Dev
1 Fuel	9.49E-02	3.66E-04	0.39
2 Zircaloy	6.82E-03	3.87E-05	0.57
3 Water (unit cell)	3.85E-01	2.26E-03	0.59
4 6061 Aluminum	2.24E-03	2.53E-05	1.13
5 304 Stainless Steel	-2.26E-04	9.59E-06	4.24
7 Water (outside)	3.06E-02	7.69E-03	25.12
^{235}U	1.44E-01	2.60E-04	0.18
^{238}U	-7.12E-02	1.49E-04	0.21

Table 47 displays the results for the direct uncertainty analysis. The benchmark evaluation $\Delta k/\Delta p$ is the values from the benchmark evaluation. The direct uncertainty analysis is the analysis performed to ensure that the process for determining the sensitivities is correct as well the model in the computer code used in the work offers the same result, within the expected uncertainty and the bias.

The relative difference is the difference between the direct uncertainty evaluation and the thesis analysis value, divided by the direct uncertainty analysis value. The enrichment and clad outer diameter match the best with the benchmark evaluation. It should be noted that the Aluminum composition is close to the benchmark evaluation, however, it was expected that these values be a lot closer (within 10%) to the expected value. The reason behind this is because the composition sensitivity is what TSUNAMI-3D generates and therefore should match.

www.manaraa.com

Table 47. Direct Uncertainty Analysis with SAFOD Analysis LCT079

	Direct Analysis		SAFOD		
Parameter	Sensitivity	Uncertainty in Sensitivity	Sensitivity	Uncertainty in Sensitivity	Relative Difference
Pitch (cm)	0.79947	0.00764	0.33357	0.00128	-58.3%
Clad OD (cm)	-0.56275	0.00269	-0.58747	0.00344	4.4%
Clad Thickness (cm)	-0.12891	0.00214	0.10227	0.00058	-179.3%
Fuel OD (cm)	-0.03008	0.00257	-0.09491	0.00037	215.5%
Fuel Enrichment	0.14830	0.00043	0.14755	0.00025	-0.5%
Clad Composition (c.u)	-0.00037	0.00007	0.00068	0.000004	-285.1%
Aluminum Composition (c.u.)	-0.00019	0.00007	0.00022	0.000003	-220.4%
Source Composition (c.u)	-0.00008	0.00005	-0.00002	0.000001	-72.1%
Temperature (K)	-0.01796	0.00057	-0.03358	0.00020	87.0%

www.manaraa.com

6.6 7uPCX TSUNAMI Correlation

The TSUNAMI correlation allows for the equations developed in Chapter 6 and the sensitivity analysis performed by the code TSUNAMI-3D to be utilized to obtain the sensitivities for each parameter in an experiment. Table 48 and Table 49 display the sensitivities obtained from the TSUNAMI-3D analysis.

Table 48. TSUNAMI-3D Sensitivities by Mixture 7uPCX 0.800 cm Pitch

	Mixture	Sensitivity	Standard Deviation	% Std. Dev.
Fuel	1	6.12E-02	4.90E-04	0.8000
Clad	2	6.27E-03	6.38E-05	0.9800
Moderator	3	4.21E-01	2.57E-03	0.6100
SS 304	4	-2.09E-05	5.00E-06	23.9100
6061 Al	5	2.53E-03	3.05E-05	1.2100
Poly	6	3.13E-04	1.54E-04	49.1100
SS 304 Spring	8	-1.36E-04	2.54E-06	1.8800
Reflector	9	3.76E-02	3.55E-03	9.4400
^{235}U	1	1.14E-01	3.82E-04	0.34
^{238}U	1	-7.39E-02	1.71E-04	0.23

Table 49. TSUNAMI-3D Sensitivities by Mixture 7uPCX 0.855 cm Pitch

855	Mixture	Sensitivity	Standard Deviation	% Std. Dev.
Fuel	1	7.07E-02	4.97E-04	0.700
Clad	2	5.08E-03	6.37E-05	1.250
Moderator	3	4.28E-01	2.91E-03	0.680
SS 304	4	-2.08E-05	5.33E-06	25.690
6061 Al	5	2.36E-03	3.06E-05	1.240
Poly	6	2.52E-04	1.14E-04	45.080
SS 304 Spring	8	-1.04E-04	2.21E-06	2.130
Reflector	9	3.98E-02	3.60E-03	9.040
^{235}U	1	1.20E-01	4.05E-04	0.34
^{238}U	1	-6.86E-02	1.65E-04	0.24

Table 50 and Table 51 contain the results for the sensitivity analysis performed for the 7uPCX using the direct uncertainty analysis method and the thesis analysis. The columns include the parameter, the sensitivity and the associated uncertainty in the

www.manaraa.com

sensitivity. The relative difference is the thesis analysis minus the direct uncertainty analysis divided by the direct uncertainty analysis.

Implementing the equations described in the previous chapter, the sensitivity and uncertainty in the sensitivity are calculated for each parameter.

Table 50. TSUNAMI-3D Sensitivity Analysis 7uPCX 0.800 cm Pitch

	Direct Uncertainty		SAFOD Analysis		
	Sensitivity	Uncertainty in Sensitivity	Sensitivity	Uncertainty in Sensitivity	Relative Difference
Pitch (cm)	0.92287	0.028800	1.680926	0.010249	82%
Clad OD (cm)	-0.70708	0.025434	-0.838606	0.003983	19%
Clad ID (cm)	-0.06590	0.020347	0.047005	0.000478	-171%
Fuel Diameter (cm)	-0.01318	0.006074	-0.061213	0.000490	364%
Fissile Column Height (cm)	-0.09100	0.254519	-0.061213	0.000490	-33%
Enrichment (wt. %)	0.10464	0.003893	0.119116	0.000369	14%
AL 6061 (c.u.)	-0.00029	0.000054	0.000253	0.000031	-187%
AL 3003 (c.u.)	-0.00058	0.000051	0.000627	0.000064	-208%
Source Composition (c.u.)	0.00002	0.000055	-0.000002	0.000005	-112%
Temperature (K)	-0.02378	0.000867	-0.036749	0.000224	55%

Table 51. TSUNAMI-3D Sensitivity Analysis 7uPCX 0.855 cm Pitch

	Direct Uncertainty		SAFOD Analysis		
	Sensitivity	Uncertainty in Sensitivity	Sensitivity	Uncertainty in Sensitivity	Relative Difference
Pitch (cm)	0.80135	0.02892	1.518325	0.011596	89%
Clad OD (cm)	-0.56996	0.01111	-0.663165	0.004506	16%
Clad ID (cm)	-0.09309	0.02419	0.038097	0.000478	-141%
Fuel Diameter (cm)	-0.01116	0.00637	-0.070723	0.000497	534%
Fissile Column Height (cm)	-0.11113	0.21822	-0.070723	0.000497	-36%
Enrichment (wt. %)	0.13256	0.00566	0.124921	0.000393	-6%
AL 6061 (c.u.)	-0.00029	0.00005	0.000236	0.002360	-181%
AL 3003 (c.u.)	-0.00053	0.000053	0.000508	0.000064	-195%
Source Composition (c.u.)	0.000057	0.000055	-0.000002	0.000005	-104%
Temperature (K)	-0.02183	0.00093	-0.037309	0.000254	71%

www.manaraa.com

The enrichment, clad outer diameter, temperature match well, while all remaining parameters differ by greater than thirty percent. It was expected that the material sensitivities match up well with the thesis analysis method, however there is some underlying reason why these values differ by a large amount.

Table 52. Final Summary Results

	LCT023	LCT070	LCT079	7uPCX 0.800 cm	7uPCX 0.855 cm
Pitch	-520%	29%	-58%	82%	89%
Clad OD	-11%	8%	4%	19%	16%
Clad ID		-97%	-179%	-171%	-141%
Enrichment	2%	3%	-1%	14%	-6%
Fuel Pellet Diameter	-586%	-13%	216%	364%	534%
Fuel Height	7%	68%		-33%	-36%
Fuel Density	3%	-24%			
Clad Mass and Composition	-3%		-285%	-208%	-195%
AL 6061 (c.u.)			-220%	-187%	-181%
Source Composition (c.u.)			-72%	-112%	-104%
Central Hole Diameter		158%			
Fuel Mass	0%				
Temperature (K)		60%	87%	55%	71%

Table 52 displays the relative difference between the direct uncertainty analysis and the SAFOD analysis for each parameter. The results in the table show that the thesis analysis works best for the clad outer diameter and enrichment. The fuel height works well for the LCT023, LCT079 and the 7uPCX experiments. The conclusion that can be drawn from these results is that the SAFOD analysis is a good starting point for sensitivity analysis.

www.manaraa.com

CHAPTER 7

7.1 Conclusions and Future Work

When an experiment is being designed, performed or evaluated, there is a requirement to know each parameter of the system as well as possible. The better the entire system is known, the more widely the information obtained from the experiment will be used.

The current method of uncertainty analysis is tedious and time consuming. The process suggested by the IHCSEBE Uncertainty Guidelines requires a nominal case be developed in an accepted Monte Carlo code, and that nominal case be perturbed individually for each parameter uncertainty. To obtain good statistics with the Monte Carlo code the files must be run with sufficient generations and neutrons per generation. This method of analysis creates hundreds of input files. Once the uncertainty in the multiplication factor for each parameter is determined, they are summed in quadrature to give an overall uncertainty in the multiplication factor for the system. This process offers a very robust and detailed analysis; however, if the time required to perform this analysis could be cut in half and still maintain the robustness of the analysis, the job of the experiment evaluator would be greatly improved.

The methods developed here offer a simpler approach to uncertainty analysis. The goal of uncertainty analysis for benchmark evaluations is to provide a single value for how well the multiplication factor is known. Each parameter evaluated in the uncertainty analysis affects the multiplication factor. If the uncertainty of the

www.manaraa.com

multiplication factor contributed by each parameter uncertainty is known, the overall uncertainty can be determined.

First order derivative equations were developed to correlate the TSUNAMI-3D sensitivity analysis with the direct uncertainty analysis process. The results varied for different types of systems.

This analysis offers a starting point for a different approach to the uncertainty quantification process. The methods developed can be implemented to obtain a general idea for the sensitivity for each parameter in the system. The evaluator can determine the system's greatest sensitivities and if needed, perform the direct uncertainty analysis for those few parameters, decreasing the overall number of parameters originally required and computer runs. An example of this is the work being performed for the Seven Percent Critical Experiment currently being conducted at Sandia. With the completion of the sensitivity and uncertainty analysis, the evaluator can now return to the experimental setup and re-measure values such as the rod outer diameter and obtain smaller uncertainties, knowing that those parameters have the largest effect on the system.

This method could be implemented previous to performing the experiment. If it is possible to determine the sensitivities for system parameters before the experiment begins, the experimenter could re-measure important values to obtain a smaller uncertainty. This would greatly decrease the overall uncertainty and give a better uncertainty in the multiplication factor.

www.manaraa.com

The primary accomplishment of this work is that the process of relating the TSUNAMI sensitivity coefficients with the method of direct uncertainty analysis had not been investigated before.

This process will be evaluated in greater detail to determine if any correlation exists between the parameters that did work and ones that did not. Providing a better understanding of why particular parameters did not work well could offer a solution to the problem, and thus offer a better overall process for uncertainty analysis.

www.manaraa.com

Appendix A. TSUNAMI-3D Control Module Sequence Description

TSUNAMI-3D-K5 is a control module that guides the execution of a sequence of calculations that are performed by other codes included in the SCALE code package. The order of the sequences executed by TSUNAMI-3D-K5 is WORKER, BONAMI, CENTRM/PMC/WORKER, KENOV.a and SAMS. WORKER is run first to convert the master library to working format library to be used by the code CENTRM.ref BONAMI ((BONdarenko AMPX Interpolator) is then executed, and performs the resonance self-shielding calculation based on the Bondarenko method and produces problem-dependent master date sets.[ref] CENTRM and PMC are executed once for every unit cell specified plus a final time for all materials that are not specified by a unit cell. WORKER is then run a final time in the sequence to convert all master format library to a working format library. The final master library is then used to obtain the resonance shielded cross section data for partial reactions that are required for the sensitivity calculations. The partial reactions include fission, capture, scatter, elastic, (n, γ), (n, n'), (n, p), (n,d), (n,α), (n,2n), chi, and nubar. These reactions can be represented for a nuclide or a mixture. Once WORKER completes the conversion for the master format library, the forward and adjoint calculations are performed using the KENO V.a module. Finally in the TSUNAMI-3D-K5 control module, the SAMS module is executed. The SAMS module calculates the sensitivity coefficients that indicate the sensitivity of the calculated value of k_{eff} to the changes in the cross sections and the uncertainty in the calculated value of k_{eff} due to the uncertainty in the nuclear data. The SAMS module then prints the energy-integrated sensitivity coefficients and the corresponding standard deviations. A sensitivity data file (.sdf) is generated along with the standard output file containing all

www.manaraa.com

of the sensitivity coefficients generated in the calculation. The .sdf file can be use for comparison with another experimental model or can be used to create sensitivity plots with the plotting code JAVAPENO. These processes with not be used in this work. Only the total sensitivities for each mixture will be utilized in this work.

www.manaraa.com

Appendix B. TSUNAMI-3D Sensitivity Coefficient Equations

From the development of the SAMS module, the total sensitivity and the associated standard deviation is given by the following equations. The full derivation of the total sensitivity and standard deviation of the total sensitivity is documented in reference 14.

$$S^i_{t,g,z} = \frac{V_z}{D}\left[\left(\Sigma^{0,i}_{s,g\to g,z} + \frac{1}{k}\nu^i_{g,z}\Sigma^i_{f,g,z}\chi^i_{g,z} - \Sigma^i_{t,g,z}\right)P^0_{g,g,z} + \sum_{\substack{g'=1\\ g\neq g'}}^{G}\left(\Sigma^{0,i}_{s,g\to g',z} + \frac{1}{k}\nu^i_{g,z}\Sigma^i_{f,g,z}\chi^i_{g',z}\right)P^0_{g,g',z} + \sum_{\ell=1}^{ISCT}\left(\Sigma^{\ell,i}_{s,g\to g,z} - (2\ell+1)\Sigma^i_{t,g,z}\right)P^l_{g,g,z} + \sum_{\substack{g'=1\\ g'\neq g}}^{G}\Sigma^{\ell,i}_{s,g\to g',z}P^l_{g,g',z}\right] \tag{173}$$

$$\sigma^2_{S^i_{t,g,z}} = \left(\frac{S^i_{t,g,z}\sigma_D}{D}\right)^2 + \frac{V_z^2}{D^2}\left[\left(\Sigma^{0,i}_{s,g\to g,z} + \frac{1}{k}\nu^i_{g,z}\Sigma^i_{f,g,z}\chi^i_{g,z} - \Sigma^i_{t,g,z}\right)^2\sigma^2_{P^0_{g,g,k}} + \sum_{\substack{g'=1\\ g\neq g'}}^{G}\left(\Sigma^{0,i}_{s,g\to g',z} + \frac{1}{k}\nu^i_{g,z}\Sigma^i_{f,g,z}\chi^i_{g',z}\right)^2\sigma^2_{P^0_{g,g',k}} + \sum_{\ell=1}^{ISCT}\left(\Sigma^{\ell,i}_{X,g\to g,z} - (2\ell+1)\Sigma^i_{t,g,z}\right)^2\sigma^2_{P^\ell_{g,g,k}} + \sum_{\substack{g'=1\\ g\neq g'}}^{G}\left(\Sigma^{\ell,i}_{X,g\to g',z}\right)^2\sigma^2_{P^\ell_{g,g',k}} + \left(\frac{\sigma_k}{k^2}\right)^2\left(\sum_{g'=1}^{G}\nu^i_{g,z}\Sigma^i_{f,g,z}\chi^i_{g',z}P^0_{g,g',z}\right)^2\right] \tag{174}$$

Where:

$$D = \frac{1}{k}\sum_{i=1}^{I}\sum_{z=1}^{R}V_z\sum_{g=1}^{G}\sum_{g'=1}^{G}\nu^i_{g,z}\Sigma^i_{f,g,z}\chi^i_{g',z}P^0_{g,g',z} \tag{175}$$

www.manaraa.com

$$\sigma_D^2 = \left(\frac{D\sigma_k}{k}\right)^2 + \frac{1}{k^2}\sum_{i=1}^{I}\sum_{z=1}^{R} V_z^2 \sum_{g=1}^{G}\sum_{g'=1}^{G}\left(\nu_{g,z}^{i}\Sigma_{f,g,z}^{i}\chi_{g',z}^{i}\right)^2 \sigma_{P_{g,g',z}^{0}}^2 \tag{176}$$

www.manaraa.com

Appendix C. Uncertainties associated with normal distributions

Assume there is a uniform distribution with the following probability density function

$$f(x) = \frac{1}{B-A} \tag{177}$$

for $A \le x \le B$. The variance and the standard deviation of a uniform distribution can be found using the following two equations.

$$Var(x) = \frac{(B-A)^2}{12} \tag{178}$$

$$\sigma(x) = \sqrt{\frac{(B-A)^2}{12}} = \frac{(B-A)}{12^{0.5}}. \tag{179}$$

In the above equations A is the "location parameter" and (B-A) is the scale parameter

$$A = \bar{x} - \delta x \tag{180}$$

$$B = \bar{x} + \delta x \tag{181}$$

where δx is the uncertainty in the parameter x. Equation 182 displays the process that results in the uncertainty divided by square root of 3 described above.

$$\sigma(x) = \sqrt{\frac{(B-A)^2}{12}} = \sqrt{\frac{[\bar{x}+\delta x-(\bar{x}-\delta x)]^2}{12}} = \sqrt{\frac{[\bar{x}+\delta x-\bar{x}+\delta x]^2}{12}} = \sqrt{\frac{[2\delta x]^2}{12}} = \sqrt{\frac{4\delta x^2}{12}} = \frac{\delta x}{\sqrt{3}} \tag{182}$$

www.manaraa.com

Appendix D. Fuel Height Measurements

	Measure Date	New MC&A Control No.	Element Identifier	Element Gross Wt	Element Tare Wt	UO2 Net Wt	Fuel Length (cm)
1	38170	P0021XXXX	1	130.37	21.79	108.58	48.9
2	38174	P0021XXXX	2	130.32	21.8	108.52	48.8
3	38174	P0021XXXX	3	130.35	21.78	108.57	48.8
4	38174	P0021XXXX	4	130.08	21.7	108.38	48.6
5	38174	P0021XXXX	5	130.37	21.75	108.62	48.8
6	38174	P0021XXXX	6	130.39	21.77	108.62	48.8
7	38174	P0021XXXX	7	129.94	21.74	108.2	48.6
8	38174	P0021XXXX	8	130.22	21.78	108.44	48.7
9	38174	P0021XXXX	9	130.43	21.89	108.54	48.8
10	38174	P0021XXXX	10	130.24	21.7	108.54	48.7
11	38174	P0021XXXX	11	130.12	21.74	108.38	48.8
12	38174	P0021XXXX	12	130.15	21.77	108.38	48.7
13	38174	P0021XXXX	13	130.5	21.9	108.6	48.8
14	38174	P0021XXXX	14	130.28	21.93	108.35	48.6
15	38175	P0021XXXX	15	132.23	21.84	110.39	49.4
16	38175	P0021XXXX	16	130.26	21.85	108.41	48.6
17	38175	P0021XXXX	17	132.26	21.81	110.45	49.5
18	38175	P0021XXXX	18	132.33	21.71	110.62	49.5
19	38175	P0021XXXX	19	130.11	21.74	108.37	48.6
20	38175	P0021XXXX	20	132.28	21.8	110.48	49.5
21	38175	P0021XXXX	21	132.43	21.75	110.68	49.5
22	38175	P0021XXXX	22	130.45	21.79	108.66	48.7
23	38175	P0021XXXX	23	130.93	21.75	109.18	48.7
24	38175	P0021XXXX	24	131.22	21.8	109.42	48.8
25	38175	P0021XXXX	25	131.04	21.79	109.25	48.8
26	38175	P0021XXXX	26	131.09	21.8	109.29	48.8
27	38175	P0021XXXX	27	131.09	21.88	109.21	48.7
28	38175	P0021XXXX	28	130.82	21.88	108.94	48.7
29	38175	P0021XXXX	29	131.13	21.8	109.33	48.8
30	38175	P0021XXXX	30	131.03	21.85	109.18	48.7
31	38175	P0021XXXX	31	131.15	21.86	109.29	48.8
32	38175	P0021XXXX	32	131.2	21.8	109.4	48.8
33	38175	P0021XXXX	33	131.03	21.91	109.12	48.8
34	38175	P0021XXXX	34	130.97	21.72	109.25	48.7
35	38175	P0021XXXX	35	131.12	21.8	109.32	48.7
36	38175	P0021XXXX	36	130.83	21.78	109.05	48.7
37	38175	P0021XXXX	37	131.05	21.84	109.21	48.8
38	38175	P0021XXXX	38	131.09	21.87	109.22	48.8
39	38175	P0021XXXX	39	130.99	21.83	109.16	48.8
40	38175	P0021XXXX	40	130.95	21.69	109.26	48.7
41	38175	P0021XXXX	41	126.28	18.29	107.99	48.7
42	38175	P0021XXXX	42	130.59	21.76	108.83	48.7
43	38175	P0021XXXX	43	130.65	21.87	108.78	48.7

www.manaraa.com

44	38175	P0021XXXX	44	130.53	21.77	108.76	48.8
45	38176	P0021XXXX	45	130.9	21.82	109.08	48.8
46	38177	P0021XXXX	46	130.87	21.73	109.14	48.8
47	38177	P0021XXXX	47	130.81	21.84	108.97	48.8
48	38177	P0021XXXX	48	131.04	21.86	109.18	48.9
49	38177	P0021XXXX	49	130.65	21.7	108.95	48.8
50	38177	P0021XXXX	50	130.95	21.87	109.08	48.8
51	38177	P0021XXXX	51	130.76	21.78	108.98	48.7
52	38177	P0021XXXX	52	130.91	21.75	109.16	48.9
53	38177	P0021XXXX	53	130.94	21.84	109.1	48.7
54	38177	P0021XXXX	54	131.01	21.83	109.18	48.8
55	38177	P0021XXXX	55	130.95	21.71	109.24	48.8
56	38177	P0021XXXX	56	130.98	21.74	109.24	48.9
57	38177	P0021XXXX	57	131.05	21.94	109.11	48.9
58	38177	P0021XXXX	58	130.94	21.75	109.19	48.8
59	38177	P0021XXXX	59	130.99	21.91	109.08	48.8
60	38177	P0021XXXX	60	130.78	21.73	109.05	48.8
61	38177	P0021XXXX	61	130.97	21.76	109.21	48.9
62	38177	P0021XXXX	62	130.78	21.81	108.97	48.8
63	38177	P0021XXXX	63	130.89	21.87	109.02	48.8
64	38177	P0021XXXX	64	130.84	21.7	109.14	48.9
65	38177	P0021XXXX	65	130.94	21.79	109.15	48.8
66	38177	P0021XXXX	66	130.99	21.72	109.27	48.8
67	38177	P0021XXXX	67	130.82	21.81	109.01	48.8
68	38177	P0021XXXX	68	130.62	21.85	108.77	48.8
69	38177	P0021XXXX	69	130.72	21.65	109.07	48.9
70	38177	P0021XXXX	70	130.78	21.77	109.01	48.9
71	38177	P0021XXXX	71	130.61	21.74	108.87	48.8
72	38177	P0021XXXX	72	130.67	21.74	108.93	48.8
73	38177	P0021XXXX	73	130.59	21.77	108.82	48.9
74	38177	P0021XXXX	74	130.79	21.81	108.98	48.8
75	38177	P0021XXXX	75	130.69	21.86	108.83	48.9
76	38177	P0021XXXX	76	130.69	21.84	108.85	48.8
77	38177	P0021XXXX	77	130.54	21.7	108.84	48.8
78	38177	P0021XXXX	78	130.74	21.82	108.92	48.9
79	38177	P0021XXXX	79	130.93	21.88	109.05	49
80	38177	P0021XXXX	80	130.47	21.75	108.72	48.8
81	38177	P0021XXXX	81	130.64	21.83	108.81	48.9
82	38177	P0021XXXX	82	130.73	21.83	108.9	48.8
83	38177	P0021XXXX	83	130.67	21.72	108.95	48.8
84	38177	P0021XXXX	84	130.77	21.8	108.97	48.9
85	38177	P0021XXXX	85	130.69	21.81	108.88	48.8
86	38177	P0021XXXX	86	130.61	21.86	108.75	48.7
87	38177	P0021XXXX	87	131.02	21.77	109.25	48.8
88	38177	P0021XXXX	88	130.87	21.92	108.95	48.8
89	38177	P0021XXXX	89	130.71	21.81	108.9	48.8
90	38177	P0021XXXX	90	130.94	21.79	109.15	48.8
91	38177	P0021XXXX	91	130.66	21.78	108.88	48.8

www.manaraa.com

92	38177	P0021XXXX	92	130.76	21.75	109.01	48.8
93	38177	P0021XXXX	93	130.79	21.79	109	48.8
94	38177	P0021XXXX	94	130.56	21.75	108.81	48.7
95	38177	P0021XXXX	95	130.81	21.9	108.91	48.7
96	38180	P0021XXXX	96	130.5	21.78	108.72	48.7
97	38180	P0021XXXX	97	130.65	21.75	108.9	48.7
98	38180	P0021XXXX	98	130.57	21.7	108.87	48.7
99	38180	P0021XXXX	99	130.8	21.81	108.99	48.8
100	38180	P0021XXXX	100	130.75	21.86	108.89	48.7
	Number					2199	
	Average			130.4586	21.74209	108.7165	48.77954
	Std. Dev.			0.360601	0.126119	0.322834	0.125101
	Std. Dev. of Mean			0.00769	0.002689	0.006884	0.002668
	Rel. SDoM					6.33E-05	5.47E-05
	Maximum			132.46	22	110.68	49.5
	Minimum			126.28	18.29	107.73	48.6

www.manaraa.com

REFERENCES

1. Oak Ridge National Laboratory, *TSUNAMI-3D: Control Module for Three-Dimensional Cross-Section Sensitivity and Uncertainty Analysis Criticality, Rev. 5.1 (ORNL/TM-2005/39), Vols.1 Book 2, Section C9.ORNL, November 2006.* Available from: Radiation Safety Information Computational Center at Oak Ridge National Laboratory.

2. Goluoglu, S. Hopper, C.M., and Rearden, B.T., "Extended Interpretation of Sensitivity Data for Benchmark Areas of Applicability." *Trans. American Nuclear Society* **88**, 77-79 (2003).

3. Rearden, B. T., Hopper, C. M., and Elam, K. R., Goluoglu, S. and Parks, C.V., "Applications of the TSUNAMI Sensitivity and Uncertainty Analysis Methodology." pp. 61-66 in *Proc. of The 7th International Conference on Nuclear Criticality Safety (ICNC2003)"*, October 20-24, 2003, Tokai-mura, Japan.

4. Rearden, B. T., Hopper, C. M., and Elam, K. R., "TSUNAMI Analysis of the Applicability of Proposed Experiments to Reactor-Grade and Weapons-Grade Mixed-Oxide Systems." presented at the International Symposium NUCEF2005, Tokai, Japan, February 9-10, 2005.

5. *International Handbook of Evaluated Criticality Safety Benchmark Experiments*, Nuclear Energy Agency Nuclear Science Committee of the Organization for Economic Co-operation and Development, NEA/NSC/DOC(95)03, (2007)

6. Gagarinski, A., Yu., Z., Oleg E., and Pavlov, V. D., "Partially Flooded Uniform Lattices of Rods with U(10%)O_2 Fuel." LEU-COMP-THERM-023. *International Handbook of Evaluated Criticality Safety Benchmark Experiments*, Nuclear Energy Agency Nuclear Science Committee of the Organization for Economic Co-operation and Development, NEA/NSC/DOC(95)03, (2007).

7. Alexeyev, N., Krainov, Y., Kravchenko, Y., and Tevetkov, V., "VVER Physics Experiments: Regular Hexagonal (1.10 cm-Pitch) Lattices of Low-Enriched U(6.5WT.% ^{235}U)O_2 Fuel Rods in Light Water at Different Core Critical Dimensions." LEU-COMP-THERM-070. *International Handbook of Evaluated Criticality Safety Benchmark Experiments*, Nuclear Energy Agency Nuclear Science Committee of the Organization for Economic Co-operation and Development, NEA/NSC/DOC(95)03, (2007).

8. Harms, G. A., "Water-Moderated U(4.31)O_2 Fuel Rod Lattices Containing Rhodium Foils." LEU-COMP-THERM-079. *International Handbook of Evaluated Criticality Safety Benchmark Experiments*, Nuclear Energy Agency Nuclear Science Committee of the Organization for Economic Co-operation and Development, NEA/NSC/DOC(95)03, (2007)

www.manaraa.com

9. Oak Ridge National Laboratory, *SCALE: A Modular Code System for Performing Standardized Computer Analyses for Licensing Evaluation, ORNL/TM-2005/39, Version 5.1, Vols. I, II, and III, November 2006.* Available from: Radiation Safety Information Computational Center at Oak Ridge National Laboratory as CCC-732.

10. Saltelli, A., Chan K., and Scott, M. E., *Sensitivity Analysis*, John Wiley & Sons LTD. 2000.

11. Saltelli, A., et al., *Global Sensitivity Analysis: The Primer*, John Wiley & Sons, 2008 [http://sensitivity-analysis.jrc.ec.europa.eu/docs/what_is_SA.htm].

12. Saltelli, A., Ratto M., Tarantola, S., and Campolongo, F.. *Sensitivity Analysis Practices: Strategies for Model-Based Inference*, European Commission, Joint Research Centre of Ispra (I). RESS Review. 2005.

13. Rearden, B. T., *TSUNAMI-3D: Control Module for Three-Dimensional Cross-Section Sensitivity and Uncertainty Analysis for Criticality*. Oak Ridge National Laboratory, Oak Ridge, Tennessee. November 2006.

14. Rearden, B. T.. *Development of SAMS: A Sensitivity Analysis Module for the SCALE Code System using KENO V.A in the CSAS25 Sequence.* Doctoral Dissertation Texas A&M University, December 1999.

15. Weisbin, C. R., et al., *Application of FORSS Sensitivity and Uncertainty Methodology to Fast Reactor Benchmark Analysis*. ORNL/TM-5563, Union Carbide Corp., Oak Ridge National Laboratory (1976).

16. Duderstadt, J.J., and Hamilton, L.J., *Nuclear Reactor Analysis*, John Wiley & Sons, New York, 1976.

17. Ott, K. O. and Neuhold, R. J. *Introductory Nuclear Reactor Dynamics* American Nuclear Society, Le Grange Park, Illinois, 1984.

18. Rearden, B. T., *SAMS: Sensitivity Analysis Module for Criticality Safety Analysis Using Monte Carlo Techniques.* Oak Ridge National Laboratory, Oak Ridge, TN 37831-6730.

19. Perry, M. A., Wynn, H. P., and Bates, R.A., *Principle Components Analysis in Sensitivity Studies of Dynamic Systems*. Probabilistic Engineering Mechanics **21** (2006) 454-460.

20. Dean, V. F., "IHECSBE Guide to the Expression of Uncertainties. International Handbook of Evaluated Critical Benchmark Experiments" in IHECSBE, September 30, 2007.

www.manaraa.com

21. Press W. H., Teukolsky S. A., Vetterling W. T., and Flannery B.. *Numerical Recipes: The Art of Scientific Computing*. 3rd Edition. Cambridge University Press, 2007.

22. ASTM B811 – 02 Standard Specification for Wrought Zirconium Alloy Seamless Tubes for Nuclear Reactor Cladding. ASTM International, 100 Barr Harbor Drive, PO Box C700, West Conshohocken, PA 19428-2959, United States.

23. ASTM B209 – 07 Standard Specification for Aluminum and Aluminum-Alloy Sheet and Plate. ASTM International, 100 Barr Harbor Drive, PO Box C700, West Conshohocken, PA 19428-2959, United States.

24. ASTM A276 – 08a Standard Specification for Stainless Steel Bars and Shapes. ASTM International, 100 Barr Harbor Drive, PO Box C700, West Conshohocken, PA 19428-2959, United States.

25. Ktech Corporation, "7uPCX Fuel Cladding Evaluation Diameter Study," Performed by the Ktech Corporation for G. A. Harms. Report submitted November 11th, 2004.

26. ASTM 8210 – 04 Standard Specification for Aluminum and Aluminum-Alloy Drawn Seamless Tubes. ASTM International, 100 Barr Harbor Drive, PO Box C700, West Conshohocken, PA 19428-2959, United States.

27. Poullot, G., Doutriaux, D., and Anno, J. *ICSBEP Guide to the Expression of Uncertainties Revision 3.* Institut de Radioprotection et de Sûreté Nucléaire (IRSN), France. September 30, 2007.

28. Saltelli, A, Chan K, and Scott E. M., *Sensitivity Analysis*. John Wiley & Sons; 2000.

29. Bevington, P. R., and Robinson, D. K., *Data Reduction and Error Analysis for the Physical Sciences*. Page numbers, 2003.

30. Areva Federal Services, "Reactor Physics and Criticality Benchmark Evaluations for Advanced Nuclear Fuel, Final Technical Report." TDR-30000849-000, Areva Federal Services, LLC, 2008.

31. Rearden, B. T., Anderson, W. J., and Harms, G. A., "Use of Sensitivity and Uncertainty Analysis in the Design of Reactor Physics and Criticality Benchmark Experiments for Advanced Nuclear Fuel." Nuclear Technology. **Vol. 151**, Number 2, August 2005 (pp. 133-158).

32. Oberkampf, W. L., Trucano T., and Hirsch C., *Verification, Validation and Predictive Capability in Computational Engineering and Physics*. Appl Mech Rev, **Vol 57** No. 5, September 2004. American Society of Mechanical Engineers.

www.manaraa.com

33. Broadhead, B.L., Hopper, C.M., Childs, R.L., and Parks, C.V., *Sensitivity and Uncertainty Analyses Applied to Criticality Validation: Volume 1: Methods Development,* NUREG/CR-6655, Vol. 1, ORNL/TM-13692/V1, U.S. Nuclear Regulatory Commission, Oak Ridge National Lab., July 1999.

www.manaraa.com